NASA CONTRACTOR REPORT

NASA CR-2374

NASA CR-2374

A PREDICTIVE PILOT MODEL FOR STOL AIRCRAFT LANDING

by David L. Kleinman and William R. Killingsworth

Prepared by
SYSTEMS CONTROL, INC.
Palo Alto, Calif. 94306
for Langley Research Center

NATIONAL AERONAUTICS AND SPACE ADMINISTRATION • WASHINGTON, D. C. • MARCH 1974

1. Report No.	2. Government Accession No.	3. Recipient's Catalog No.
NASA CR-2374		

4. Title and Subtitle	5. Report Date
A PREDICTIVE PILOT MODEL FOR STOL AIRCRAFT LANDING	March 1974
	6. Performing Organization Code

7. Author(s)	8. Performing Organization Report No.
David L. Kleinman and William R. Killingsworth	

9. Performing Organization Name and Address	10. Work Unit No.
	504-29-13-01
Systems Control, Inc. Palo Alto, California	11. Contract or Grant No.
	NAS1-11727
12. Sponsoring Agency Name and Address	13. Type of Report and Period Covered
National Aeronautics and Space Administration Washington, D.C. 20546	Contractor Report
	14. Sponsoring Agency Code

15. Supplementary Notes

This is a final report.

16. Abstract

An optimal control approach has been used to model pilot performance during STOL flare and landing. The model is used to predict pilot landing performance for three STOL configurations, each having a different level of automatic control augmentation. Model predictions are compared with flight simulator data. It is concluded that the model can be an effective design tool for studying analytically the effects of display modifications, different stability augmentation systems, and proposed changes in the landing area geometry.

17. Key Words (Suggested by Author(s))	18. Distribution Statement
Optimal control STOL landing model STOL simulation Landing simulation Math model	Unclassified - Unlimited

19. Security Classif. (of this report)	20. Security Classif. (of this page)	21. No. of Pages	22. Price*
Unclassified	Unclassified	128	$4.50

*For sale by the National Technical Information Service, Springfield, Virginia 22151

A PREDICTIVE PILOT MODEL FOR STOL AIRCRAFT LANDING

by

David L. Kleinman and William R. Killingsworth
Systems Control, Inc.

SUMMARY

The optimal control approach to pilot vehicle systems analysis provides the framework for modeling pilot performance during STOL flare and landing. The model includes both the terminal time aspects and the short-term open/closed interrelationship for the landing task, and pilot reaction to ground effect. Model output predictions include the probability densities of the touchdown time and velocity, flare path dispersions and pilot control inputs. The model is used to predict pilot landing performance for three STOL configurations, each having a different level of automatic control augmentation. Model predictions are compared with NASA flight simulator data. It is concluded that the model can be an effective design tool for studying analytically the effects of display modifications, different stability augmentation systems, and proposed changes in the landing area geometry.

TABLE OF CONTENTS

TABLE OF CONTENTS (CONCLUDED)

LIST OF FIGURES

SYMBOLS

$\underline{A}$	system matrix
a_T^{-1}	throttle-thrust time-constant
a_i	pilot threshold on output y_i
$\tilde{\underline{A}}$	augmented system matrix
$\underline{B}$	control matrix
$\tilde{\underline{B}}$	augmented control matrix
$\underline{C}$	output matrix
C_T	thrust coefficient
c	chord length
$\tilde{\underline{C}}$	augmented output matrix
$\underline{c}$	terminal condition vector
$C_{L,ge}$	lift ground effect
$C_{M,ge}$	pitching moment ground effect
$\underline{D}$	output matrix
$E\{\cdot\}$	expectation operator
$\underline{E}$	noise driving matrix

$\underline{e}_1$	estimation error
$\underline{e}_2$	prediction error
$\underline{E}_1$, $\underline{E}_2$	estimation, prediction error covariance matrices
$\underline{F}$	forcing function matrix
F_x, F_y, F_z	longitudinal, side and vertical forces
ΔF_x, ΔF_y, ΔF_z	incremental longitudinal, side and vertical forces
g	acceleration due to gravity
$\underline{H}$	terminal condition matrix
h	altitude
δh	altitude deviations from glideslope
$\delta h'$	normalized deviations, $\delta h/V_a$
h_{CG}	altitude of aircraft center of gravity
h_{LG}	altitude of aircraft landing gear
I_x, I_y, I_z	moments of inertia about x, y, and z body axes
I_{xz}	product of inertia
$J(\underline{u})$	cost functional
$\underline{K}$	Kalman filter gain matrix
$\underline{L}$	feedback gains

$\underline{M}$	cross covariance matrix
m	mass
M_y	pitching moments
ΔM_y	incremental, pitching moments
$\underline{p}$	best estimate of delayed state
p(x)	probability density of variable x
p(x/y)	conditional density of x given y
Q	pitching angular velocity
$\bar{q}$	dynamic pressure, $\rho V_a^2/2$
$\underline{Q}_y$	output weighting matrix, diag $[q_{yi}]$
$\underline{Q}_u$	control weighting matrix, diag $[q_{ui}]$
$\underline{Q}_u^{\bullet}$	control rate weighting matrix, diag $[q_{ui}]$
S	wing area
s	Laplace operator
T	total thrust
t	time
$\underline{T}_N$	neuromotor lag matrix
T_d	intended touchdown time

U, W	aircraft total speed components in x and z body axes
u	incremental speed in longitudinal axis
u'	normalized incremental speed, u/V_a
$\underline{u}$	control vector, $[u_1,u_2,\ldots,u_r]$
$\underline{u}_c$	commanded control (internal to pilot model)
$\underline{u}_o$	nominal flare control
V	airspeed
V_a	resultant aerodynamic velocity of airplane
$\underline{v}_y$	observation noise vector, components v_{yi}
$\underline{V}_y$	diagonal observation noise covariance matrix, elements V_{yi}
$\underline{v}_u$	motor noise vector, components v_{ui}
$\underline{V}_u$	diagonal motor noise covariance matrix, elements V_{ui}
$\tilde{\underline{V}}_y$	modified observation noise covariance matrix
w	incremental speed in vertical axes
$\underline{w}$	white driving noise vector
$\underline{W}$	driving noise covariance matrix
$\tilde{\underline{W}}$	augmented driving noise covariance matrix
$\underline{x}$	state vector, $[x_1,x_2,\ldots,x_n]$

$\hat{\underline{x}}$	estimated state vector
$\underline{X}$	state covariance matrix
$\hat{\underline{X}}$	state estimate covariance matrix
$\underline{x}_o$	nominal state trajectory for flare
$\underline{Y}$	output covariance matrix
$\underline{y}$	display output vector, $[y_1, y_2, \ldots, y_m]$
$\underline{y}_p$	pilot-perceived outputs
$\underline{y}_o$	nominal outputs during flare
$\dot{\underline{z}}$	"deterministic" input forcing function
α, α'	angle of attack
γ	flight path angle
δf_3	deflection of rear trailing edge flap (from 60°)
δt	horizontal tail deflection
δT	incremental thrust
δT_c	incremental throttle deflection
$\delta\underline{x}$, $\delta\underline{y}$, $\delta\underline{u}$	deviations from nominal flare trajectory $\underline{x}_o$, $\underline{y}_o$, $\underline{u}_o$
$\underline{\Sigma}$	solution of Riccati (variance) equation
σ_x	standard deviation of variable x

η_k	fractional attention to display k
Θ	pitch angle
θ	incremental pitch angle
ρ	air density
ρ_{yi}	observation noise ratio on output y_i
ρ_{ui}	motor noise ratio on control u_i
τ	time delay
$\underline{X}$	augmented state vector, $[\underline{x}, \underline{u}]$
$\overline{\underline{X}}$	mean augmented state vector, $[\overline{\underline{x}}, \overline{\underline{u}}]$

UNIT CONVERSION FACTORS

The numerical results presented in this report are in the U.S. system of units. The conversions between the U.S. units and the S.I. system of units is given below for those quantities appearing in this report.

U.S. UNITS	S.I. UNITS
ft	.305 m
ft^2	.0925 m^2
lb (force)	4.45 N
slug	14.6 kg
slug-ft^2	1.35 kg-m^2
knot	.515 m/sec

I. INTRODUCTION

Increasing traffic density and resistance to airport expansion have led to the consideration of short take-off and landing (STOL) aircraft. These aircraft are designed with special high lift devices that enable them to land at lower airspeeds with steeper glideslope angles than conventional aircraft. Less runway is needed and less ground noise is heard. Because of the steeper approach paths and smaller landing zones, the flare portion of the landing takes a much shorter time and the pilot is allowed little margine for error. Previous studies[1] have indicated a high level of difficulty for STOL landing and wide dispersions in the touchdown data. Much of the difficulty is caused by adverse ground effects to which the pilot must adapt very quickly.

This study addresses pilot performance for instrument approach and landing of a STOL aircraft, i.e., no external visual cues are available to the pilot, only the cockpit displays. Pilot models based on modern control theory are developed and used in conjunction with mathematical models of the STOL to predict pilot performance in the longitudinal mode of the landing task.

The STOL aircraft design investigated in this effort was a four engine subsonic jet transport with high-bypass-ratio turbofan engines and a high wing equipped with an external-flow jet flap. The engines were pod-mounted under the wing in such a manner that the jet exhaust impinged directly on the trailing-edge flap system. This arrangement provided the high lift required for short field operations.

This basic aircraft possessed several inherent stability and control problems. In the approach configuration, the equilibrium trim pitch attitude was -4.1°. Pilots disliked this condition due to the large change required in pitch attitude just prior to touchdown. Average pilot rating assigned to the longitudinal handling qualities of the basic aircraft was 6.5[1], with the major objections being poor airspeed control, sluggish initial pitch response, large pitch attitude excursions associated with changes in thrust and flaps, a phugoid of short period that cuased pilot induced oscillations, and low apparent pitch damping.

In attempting to overcome these control difficulties, several longitudinal augmentation schemes were investigated by NASA-LRC. One augmentation scheme was an autospeed system that drove the third segment flap to maintain a desired airspeed. The autospeed system accomplished three objectives. It eliminated the phugoid mode that gave rise to many of the basic longitudinal handling qualities, it provided good speed control, and it relieved the pilot of the speed control task, thus reducing pilot workload. More importantly, since the autospeed system moved the flaps to maintain speed, the airplane could be trimmed to a nose-up attitude on the approach path. However, the pilot still had to actively control pitch to maintain this attitude.

A second augmentation scheme incorporated a pitch attitude command and hold system with autospeed. The attitude command system allowed the pilot to trim the aircraft to the pitch attitude required for touchdown early in the approach. Once trimmed, no subsequent pitch control was required since the command system automatically maintained the desired attitude. The longitudinal piloting task was thus reduced to altitude control with throttles.

In landing the aircraft, the pilot has a standard set of instruments. An eight-ball was used to display pitch attitude, an altimeter and sink-rate instrument displayed vertical information, and an airspeed indicator provided velocity information. A light was automatically turned on at an altitude of 53' to notify the pilot at flare initiation altitude.*

The STOL iarcraft approached the runway on a 6° glideslope at a velocity of 75 knots. The primary longitudinal requirements for a satisfactory landing were: touchdown within a prescribed landing zone 450 ft long starting 250 ft from the runway threshold; and touchdown with an acceptable rate of sink, no greater than 3 ft/sec. Since flare initiation is a h_{CG} = 53 ft touchdown occurs in approximately 5 sec. As a result, the pilot has little time to correct any errors. The difficulty of the landing task is compounded by adverse ground effects that arise from the deflected thrust. Specifically, a nose-down pitching moment, a loss in lift, and a decrease in drag occur as the ground is

*An additional "get ready" light came on ≈5 sec prior to flare initiation.

approached.

In the analytic effort described herein, mathematical models were developed for the STOL aircraft and for the pilot. These models were then used to predict pilot performance in the STOL landing task for the basic aircraft, aircraft with autospeed and the fully augmented STOL. The pilot model was developed using techniques of modern control and estimation theory, and contains explicit representations of the pilot's inherent limitations, information processing and control behavior. The model extends existing results in man-machine systems analysis by considering human adaptation to ground effects as well as the terminal aspects and the open/closed loop interrelationships.

The outline of the report is as follows. In Chapter II, linearized models for the three different STOL configurations are developed from NASA supplied wind tunnel data. In Chapter III, the modern control approach to human operator modeling is outlined, and the extensions necessary to treat the landing task are presented. Expressions for the touchdown statistics are derived from model covariance predictions. For the three cases studied, numerical values for the pilot model parameters are chosen a priori. In Chapter IV, the resulting model covariance predictions are compared with ensemble averages of actual pilot response data obtained on the Real Time Dynamic Simulation Facility at NASA Langley Research Center. The comparisons were favorable. Discrepancies between the model prediction and the data are discussed, and are used to indicate potential areas for model improvement. Our conclusions and suggestions for further work are contained in Chapter V.

II. STOL MODEL DEVELOPMENT

In this chapter, mathematical representations are developed for the STOL aircraft during approach and landing. In particular, linearized dynamics are derived from available wind tunnel data. The linear models are needed in the subsequent development of the optimal control model for pilot response that includes the terminal control aspects of the landing task.

2.1 BASIC EQUATIONS OF MOTION

The equations of motion for the aircraft can be derived from Newton's laws of motion,

$$\Sigma F = \frac{d}{dt}(mV)\Big]_I \tag{1}$$

$$\Sigma M = \frac{dH}{dt}\Big]_I \tag{2}$$

where the subscript I indicates the time change with respect to inertial space.

Assuming: (a) the mass of the aircraft remains constant during any particular dynamic analysis; (b) the body fixed axes OX and OZ lie in the plane of symmetry of the aircraft; (c) the aircraft is a rigid body; and (d) the earth is an inertial reference, Eqs. (1) and (2) may be expanded to yield

$$\begin{aligned} \Sigma F_x &= m(\dot{U} + WQ - VR) \\ \Sigma F_y &= m(\dot{V} + UR - WP) \\ \Sigma F_z &= m(\dot{W} + VP - UQ) \end{aligned} \tag{3}$$

and

$$\Sigma M_x = PI_x - RI_{xz} + QR(I_z - I_y) - PQI_{xz}$$

$$\Sigma M_y = QI_y + PR(I_x - I_z) + (P^2 - R^2)I_{xz} \tag{4}$$

$$\Sigma M_z = RI_z - PI_{xz} + PQ(I_y - I_x) + QRI_{xz}$$

These six simultaneous nonlinear equations of motion completely describe the behavior of a rigid aircraft. In this form, a solution can be obtained only by use of analog or digital computers. In most cases, however, by use of proper assumptions, the equations can be broken down into two sets of three equations each and these linearized to obtain equations amenable to analytic solutions of sufficient accuracy. The six equations are first broken up into two sets of three simultaneous equations. To accomplish this, the aircraft is considered to be in straight and level unaccelerated flight and then to be disturbed by deflection of the elevator. This deflection applies a pitching moment about the OY axis, causing a rotation about this axis which eventually causes a change in F_x and F_z, but does not cause a rolling or yawing moment or any change in F_y; thus, P=R=V=0 and the ΣF_y, ΣM_x, ΣM_z equations may be eliminated. This leaves three equations describing the so-called longitudinal motion:

$$\Sigma F_x = m(\dot{U} + WQ) \tag{5}$$

$$\Sigma F_z = m(\dot{W} - UQ) \tag{6}$$

$$\Sigma M_y = \dot{Q}I_y \tag{7}$$

The applied forces and moments acting upon the aircraft will next be considered, and then the equilibrium longitudinal flight conditions will be examined.

2.2 APPLIED FORCES AND MOMENTS

To complete the mathematical representation, it is necessary to expand the applied forces and moments which are of an aerodynamic or gravitational origin. For example, the components of gravity along the X and Z axes are a single function of the angle θ between the X axis and the horizontal,

$$F_x, \text{ gravity} = mg \sin \theta$$
$$F_z, \text{ gravity} = mg \cos \theta \tag{8}$$

For the longitudinal analysis, the forces in the X direction and the Z direction may be considered to be functions of: (a) the coefficient of thrust, C_T; (b) the angle of attack, α; and (c) the controls δt = tail deflection, and δf_3 = flap deflection from 60°. These forces may be expressed as:[1,8]

$$\Sigma F_x = \frac{\rho V_a^2 S}{2}\left[C_{x_o}(C_T,\alpha) + C_{x_{\delta t}}(C_T,\alpha)\delta t + C_{x_{\delta f_3}}(C_T,\alpha)\delta f_3\right] - mg \sin\theta \tag{9}$$

$$\Sigma F_z = \frac{\rho V_a^2 S}{2}\left[C_{z_o}(C_T,\alpha) + C_{z_{\delta t}}(C_T,\alpha)\delta t + C_{z_{\delta f_3}}(C_T,\alpha)\delta f_3\right] + mg \cos\theta \tag{10}$$

where the coefficients C_{x_o}, $C_{x_{\delta t}}$, etc., are determined empirically by wind tunnel testing. (In this testing, thrust variation was studied by blowing compressed air through the engines of the model. The coefficients are tabulated and/or presented graphically in Ref. [1].) The Y-moment equation describing pitching motion is given as

$$\Sigma M_y = \frac{\rho V_a^2 Sc}{2}\left[C_{m_o}(C_T,\alpha) + C_{m_{\delta t}}(C_T,\alpha)\delta t + C_{m_{\delta f_3}}(C_T,\alpha)\delta f_3\right]$$
$$+ \frac{\rho V_a^2 Sc^2}{4}\left[C_{m_q}(C_T,\alpha)Q + C_{m_{\dot\alpha}}(C_T,\alpha)\dot\alpha\right] \tag{11}$$

where the C_m coefficients are obtained from Ref. [1]. The differential equations describing the longitudinal dynamics are then given as

$$\dot{U} = -g \sin\theta - WQ + \frac{\rho V_a^2 S}{2m}\left[C_{x_o} + C_{x_{\delta t}}\delta t + C_{x_{\delta f_3}}\delta f_3\right] \tag{12}$$

$$\dot{W} = g \cos\theta + UQ + \frac{\rho V_a^2 S}{2m}\left[C_{z_o} + C_{z_{\delta t}}\delta t + C_{z_{\delta f_3}}\delta f_3\right] \tag{13}$$

$$\dot{Q} = \frac{\rho V_a^2 Sc}{2I_y}\left[C_{m_o} + C_{m_{\delta t}}\delta t + C_{m_{\delta f_3}}\delta f_3\right] + \frac{\rho V_a^2 Sc^2}{4I_y}\left[C_{m_q} Q + C_{m_{\dot{\alpha}}}\dot{\alpha}\right] \tag{14}$$

The equilibrium flight conditions that satisfy these equations will next be determined.

2.3 EQUILIBRIUM FLIGHT CONDITIONS

For steady flight conditions, the rates of change in the dynamic equations are zero, i.e., U=W=Q=0. For the basic aircraft, we shall consider that the horizontal tail is the only control used to maintain equilibrium flight conditions and that the flap is set at full 60° deflection, i.e., $\delta f_3 = 0$. Therefore, the equilibrium conditions are described by

$$0 = -g \sin\theta + \frac{\rho V_a^2 S}{2m}\left[C_{x_o} + C_{x_{\delta t}}\delta t\right] \tag{15}$$

$$0 = g \cos\theta + \frac{\rho V_a^2 S}{2m}\left[C_{z_o} + C_{z_{\delta t}}\delta t\right] \tag{16}$$

$$0 = \frac{\rho V_a^2 Sc}{2I_y}\left[C_{m_o} + C_{m_{\delta t}}\delta t\right] \tag{17}$$

2.3.1 Steady Level Flight

For straight and level steady flight, the flight path angle γ equals zero. Thus, since γ is defined as

$$\gamma = \theta - \alpha, \tag{18}$$

for level flight we have $\theta = \alpha$. The X force equation is then

$$-g\alpha + \frac{\rho V_a^2 S}{2m} C_{x_o}(C_T,\alpha) + C_{x_{\delta t}} \delta t = 0 \tag{19}$$

For straight and level flight prior to initiating the glide slope, $V_a = 75$ knots and Thrust = 23,000 lbs. This yields a coefficient of thrust

$$C_T = \frac{T}{\frac{\rho V_a^2 S}{2}} = 1.71 \tag{20}$$

In solving for α, $C_{x_o}(C_T = 1.71, \alpha)$ is approximated as

$$C_{x_o}(C_T = 1.71,\alpha) = C_{x_o}(C_T=1.71, \alpha=0) + \left(\frac{\partial C_{x_o}}{\partial \alpha}\right)(C_T=1.71,\alpha=0) \tag{21}$$

where from curves of C_{x_o}, we obtain*

$$C_{x_o}(C_T = 1.7.,\alpha=0) \simeq (-.25)\,\bar{C}_{x_\alpha}(C_T = 1.71,\alpha=0) \simeq 0.0 \tag{22}$$

For α within a region near zero, $C_{x_{\delta t}}$ may also be neglected.

---

*The notation $\bar{C}_{x_\alpha} \equiv \frac{\partial C_{x_o}}{\partial \alpha}$ is used.

Hence

$$\alpha_o = \frac{\rho V_a^2 S}{2mg} C_{x_o}(C_T = 1.71, \alpha=0) \tag{23}$$

or

$$\alpha_o = (.284)(-.25) = -.071 \text{ rad} = -4.1 \text{ deg} = \theta_o \tag{24}$$

To maintain constant pitch, it is necessary to introduce a constant longitudinal trim δt. This is calculated using the equilibrium Y-moment equation,

$$0 = \frac{\rho V_a^2 Sc}{2I_y}\left[C_{m_o}(C_T,\alpha) + C_{m_{\delta t}}(C_T,\alpha)\delta t\right] \tag{25}$$

This requires

$$C_{m_o}(C_T = 1.71,\ \alpha_o = -4.1°) = C_{m_{\delta t}}(C_T = 1.71,\ \alpha = -4.1°)\delta t \tag{26}$$

or

$$\delta t = \frac{0.15}{-0.086} = -1.75 \text{ deg}$$

Hence, for straight and level flight at V_a = 75 kts, T = 23,000, the aircraft is pitched down at -4.1° and the horizontal tail has a trim value of -1.75°.

2.3.2 Steady Flight Down Glideslope

On the glideslope, the velocity is held at 75 knots and the glideslope and flight path angle are -6°. The relationship between flight path angle and angle-of-attack is given by Eq. (18). Thus, $\theta = \alpha - .105$. The X-force equation is then given as

$$0 = -g(\alpha - 0.105) + \frac{\rho V_a^2}{2m}\left[C_{x_o}(C_T,\alpha) + C_{x_{\delta t}}(C_T,\alpha)\ \delta t\right] \tag{27}$$

again neglecting $C_{x_\alpha}(C_T, \alpha=0)$ and $C_{x_{\delta t}}(C_T, \alpha=0)$,

$$\alpha = .105 + \frac{\rho V_a^2}{2mg} C_{x_o}(C_T, \alpha=0) \tag{28}$$

Now noting for a range of C_T about 1.0 that $C_{x_o}(C_T, \alpha=0)$ is approximately constant at -.25 yields

$$\alpha_o = 0.034 \text{ rad} = 1.94° \tag{29}$$

and

$$\theta_o = -4.1°$$

The vertical equation in equilibrium is given as

$$0 = g \cos \theta + \frac{\rho V_a^2}{2m} \left[C_{z_o}(C_T, \alpha_o) + C_{z_{\delta t}}(C_T, \alpha_o) \delta t \right] \tag{30}$$

Neglecting the contribution of the tail yields

$$C_{z_o}(C_T, \alpha_o) = -4.1° \tag{31}$$

This condition for C_{z_o} is satisfied at $C_{T_o} \cong 1.32$ or $T = 17,500$. From the pitch equation, the longitudinal trim is given by

$$-C_{m_o}(C_{T_o}, \alpha_o) = C_{m_{\delta t}}(C_{T_o}, \alpha_o) \delta t$$

yielding

$$\delta t = \frac{-.08}{+.08} = -1° \tag{32}$$

These equilibrium points analytically determined agree very closely to those obtained via NASA simulation of the nonlinear equations and relationships.[9]

2.3.3 Steady Pitched-Up Flight Down Glideslope

In NASA simulations,[1] subject pilots objected to the nose-down attitude because of the relatively large change in pitch attitude required prior to landing. In order to fly the plane in a pitched-up attitude, less than 60° of flap deflection must be used. An equilibrium pitched-up condition with a δf_3 input is now calculated.

In the approach condition, the thrust is set at 13,200 lbs and the desired attitude is 2° pitched up. Since the aircraft is approaching on a 6° glideslope, the angle-of-attack is therefore 8°. For equilibrium flight, the X force equation satisfies the relationship

$$0 = -\sin\theta + \frac{\rho V_a^2 S}{2mg}\left[C_{x_o} + C_{x_{\delta t}}\delta t + C_{x_{\delta f_3}}\delta f_3\right] \tag{33}$$

Using coefficients from NASA data, this equation becomes

$$.0048\delta t + .016\ \delta f_3 = -.224\ .$$

The moment equation must satisfy

$$0 = \frac{\rho V_a^2 Sc}{2Iy}\left[C_{m_o} + C_{m_{\delta t}}\delta t + C_{m_{\delta f_3}}\delta f_3\right] \tag{34}$$

or

$$-.093\ \delta t + .0025\ \delta f_3 = .3\ .$$

Solution of these simultaneous equations yields $\delta f_3 = -13.1°$ and $\delta t = -3.5°$.

2.4 LINEAR MODEL DEVELOPMENT

Since the general nonlinear longitudinal equations are not amenable to analytic study, linear models of the aircraft are now developed. In the analysis to follow, the aircraft is always considered to be in equilibrium flight before a disturbance is introduced. The linearized model of the aircraft then describes the dynamic behavior of the aircraft about the equilibrium operating point.

2.4.1 Linear Equations of Motion

Previously, the components of the total instantaneous values of the linear and angular velocity resolved into the aircraft axes were designated as U, V, W, P, Q and R. Since these values include an equilibrium value and the change from the steady state, they may be expressed as

$$\left.\begin{aligned} U &= U_o + u \\ W &= W_o + w \\ Q &= Q_o + q \end{aligned}\right\} \qquad (35)$$

where U_o, W_o, etc., are the equilibrium values and u, w, etc., are the changes in these values resulting from some disturbance.

Similarly, the external forces and moments are written as the sum of equilibrium components and deviation from equilibrium, e.g.,

$$\Sigma F_x = \Sigma F_{x_o} + \Sigma \Delta F_x .$$

For the development of the linear model, a body axes system known as the "stability axes system" is introduced. This system is widely utilized in aircraft analysis and introduces several simplifications. For example, the OX axis could be aligned with the longitudinal axis of the aircraft; however, if it is originally aligned with the equilibrium direction of the velocity vector

of the aircraft, then $W_o = 0$. This is illustrated in Figure 1. In Figure 1 the axes X_e, Y_e, Z_e are earth reference axes; the X_o, Y_o, Z_o, are equilibrium aircraft axes. For any particular problem the aircraft axes, after being aligned with the X axis into the relative wind, remain fixed to the aircraft during the study of perturbations from that initial flight condition. Such a set of aircraft axes are referred to as "stability axes". The stability axes will be used in all the dynamic analysis to follow. As can be seen from Figure 1, Θ_o and γ_o are measured from the horizontal to the stability X_o axis. The angle γ is often referred to as the "flight path angle" and is defined as the angle measured, in the vertical plane, between the horizontal and the velocity vector of the aircraft. By using stability axes, Θ_o and γ_o are equal. The definition of attack is standard, that is, the angle between the velocity vector (or the relative wind) and the wind chord. As the change in Θ, which is equal to θ, is caused by a rotation about the Y axis then $q = \dot{\theta}$. Under these conditions $U = U_o + u$, $W = w$. and, as U_o is constant, $\dot{U} = \dot{u}$ and $\dot{W} = \dot{w}$. As the aircraft is initially in unaccelerated flight, Q_o must be zero, thus $Q = q$. Making these substitutions, the force equations (5) and (6) become

$$\Sigma\Delta F_x = m(\dot{u} + wq) \tag{36}$$

$$\Sigma\Delta F_z = m(\dot{w} - U_o q - uq) \tag{37}$$

By restricting the disturbances to small perturbations about the equilibrium condition, the product of the variations will be small in comparison with the variations and can be neglected, and the small angle assumptions can be made relative to the angles between the equilibrium and disturbed axes. This last assumption somewhat limits the applicability of the equations, but reduces them to linear equations. Thus, Eqs. (36) and (37) may be written as follows with the addition of the pitching moment equation

$$\Sigma\Delta F_x = m\dot{u} \tag{38}$$

$$\Sigma\Delta F_z = m(\dot{w} - U_o q) \tag{39}$$

$$\Sigma\Delta M_y = I_y \dot{q} \tag{40}$$

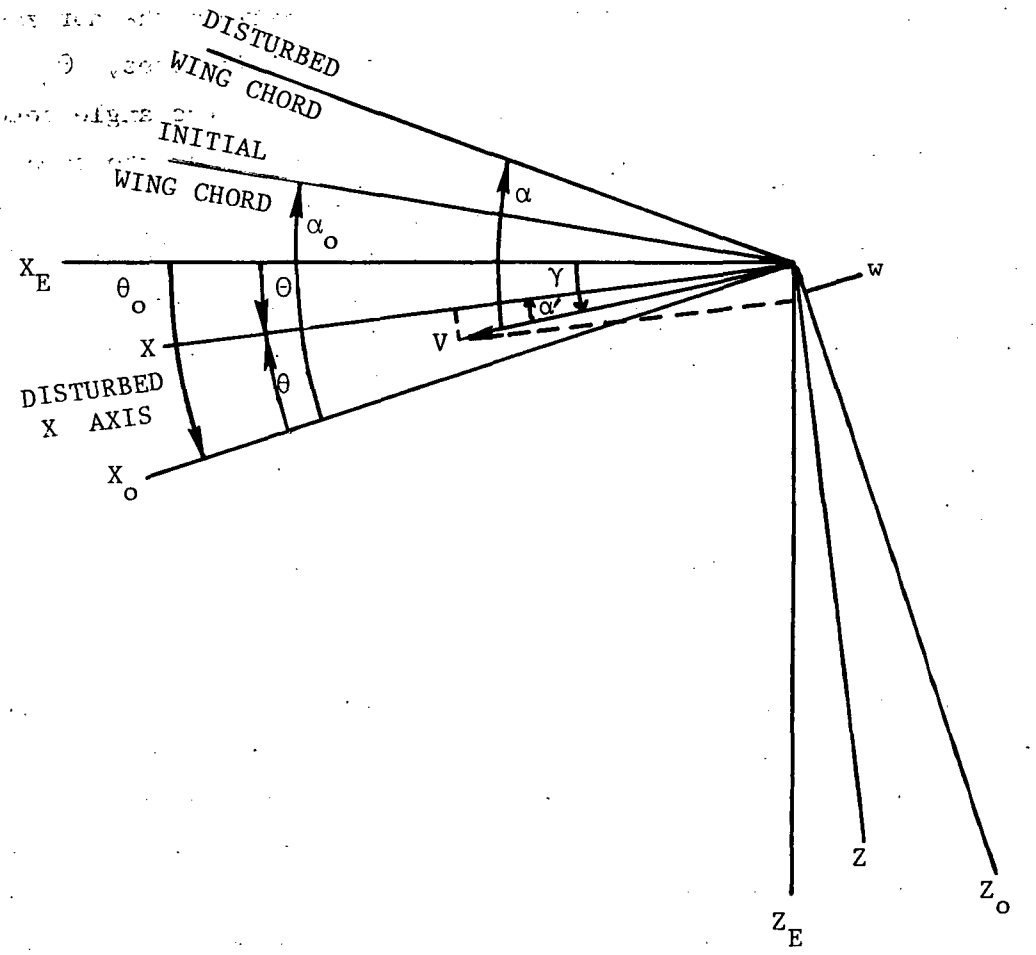

FIGURE 1 STABILITY AXIS SYSTEM

It is now necessary to include the applied forces and moments in the linearized framework. From Eq. (9), the force in the X direction is given as

$$\frac{1}{m}\left(\Sigma F_{x_o} + \Sigma \Delta F_x\right) = -g \sin \Theta + \frac{\rho V_a^2 S}{2m}\left[C_{x_o}(C_T,\alpha) + C_{x_{\delta t}}(C_T,\alpha)\delta t + C_{x_{\delta f_3}}(C_T,\alpha)\delta f_3\right] \tag{41}$$

Thus, the force in the X direction may be considered to be a function of α (angle-of-attack), T (thrust), and Θ. Linearization about the equilibrium operating point yields

$$\begin{aligned}\frac{1}{m}\left(\Sigma F_{x_o} + \Sigma \Delta F_x\right) = -g \sin \Theta_o - (g \cos \Theta_o) + \frac{\rho V_a^2 S}{2m}\Bigg\{ & \bar{C}_{x_o}(C_{T_o},\alpha_o) \\ & + (2/V_a)\bar{C}_{x_o} u + \bar{C}_{x_\alpha}\alpha + \bar{C}_{x_{\delta T}}\delta T + \Big[\bar{C}_{x_{\delta t}}(C_{T_o},\alpha_o) + \bar{C}_{x_{\delta t_\alpha}}\alpha \\ & + \bar{C}_{x_{\delta t_{\delta T}}}\delta T\Big](\delta t_o + \delta t) + \Big[\bar{C}_{x_{\delta f_3}}(C_{T_o},\alpha_o) + \bar{C}_{x_{\delta f_{3_\alpha}}}\alpha \\ & + \bar{C}_{x_{\delta t_{\delta T}}}\delta T\Big](\delta f_e)\Bigg\}\end{aligned} \tag{42}$$

where

$$\bar{C}_{x_\alpha} \triangleq \left(\frac{\partial C_{x_o}}{\partial \alpha}\right)(C_{T_o},\alpha_o) \tag{43}$$

$$\bar{C}_{x_{\delta t_\alpha}} \triangleq \left(\frac{\partial C_{x_t}}{\partial \alpha}\right)(C_{T_o},\alpha_o), \quad \text{etc.} \tag{44}$$

Then since the equilibrium condition is

$$\frac{1}{m}\Sigma F_{x_o} = -g \sin \Theta_o + \frac{\rho V_a^2}{2m} C_{x_o}(C_{T_o}, \alpha_o) = 0 \tag{45}$$

and neglecting second order terms, the force in the X direction is

$$\frac{1}{m}\Sigma \Delta F_x = -(g \cos \Theta_o) + \frac{\rho V_a^2 S}{2m}\left\{\bar{C}_{x_\alpha}\alpha + \bar{C}_{x_{\delta t}}\delta T + C_{x_{\delta t}}\delta t + \bar{C}_{x_{\delta f_3}}\delta f_3\right\}$$

$$+ (\rho V_a S/m)\,\bar{C}_{x_o} u \tag{46}$$

where $\bar{C}_{x_{\delta t}} = C_{x_{\delta t}}(C_{T_o}, \alpha_o)$, etc.

The differential equation describing velocity variation in the X direction is therefore given as

$$\dot{u} + (g \cos \Theta_o)\theta - \frac{\rho V_a^2 S}{2m} C_{x_\alpha}\alpha = \frac{\rho V_a^2 S}{2m}\left[\bar{C}_{x_{\delta T}}\delta T + \bar{C}_{x_{\delta t}}\delta t + \bar{C}_{x_{\delta f_3}}\delta f_3\right]$$

$$+ (\rho V_a S/m)\,\bar{C}_{x_o} u \tag{47}$$

Similarly, the linear differential equations describing the variations in the Z direction and the pitching motion may be derived as

$$U_o\dot{\alpha} - U_o q + (g \sin \Theta_o)\theta - \frac{\rho V_a^2 S}{2m}\left[C_{z_\alpha}\alpha\right] = \frac{\rho V_a^2 S}{2m}\left[\bar{C}_{z_{\delta T}}\delta T + \bar{C}_{z_{\delta t}}\delta t + C_{z_{\delta f_3}}\delta f_3\right]$$

$$+ (\rho V_a S/m)\,\bar{C}_{z_o} u \tag{48}$$

and

$$\dot{q} - \frac{\rho V_a Sc^2}{4Iy} \bar{C}_{m_q} q - \frac{\rho V_a Sc^2}{4I_y} \bar{C}_{m_{\dot{\alpha}}} \dot{\alpha} - \frac{\rho V_a^2 Sc}{2I_y} C_{m_\alpha} \alpha = \frac{\rho V_a^2 Sc}{2I_y} \left[\bar{C}_{m_{\delta T}} \delta T + C_{m_{\delta t}} \delta t + C_{m_{\delta f_3}} \delta f_3 \right] \tag{49}$$

It should be noted that the coefficients $\bar{C}_{x_\alpha}$, $\bar{C}_{x_{\delta t}}$, $\bar{C}_{z_\alpha}$, $\bar{C}_{z_{\delta T}}$, $\bar{C}_{m_\alpha}$, and $\bar{C}_{m_{\delta t}}$, are obtained from slope measurements of curves of C_x, etc. Also note that

$$\bar{C}_{m_q} = C_{m_q}(C_{T_o}, \alpha_o)$$

$$\bar{C}_{m_\alpha} = C_{m_\alpha}(C_{T_o}, \alpha_o)$$

2.4.2 Short-Period Mode Approximation and Model Validation

1. Short-Period Mode Analysis: The characteristic modes for nearly all aircraft in most flight conditions have two oscillations: one of short period with relatively heavy damping, the other of long period with very light damping. The "short-period mode" consists primarily of variations in α and θ with very little change in the forward velocity. Therefore, to approximate the short-period mode, let $u = 0$ in the equations of motion and also, since forces in the X direction contribute mostly to changes in forward speed, the X equation is neglected. The equation may then be put into the following form (using Laplace variables for this segment of the analysis)

$$\left(\frac{mU}{S\bar{q}} s - \bar{C}_{z_\alpha} \right) \alpha(s) + \left[-\frac{mU}{S\bar{q}} s + \frac{mg}{S\bar{q}} \sin \Theta_o \right] \theta(s) = \bar{C}_{z_{\delta T}} \delta T + \bar{C}_{z_{\delta t}} \delta t + \bar{C}_{z_{\delta f_3}} \delta f_3 \tag{50}$$

$$- \frac{c}{2U} \bar{C}_{m_{\dot{\alpha}}} s - \bar{C}_{m_\alpha} \quad \alpha(s) + \frac{I_y}{S\bar{q}c} s^2 - \frac{c}{2U} \bar{C}_{m_q} s \quad \theta(s) = \bar{C}_{m_{\delta T}} \delta T + \bar{C}_{m_{\delta t}} \delta t$$

$$+ \bar{C}_{m_{\delta f_3}} \delta f_3 \tag{51}$$

where $\bar{q} = \frac{\rho V_a^2}{2}$. Letting $\Theta_o = 0$, the determinant of the homogeneous equation may be put into the form

$$s(D_2 s^2 + D_1 s + D_o) = 0 \tag{52}$$

where

$$D_2 = \left(\frac{I_y}{S\bar{q}c}\right)\left(\frac{mU}{S\bar{q}}\right)$$

$$D_1 = \left(\frac{-c}{2U} C_{m_q}\right)\left(\frac{mU}{S\bar{q}}\right) - \frac{I_y}{S\bar{q}c} C_{z_\alpha} - \left(\frac{c}{2U} C_{m_{\dot{\alpha}}}\right)\left(\frac{mU}{S\bar{q}}\right) \tag{53}$$

$$D_o = \frac{c}{2U} C_{m_q} C_{z_\alpha} - \frac{mU}{S\bar{q}} C_{m_\alpha}$$

Dividing Eq. (52) by D_2 and writing in the standard quadratic form with ζ and ω_n, then

$$2\zeta\omega_n = \frac{D_1}{D_2} \quad \text{and} \quad \omega_n^2 = \frac{D_o}{D_2} \tag{54}$$

Explicitly we obtain

$$\omega_n = \frac{U\rho Sc}{2}\left(\frac{\frac{C_{m_q} C_{z_\alpha}}{2} - \frac{2m}{Sc} C_{m_\alpha}}{I_y m}\right)^{\frac{1}{2}} \tag{55}$$

and

$$\zeta \approx -\frac{1}{4}\left(C_{m_q} + C_{m_{\dot{\alpha}}} + \frac{2I_y}{mc^2} C_{z_\alpha}\right)\left[\frac{mc^2}{I_y\left(\frac{C_{m_q} C_{z_\alpha}}{2} - \frac{2mC_{m_\alpha}}{\rho Sc}\right)}\right] \tag{56}$$

2. Linearized Model Validation: The STOL transport aircraft has been simulated at NASA-Langley Research Center using the general nonlinear equations with the aerodynamic coefficients obtained via table look-up. The short-period dynamic response characteristics of the aircraft have been determined empirically by measuring the response of the simulated aircraft to simple inputs. Results for the basic aircraft at 75 knots and $T = 23{,}000$ are,

$$\omega_n = 1.41 \qquad \zeta = 0.71 \ .$$

These numbers provide an opportunity to evaluate the linear model developed herein by calculating ω_n and ζ using the derived short-period expressions.

From the aerodynamic data, we obtain

$$\bar{C}_{m_q} = C_{m_q}(C_{T_o}, \alpha_o) = -27.00$$

$$\bar{C}_{z_\alpha} = \left(\frac{\partial C_z}{\partial \alpha}\right)(C_{T_o}, \alpha_o) = -7.45$$

$$\bar{C}_{m_\alpha} = \left(\frac{\partial C_m}{\partial \alpha}\right)(C_{T_o}, \alpha_o) = -2.1$$

$$\bar{C}_{m_{\dot{\alpha}}} = C_{m_{\dot{\alpha}}}(C_{T_o}, \alpha_o) = -11.0$$

Substituting these values into Eqs. (55) and (56) yields

$$\omega_n = 1.44 \qquad \zeta = 0.66$$

These results agree very well with those values obtained experimentally with the nonlinear simulation and lend credence to the linearized model.

2.4.3 Development of State Space STOL Models

The linearized differential equation describing velocity variation in the X direction given in Eq. (47) may be rewritten as

$$\dot{u}' = (2\bar{q}S\bar{C}_{x_o}/mV_a)u' + (\bar{q}S/mVa)\alpha' - (g \cos \theta_o/V_a)$$

$$+ (\bar{q}S/mV_a)\left[\bar{C}_{x_{\delta T}}\delta T + \bar{C}_{x_{\delta t}}\delta t + \bar{C}_{x_{\delta f_3}}\delta f_3\right] \tag{57}$$

the equation describing variation in angle-of-attack as

$$\dot{\alpha}' = (2\bar{q}S/mV_a)\,\bar{C}_{z_o}u' + (\bar{q}S/mV_a)C_{z_\alpha}\alpha' + q - (g \sin \theta_o/V_a)\theta$$

$$+ (\bar{q}S/mV_a)\left[\bar{C}_{z_{\delta T}}\delta T + \bar{C}_{z_{\delta t}}\delta t + \bar{C}_{z_{\delta f_3}}\delta f_3\right] \tag{58}$$

and the pitching moment equation as

$$\dot{q} + (\bar{q}Sc/I_y)\bar{C}_{m_\alpha}\alpha' + (\rho V_a Sc^2/4I_y)\bar{C}_{m_{\dot{\alpha}'}}\dot{\alpha}' + (\rho V_a Sc^2/4I_y)\bar{C}_{m_q}q$$

$$= (\bar{q}Sc/I_y)\left[\bar{C}_{m_{\delta T}}\delta T + \bar{C}_{m_{\delta t}}\delta t + \bar{C}_{m_{\delta f_3}}\delta f_3\right] \tag{59}$$

where we have introduced the variables

$$u' = u/V_a \qquad \alpha' = w/V_a \qquad \bar{q} = (\rho V_a^2/2).$$

Substituting the expression for $\dot{\alpha}'$ given by Eq. (48) into Eq. (59) yields

$$\dot{q} = (\rho V_a Sc^2/4I_y)(2\bar{q}S/mV_a)\bar{C}_{z_o} u' + \left\{(\bar{q}Sc/I_y)\bar{C}_{m_\alpha} + (\rho V_a Sc^2/4I_y)(\bar{q}S/mV_a)\bar{C}_{m_{\dot{\alpha}}} C_{z_\alpha}\right\}\alpha + \left\{(\rho V_a Sc^2/4I_y)\bar{C}_{m_q} + (\rho V_a Sc^2/4I_y)\bar{C}_{m_{\dot{\alpha}}}\right\} q - \left\{(\rho V_a Sc^2/4I_y)(g \sin\theta_o/V_a)C_{m_{\dot{\alpha}}}\right\}\theta + (\bar{q}Sc/I_y)\left[\bar{C}_{m_{\delta T}}\delta T + \bar{C}_{m_{\delta t}}\delta t + \bar{C}_{m_{\delta f_3}}\delta f_3\right] + (\rho V_a Sc^2/4I_y)(\bar{q}S/mV_a)C_{m_{\dot{\alpha}}}\left[\bar{C}_{z_{\delta T}}\delta T + \bar{C}_{z_{\delta t}}\delta t + C_{z_{\delta f_3}}\delta f_3\right] \tag{60}$$

Now defining a state vector $\underline{x} = \text{col}[u', \alpha', q, \theta]$ and a control vector $\underline{u} = \text{col}[\delta T, \delta t, \delta f_3]$. Equations (57), (58) and (60) may be put into the vector matrix form

$$\dot{\underline{x}}(t) = \underline{A}\,\underline{x}(t) + \underline{B}\,\underline{u}(t) \tag{61}$$

where the matrix elements $a(i,j)$, $b(i,j)$ are

$$a(1,1) = (2\bar{q}SC_{x_o}/mV_a)$$

$$a(1,2) = (\bar{q}S/mV_a)$$

$$a(1,3) = 0.0$$

$$a(1,4) = -(g \cos\theta_o/V_a)$$

$$a(2,1) = (2\bar{q}S/mV_a)$$

$$a(2,2) = (\bar{q}S/mV_a)\bar{C}_{z_\alpha}$$

$$a(2,3) = 1.0$$

$$a(2,4) = -(g \sin \theta_o / V_a)$$

$$a(3,1) = (\rho V_a Sc^2/4I_y)(2\bar{q}S/mV_a)\bar{C}_{z_o}$$

$$a(3,2) = (\bar{q}Sc/I_y)\bar{C}_{m_\alpha} + (\rho V_a Sc^2/4I_y)(\bar{q}S/mV_a)\bar{C}_{m_\alpha}\bar{C}_{z_\alpha}$$

$$a(3,3) = (\rho V_a Sc^2/4I_y)\bar{C}_{m_q} + (\rho V_a Sc^2/4I_y)\bar{C}_{m_{\dot{\alpha}}}$$

$$a(3,4) = -(\rho V_a Sc^2/4I_y)(g \sin \theta_o / V_a)\bar{C}_{m_{\dot{\alpha}}}$$

$$a(4,1) = 0.0$$

$$a(4,2) = 0.0$$

$$a(4,3) = 1.0$$

$$a(4,4) = 0.0$$

$$b(1,1) = (\bar{q}S/mV_a)\bar{C}_{x_{\delta T}}, \text{ etc.}$$

The remaining elements of the $\underline{B}$ matrix are readily obtained from Equations (57) - (60). To obtain models for various conditions, the aerodynamic coefficients are simply evaluated for the particular flight condition of interest. Stability derivatives such as $\bar{C}_{m_\alpha}$ are calculated from slope measurement.

To investigate approach and landing, it is necessary to include altitude variations within the model. Since the linear model describes variations about an equilibrium flight condition coming down the glideslope, the altitude

perturbation equation will describe altitude variations off the glideslope at a particular instant. Specifically, the sink rate is given as

$$\dot{h} = V \sin \gamma \tag{62}$$

and from the definition of the stability axis system,

$$\dot{h} = V \sin (\Theta_o + \theta - \alpha') \tag{63}$$

Assuming small angles, the linear perturbation equation for vertical distance off the glideslope is given as

$$\delta\dot{h} = -V\alpha' + V\theta + u\Theta_o \tag{64}$$

or dividing by V,

$$\delta\dot{h}' = -\alpha' + \theta + u'\Theta_o \ . \tag{65}$$

One additional variable must be included to model the fact that changes in throttle do not lead to instantaneous changes in thrust. The dynamics of the engines are modeled as a first order lag in our linearized dynamic model of the STOL. Specifically,

$$\dot{\delta T} = a_T \delta T + a_T \delta T_c \tag{66}$$

where δT_c is the throttle commanded change in thrust level. Curves of δT response to step changes in the δT_c are given in Ref. [1]. From this data an approximate thrust time constant $a_T^{-1} = .5$ sec was selected.

2.4.4 Wind Gusts and Ground Effect Disturbances

Wind Gusts: The STOL aircraft is subject to vertical random turbulence during the approach phase. This is modeled by passing Gaussian white noise through a first order shaping filter, i.e.,

$$\dot{w}_g = -\left(\frac{V_o}{L_w}\right) w_g + \sigma_w \sqrt{\frac{2V_o}{L_w}}\, n(t) \tag{67}$$

or,

$$\dot{\alpha}'_g = -\left(\frac{V_o}{L_w}\right) \alpha'_g + \left(\frac{\sigma_w}{V_o}\right)\sqrt{\frac{2V_o}{L_w}}\, n(t) \tag{68}$$

where w_g is vertical wind gust velocity, α'_g is the increment in angle-of-attack created by the wind gust and where $E\{n(t)n(\tau)\} = \delta(t-\tau)$. L_w is taken to be a nominal value of 500 and σ_w is 2, 4, and 6 for light, moderate, and heavy turbulence, respectively. (These numbers are chosen to correspond with NASA simulation parameters and, as in the simulation, the vertical gusts are reduced to zero between 100 and 50 feet altitude.) In studying the flare and landing portion of the flight, the turbulence may be neglected, since flare begins at $h_{\ell g} \simeq 41$ ft. ($h_{cg} \simeq 53$ ft.).*

Ground Effect: As the externally blown flap STOL approaches the ground, adverse ground effects arise. Specifically, a nose down pitching moment, a loss in lift, and a decrease in drag are created. The effects of ground proximity on C_o and C_m begin at an altitude of approximately 60 ft and increase in severity, almost linearly with (60 - h), to touchdown. The effects of ground proximity on C_L begins at a lower altitude and increases rapidly in an almost linear manner. The incremental changes in pitching moment, lift, and drag coefficients due to ground effect are presented in Figure 2.

The dynamic changes in the aircraft states due to the ground effect input may be expressed as

*The turbulence, by acting during approach, does effect the initial conditions at the flare altitude. This indirect influence of the turbulence is considered setting up conditions at flare initiation.

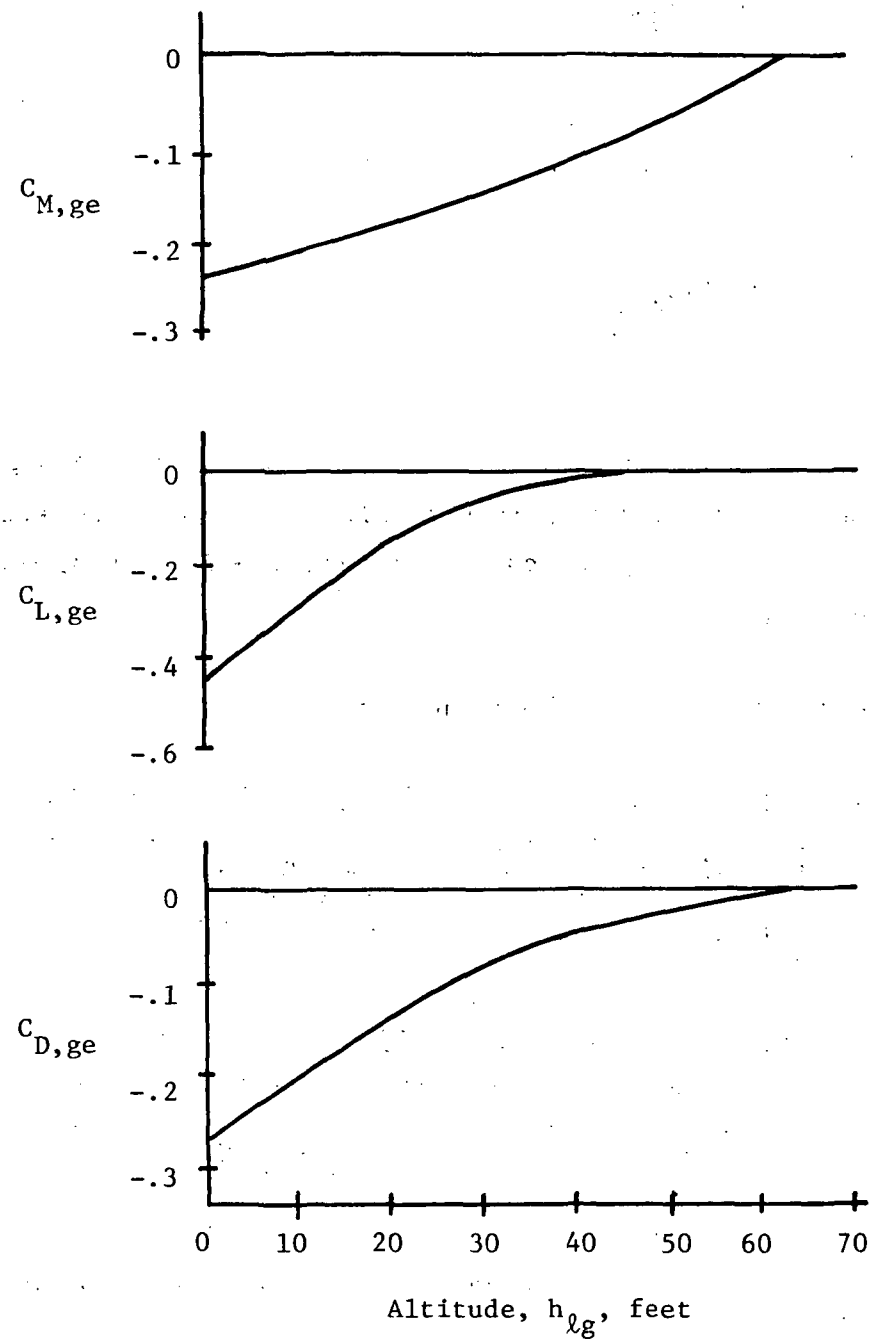

FIGURE 2 CHANGES IN AIRCRAFT COEFFICIENTS DUE TO GROUND EFFECT

$$\begin{bmatrix} \dot{u}' \\ \dot{\alpha}' \\ \dot{q} \end{bmatrix}_{ge} = \begin{bmatrix} \frac{\bar{q}S}{mV_o} C_D(h(t))_{ge} \\ \frac{\bar{q}S}{mV_o} C_L(h(t))_{ge} \\ \frac{\bar{q}Sc}{I_y} C_M(h(t))_{ge} \end{bmatrix} \tag{69}$$

However, assuming a nominal value for $C_D(h) = -0.15$ and a nominal flare time ($\simeq$5 sec.), the change in airspeed due to ground effect is a small increase of approximately two and a half feet per second. This small effect is neglected in the subsequent modeling.

The lift and moment coefficients may be approximated as

$$C_L(h(t)) = \begin{cases} 0.0 & 4.1 < h \\ (.0045)(h(t) - 41.) & 28. \leq h \leq 41. \\ (.014)(h(t) - 32.) & 0 \leq h \leq 28. \end{cases} \tag{70}$$

$$C_M(h(t)) = \begin{cases} 0.0 & 60. < h \\ \\ (.004)(h(t) - 60.) & 0 \leq h \leq 60. \end{cases} \tag{71}$$

To include the ground effect within the dynamic model, two states are defined as

$$\begin{aligned} x_1(t) &= C_L(t) && 0 \leq h \leq 41. \\ x_2(t) &= C_M(t) && 0 \leq h \leq 60. \end{aligned} \tag{72}$$

Thus, the perturbations due to the ground effect may be expressed as

$$\begin{bmatrix} \dot{\alpha}' \\ \\ \dot{q} \end{bmatrix}_{ge} = \begin{bmatrix} \frac{\bar{q}S}{mV_o} & x_1 \\ \\ \frac{\bar{q}Sc}{I_y} & x_2 \end{bmatrix} \qquad \begin{matrix} 0 \leq h \leq 41. \\ \\ 0 \leq h \leq 60. \end{matrix} \tag{73}$$

and the variations in x_1 and x_2 given as

$$\begin{bmatrix} \dot{x}_1 \\ \\ \dot{x}_2 \end{bmatrix} = \begin{bmatrix} m(t)\dot{h}(t) \\ \\ .004\ \dot{h}(t) \end{bmatrix} \qquad \begin{matrix} 0 \leq h \leq 41. \\ \\ 0 \leq h \leq 60. \end{matrix} \tag{74}$$

where $m(t) = .0045$ for $28 < h < 41$, $.014$ for $0 < h < 28$. The total sink rate is

$$\dot{h}(t) = V_o\gamma_o + V_o(-\alpha' + \theta + u'\Theta_o) \tag{75}$$

Equation (74) may be most conveniently modeled as a deterministic time varying input given as

$$\begin{bmatrix} \dot{x}_1(t) \\ \\ \dot{x}_2(t) \end{bmatrix} = \begin{bmatrix} \dot{z}_1(\alpha'(t),\ \theta(t),\ u'(t)) \\ \\ \dot{z}_2(\alpha'(t),\ \theta(t),\ u'(t)) \end{bmatrix} = \begin{bmatrix} \dot{z}_1(t) \\ \\ \dot{z}_2(t) \end{bmatrix} \tag{76}$$

Equations (76) and (74) may then be used to include ground effects as an external input disturbance in the STOL model.

2.4.5 Dynamical Models of the STOL

Basic Aircraft: An overall dynamic model of the basic STOL aircraft during flare may be obtained by combining the equations describing the aircraft, and the ground effects. This model is given as

$$\dot{\underline{x}} = \underline{A}\,\underline{x} + \underline{B}\,\underline{u} + \underline{F}\,\dot{\underline{z}}(t) \tag{77}$$

where $\underline{x} = \text{col}[C_L, C_M, u', \alpha', q, \theta, \delta h', \delta T]$, $\underline{u} = \text{col}[\delta T_c, \delta t]$

$$\underline{A} = \begin{bmatrix} 0 & 0 & 0 & 0 & 0 & 0 & 0 & 0 \\ 0 & 0 & 0 & 0 & 0 & 0 & 0 & 0 \\ 0 & 0 & a_{11} & a_{12} & 0 & a_{14} & 0 & b_{11} \\ a_{gL} & 0 & a_{21} & a_{22} & 1 & a_{24} & 0 & b_{21} \\ 0 & a_{gp} & a_{31} & a_{32} & a_{33} & a_{34} & 0 & b_{31} \\ 0 & 0 & 0 & 0 & 1 & 0 & 0 & 0 \\ 0 & 0 & 0 & -1 & 0 & 1 & 0 & 0 \\ 0 & 0 & 0 & 0 & 0 & 0 & 0 & -a_T \end{bmatrix} \qquad \underline{B} = \begin{bmatrix} 0 & 0 \\ 0 & 0 \\ 0 & b_{12} \\ 0 & b_{22} \\ 0 & b_{32} \\ 0 & 0 \\ 0 & 0 \\ a_T & 0 \end{bmatrix}$$

and

$$\underline{F}' = \begin{bmatrix} 1 & 0 & 0 & 0 & 0 & 0 & 0 & 0 \\ 0 & 1 & 0 & 0 & 0 & 0 & 0 & 0 \end{bmatrix} \tag{78}$$

where

$$a_{gL} = \left(\frac{\bar{q}S}{mV_o}\right)$$

$$a_{gp} = \left(\frac{\bar{q}Sc}{I_y}\right) \tag{79}$$

$$z_1(t) = .0045[-V_o\gamma_o + V_o(-\alpha' + \theta + u'\Theta_o)] \quad 28 \leq h \leq 41.$$

$$z_1(t) = .014[-V_o\gamma_o + V_o(-\alpha' + \theta + u'\Theta_o)] \quad 0 \leq h \leq 28.$$

$$z_2(t) = .004[-V_o\gamma_o + V_o(-\alpha' + \theta + u'\Theta_o)] \quad 0 \leq h \leq 60.$$

The coefficients are evaluated for the aircraft in the basic pitched-down equilibrium condition.

Autospeed: Through simulation experiments, the basic STOL aircraft represented by Eq. (78) was found to possess several major longitudinal deficiencies:

- sluggish initial pitch response;
- low apparent pitch damping;
- large pitch excursions associated with changes in thrust, flaps, and spoilers; and
- a phugoid with an unusually short period.

Due to these characteristics, there is poor pilot control of pitch attitude and, hence, poor control of airspeed. As a result of these difficulties, several augmentation schemes have been developed to improve the stability and control characteristics of the aircraft.

The first augmentation system to be considered was an autospeed system that maintained the desired airspeed by driving the third segment flap. To neutralize the lift increment resulting from flap deflection, an interconnect to the symmetric spoilers was provided, thus effectively decoupling the forward and vertical modes. The autospeed system accomplished three objectives: (1) it eliminated the phugoid mode which was the source of much of the basic longitudinal handling difficulties, (2) it provided good speed control, and (3) it relieved the pilot of the speed control task and, hence, considerably reduced pilot workload. In addition, since the autospeed system moves the flaps to maintain speed, the pilot is able to trim the STOL in a nose-up attitude (as described in Section 2.3.3). It should be noted, however, that the pilot must still control pitch.

A dynamic model describing the state variables of the STOL aircraft with autospeed is developed by removing forward velocity variation from the model

presented by (78). This is a justifiable modeling approach because of the decoupling nature of the autospeed system. This model is given in the form of Eq. (77) with $\underline{x} = \text{col}[C_L, C_M, \alpha', q, \theta, \delta h', \delta T]$

$$\underline{A} = \begin{bmatrix} 0 & 0 & 0 & 0 & 0 & 0 & 0 \\ 0 & 0 & 0 & 0 & 0 & 0 & 0 \\ a_{gL} & 0 & a_{22} & 1 & a_{24} & 0 & b_{21} \\ 0 & a_{gp} & a_{32} & a_{33} & a_{34} & 0 & b_{31} \\ 0 & 0 & 0 & 1 & 0 & 0 & 0 \\ 0 & 0 & -1 & 0 & 1 & 0 & 0 \\ 0 & 0 & 0 & 0 & 0 & 0 & -a_T \end{bmatrix} \quad \underline{B} = \begin{bmatrix} 0 & 0 \\ 0 & 0 \\ 0 & b_{22} \\ 0 & b_{32} \\ 0 & 0 \\ 0 & 0 \\ a_T & 0 \end{bmatrix} \quad \underline{F} = \begin{bmatrix} 1 & 0 \\ 0 & 1 \\ 0 & 0 \\ 0 & 0 \\ 0 & 0 \\ 0 & 0 \\ 0 & 0 \end{bmatrix} \tag{80}$$

where the coefficients are evaluated for the pitched up equilibrium position.

Autospeed plus Pitch Command and Hold: Due to continued difficulty in controlling pitch, a pitch attitude command system was incorporated with the autospeed. This system allowed the pilot to trim the aircraft to the pitch attitude required for touchdown early in the approach. No subsequent pitch changes are necessary since the command system automatically maintains the attitude throughout the remainder of the approach and landing. This configuration of the aircraft is modeled by removing pitch rate, pitch, and horizontal tail from Equation (80). This yields the following model for the fully augmented STOL aircraft

$$\begin{bmatrix} \dot{C}_L \\ \dot{\alpha}' \\ \dot{\delta h}' \\ \dot{\delta T} \end{bmatrix} = \begin{bmatrix} 0 & 0 & 0 & 0 & 0 & C_L \\ a_{gL} & a_{22} & a_{22} & 0 & b_{21} & \alpha' \\ 0 & 0 & -1 & 0 & 0 & \delta h' \\ 0 & 0 & 0 & 0 & -a_T & \delta T \end{bmatrix} + \begin{bmatrix} 0 \\ 0 \\ 0 \\ a_T \end{bmatrix} \delta T_c + \begin{bmatrix} 1 \\ 0 \\ 0 \\ 0 \end{bmatrix} \dot{z}_1(t) \tag{81}$$

where the coefficients are evaluated for the pitched-up equilibrium condition. In this configuration, the pilot's only task is to control altitude and sink rate with thrust.

In summary, state space models in the form

$$\dot{\underline{x}}(t) = \underline{A}\,\underline{x}(t) + \underline{B}\,\underline{u}(t) + \underline{F}\,\dot{\underline{z}}(t) \tag{82}$$

have been developed for three different STOL configurations:

1. Basic Aircraft,

2. Autospeed, and

3. Autospeed plus pitch command and hold.

Numerical values for the $\underline{A}$ and $\underline{B}$ matrices are given in Appendix B. In the next chapter, a model for the pilot will be developed for the flare task that can be used to predict pilot response.

III. PILOT MODEL DEVELOPMENT

A model for the pilot is developed, based on the optimal control model for human response,[2-5] that includes the terminal control aspects of the landing task and pilot adaptation to the ground effect. The treatment of the finite time aspects and open/closed loop interrelationship is an important extension of existing results in man-machine systems analysis.

3.1 PILOT MODELING - GENERAL BACKGROUND

The pilot modeling techniques used in this study are rooted in optimal control and estimation theory. They are based on the assumption that the well-trained, highly motivated pilot behaves in an optimal manner subject to his inherent limitations and constraints. This modeling approach is capable of treating multivariable, and time-varying systems within a single conceptual framework using state-space and time-domain techniques. It is, therefore, well-suited to the pilot-STOL system described in the previous sections. The generalized modeling framework facilitates extensions to cover the terminal control aspects of pilot response.

The basic operator modeling techniques are documented extensively in the literature;[2-5] therefore, only the salient features are described below in a general context. The model extensions necessary to treat the terminal time aspects of the landing task are developed in the following sections.

3.1.1 System Description

The structure of the optimal control model of human response is shown in Figure 3. It is assumed that the system dynamics (which also include any pertinent noise shaping filters) are described by the linear time-invariant* equations

*The time-varying case is discussed in Ref. [5]. For the STOL problem studied here, the linearized system dynamics are time-invariant.

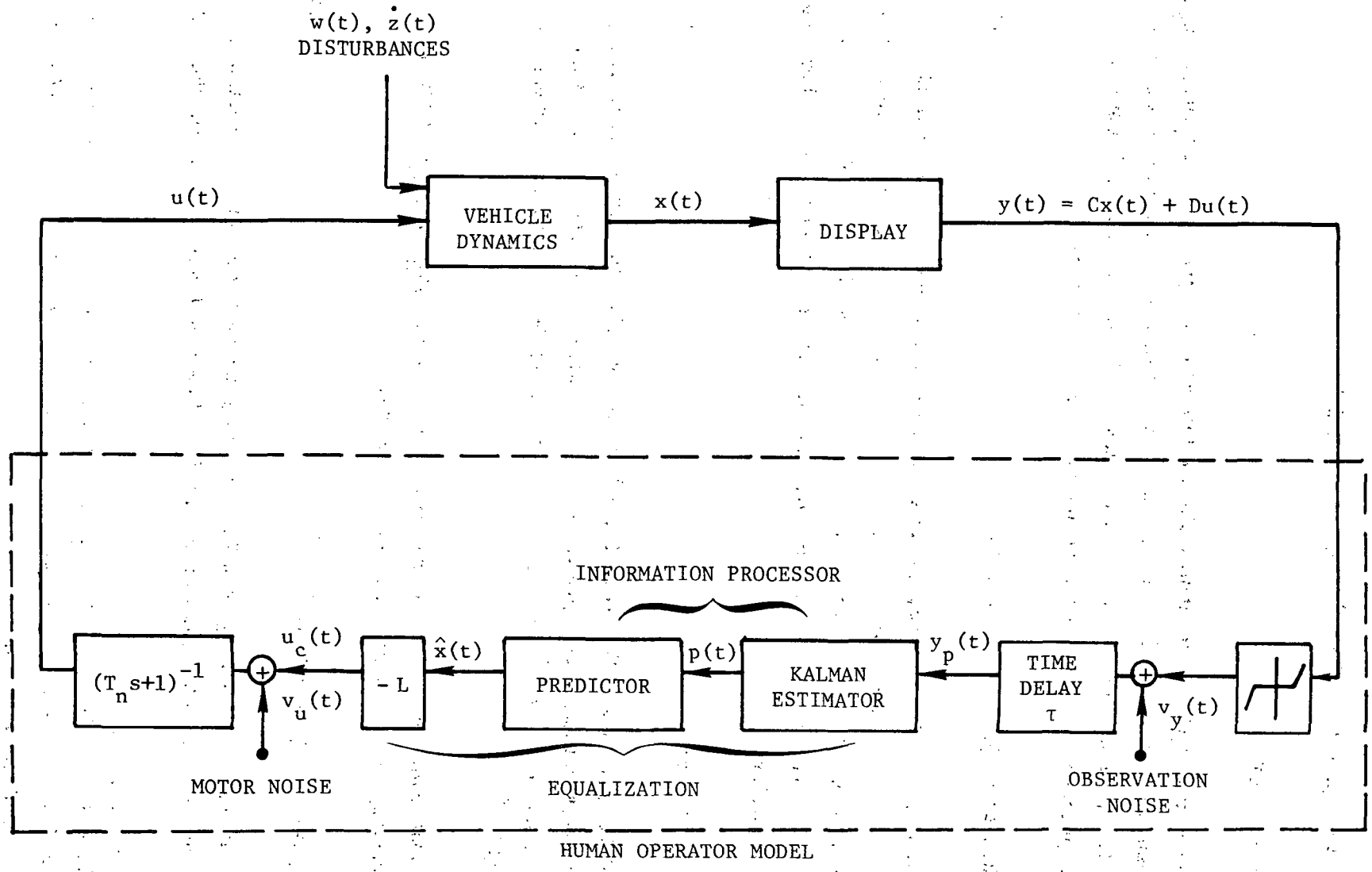

FIGURE 3 OPTIMAL CONTROL MODEL OF HUMAN RESPONSE

$$\dot{\underline{x}}(t) = \underline{A}\,\underline{x}(t) + \underline{B}\,\underline{u}(t) + \underline{E}\,\underline{w}(t) + \underline{F}\,\dot{\underline{z}}(t) \tag{83}$$

$$\underline{x}(0) = \text{given}$$

where the n-vector $\underline{x}(t)$ represents the system state, $\underline{u}(t) = \text{col}[u_1, u_2, \ldots u_r]$ are the human's control inputs, and where $\underline{w}(t)$ represents random input forcing functions, e.g., wind gusts. $\underline{w}(t)$ is assumed to be a zero-mean, Gaussian white noise process (possibly nonstationary) with covariance

$$E\{\underline{w}(t)\,\underline{w}'(\sigma)\} = \underline{W}(t)\,\delta(t-\sigma) \tag{84}$$

The term $\underline{z}(t)$ in Eq. (83) is used to generate input forcing functions that are not stochastic in nature, but are more aptly regarded as "deterministic" inputs. In the modeling of pilot response, it is assumed that $\dot{\underline{z}}(t)$ is the time rate of change of inputs such as wind shear, ground effect, etc. For example, the scalar equation

$$\dot{x}_1(t) = \dot{z}(t) \tag{85}$$

can be used to generate a "deterministic" input $x_1(t)$. We assume that the pilot can continuously estimate the quantity $x_1(t) = z(t)$ from displayed information, but does not so estimate $\dot{z}(t)$. Thus, $x_1(t)$ must be modeled as a state variable as in Eq. (85).*

The human observes a set of outputs $\underline{y}(t) = \text{col}[y_1, y_2, \ldots, y_m]$ that is related linearly to the system state and control,

$$\underline{y}(t) = \underline{C}\,\underline{x}(t) + \underline{D}\,\underline{u}(t) \tag{86}$$

where the matrices $\underline{C}$ and $\underline{D}$ can be time varying to model gains on display variables that change with time or altitude. The usual assumption in the model

---

*A generalization to Eq. (85) is $\dot{x}_1(t) = x_2(t)$, $\dot{x}_2(t) = \ddot{z}(t)$. This would be used of $x_2(t)$ appeared explicitly in the system equations (83) or contributed directly to a displayed signal.

is that if a quantity y_i is explicitly displayed to the man, he also derives the rate of change $\dot{y}_i$. Thus, $\underline{y}(t)$ contains both position and velocity information of a displayed signal, but no higher derivative information.

3.1.2 Human Limitations

The human has inherent limitations of time-delay and perceptual noise (i.e., remnant). These quantities are associated with the observational process in the man model, so that the human is assumed to perceive $\underline{y}_p(t)$, a delayed, noisy replica of $y(t)$. Thus,

$$\underline{y}_p(t) = \underline{y}(t-\tau) + \underline{v}_y(t-\tau) \ .$$

The time-delay τ is nominally $\tau = .2 \pm .05$ sec. The "observation" noises are white, independent, and have covariance

$$E\{v_{yi}(t)\ v_{yi}(\sigma)\} = V_{yi}(t)\ \delta(t-\sigma) \quad i=1,2,\ldots,m \tag{87}$$

When directly viewing $y_i(t)$, the associated covariance V_{yi} is assumed to scale with the variance of $y_i(t)$, i.e.,

$$V_{yi}(t) = \rho_{yi} E\{y_i^2(t)\} \tag{88}$$

For full attention on a single display indicator, the noise/signal ratios ρ_{yi} on position and rate typically have a value of $.01\pi$, i.e., $v_{yi}(t)$ has a -20dB normalized power density level. When there are $K > 1$ display indicators, the human must allocate his attention among the various displays. Let η_k denote the attentional allocation to display indicator k. Then, neglecting the time spent in interinstrument scanning, we have

$$\sum_{k=1}^{K} \eta_k = 1, \quad 0 \leq \eta_k \leq 1 \tag{89}$$

If displayed variable $y_i(t)$ is obtained from indicator k, the effect of attentional allocation is to modify the noise/signal ratio ρ_i according to

$$\rho_{yi} = \rho^{\circ}_{yi}/\eta_k \tag{90}$$

where $\rho^{\circ}_{yi} \simeq .01\pi$ is the noise/signal ratio that corresponds to full attention on indicator k. Methods for determining η_k within the optimal control modeling context are discussed in Refs. [2] and [5]. However, these methods are difficult to apply, and are generally applicable for steady-state situations only. In the present STOL effort, we do not attempt to solve the display attentional allocation problem in the time-varying or finite time case. However, in order to include some effects of attentional allocation, albeit in a crude manner, we set $\eta_k = 1/K$. Thus, we assume an equal division of pilot attention among the primary instruments needed for control.

In addition to time-delay and perceptual noise, we include perceptual/indifference thresholds on displayed information. Clearly, a pilot will not react to changes in a displayed variable if the indicator motion is smaller than his observational thresholds. Thus, in perceiving quantity $y_i(t)$, we write

$$y_{pi}(t) = f_i(y_i(t-\tau)) + v_{yi}(t-\tau) \tag{91}$$

where the threshold nonlinearity $f_i(\cdot)$ is

$$f(x) = \begin{cases} x-a & x \geq a \\ 0 & -a \leq x \leq a \\ x+a & x \leq -a \end{cases} \tag{92}$$

The nonlinearity $f(\cdot)$ is replaced in the pilot model by its equivalent "Random Input Describing Function". This statistical linearization gives

$$f(x) \simeq \overline{f}_x \cdot x \tag{93}$$

where $\overline{f}_x$ is a gain that varies with the mean and standard deviation of $x(t)$. Expressions for $\overline{f}_x$ are given in [4]. Values for the thresholds a_i depend, in part, on the physiological limitations of the eye in sensing motion, as well as on the specific instrument markings used.

3.1.3 Task Definition

It is assumed that the human's control task is adequately reflected in the choice of a control $\underline{u}(\cdot)$ that minimizes the cost functional

$$J(\underline{u}) = \lim_{T\to\infty} E \frac{1}{T} \int_0^T [\underline{y}'(t)\, \underline{Q}_y \underline{y}(t) + \underline{u}'(t)\underline{Q}_u \underline{u}(t) + \dot{\underline{u}}'(t)\underline{Q}_{\dot{u}}\dot{\underline{u}}(t)]dt \qquad (94)$$

conditioned on the perceived information $\underline{y}_p(\cdot)$. The first term in $J(\underline{u})$ is a generalized mean-squared error criterion where $\underline{Q}_y$ depends on the task specifics. The control rate term is used to account for the human's limitation on the rate of control motion, and introduces "neuro-motor" dynamics in the man model.

The selection of the weightings $\underline{Q}_y = \text{diag}\,[q_{yi}]$, $\underline{Q}_u = \text{diag}\,[q_{ui}]$ and $\underline{Q}_{\dot{u}} = \text{diag}\,[q_{\dot{u}i}]$ in $J(\underline{u})$ is a non-trivial step in applying the man-model. In any specific situation, these parameters are dependent on both the human's objective task requirements and his subjective mode of behavior. One useful method for selecting reasonable a priori estimates for q_{yi} and q_{ui} is by associating these quantities with allowable deviations in the system variables. Thus, we let

$$q_{yi} = \left|\frac{1}{y_{i,max}}\right|^2 \quad , \quad q_{ui} = \left|\frac{1}{u_{i,max}}\right|^2 \qquad (95)$$

where $y_{i,max}$ is the maximum desired, or allowable, value of y_i; $u_{i,max}$ is the maximum control deflection. This method of choosing weightings has intuitive appeal. First, maximum or limiting values of system quantities are often easy to specify, or elicit by pilot questionnaire. Second, the contribution of each

term $q_{yi}y_i^2(t)$ to the total cost depends on how close y_i is to its maximum value. Because of the normalization (95), each $y_i(t)$ will not contribute significantly to $J(\underline{u})$ provided $|y_i| \leq |y_{i,max}|$. When $|y_i| > |y_{i,max}|$, the contribution to $J(\underline{u})$ of $q_i y_i^2(t)$ increases rapidly with $y_i^2(t)$. The analogy to manual control is that there will be little concern over minimizing $y_i(t)$ if this quantity is well within allowable limits.

One method that can be used for selecting the weightings $q^{\bullet}_{ui}$ on the human's control rate is similar to that for q_{yi}, i.e., let

$$q^{\bullet}_{ui} = \left| \frac{1}{\dot{u}_{i,max}} \right|^2 \tag{96}$$

Here, $\dot{u}_{i,max}$ is the maximum rate that a human can (or will) input a control u_i. However, we choose to associate the weightings $q^{\bullet}_{u}$ with the human limitations directly. Weighting $\dot{u}$ in the cost functional results in first order lags being introduced in the man model. There is a first order lag time constant τ_{n_i} that corresponds to each control rate weighting $q^{\bullet}_{ui}$; the smaller one sets $q^{\bullet}_{ui}$, the smaller is the resulting τ_{n_i}. In the model, the lags τ_{n_i} are associated with the man's "neuromotor" dynamics, where past modeling efforts show typically $\tau_{n_i} \simeq .1$ sec.[2] Thus, the weightings $q^{\bullet}_{ui}$ are adjusted iteratively until each $\tau_{n_i} \simeq .1$ sec.*

3.1.4 The Pilot Model

The "human's" control input (i.e., the control that minimizes $J(\underline{u})$) is generated by the feedback law

$$\underline{T}_n \dot{\underline{u}}(t) + \underline{u}(t) = -\underline{L}\,\hat{\underline{x}}(t) + \underline{v}_u(t) = \underline{u}_c(t) + \underline{v}_u(t) \tag{97}$$

*If the resulting $q^{\bullet}_{ui}$ weighting is such that $1/\sqrt{q^{\bullet}_{ui}}$ is much greater than the physical rate at which one can move control u_i, then Eq. (96) must be used.

where $\hat{\underline{x}}(t)$ is the best estimate of the system state $\underline{x}(t)$. $\underline{v}_u(t)$ is a white "motor-noise" that represents a human's imprecise knowledge of generated control inputs and has covariance

$$E\left\{v_{u_i}(t)v'_{u_i}(\sigma)\right\} = V_{u_i}(t)\ \delta(t-\sigma) \quad i=1,2,\ldots,r \tag{98}$$

where a good approximation to the covariance $V_{u_i}(t)$ is

$$V_{u_i}(t) = \rho_{u_i} \cdot E\{u_i^2(t)\} \quad i=1,2,\ldots,r \tag{99}$$

The motor noise/signal ratio $\rho_{u_i} \simeq .003\pi$, i.e., $v_{u_i}(t)$ has approximately -25dB normalized power density level.

The feedback gains $\underline{L}$ and the r x r matrix $\underline{T}_n$ are given by

$$\begin{aligned} \underline{T}_n &= \underline{P}_{22}^{-1}\ \underline{Q}_u^{\bullet} \\ \underline{L} &= \underline{P}_{22}^{-1}\ \underline{P}'_{12} \end{aligned} \tag{100}$$

where

$$\underline{P} = \left[\begin{array}{c|c} \underline{P}_{11} & \underline{P}_{12} \\ \hline \underline{P}'_{12} & \underline{P}_{22} \end{array}\right]$$

satisfies the equation

$$\begin{aligned} &\underline{P}_{11}\underline{A} + \underline{A}'\underline{P}_{11} + \underline{C}'\underline{Q}_y\underline{C} - \underline{P}_{12}\underline{Q}_u^{\bullet -1}\ \underline{P}'_{12} = \underline{0} \\ &\underline{P}_{11}\underline{B} + \underline{A}'\underline{P}_{12} + \underline{C}'\underline{Q}_y\underline{D} - \underline{P}_{12}\underline{Q}_u^{\bullet -1}\ \underline{P}_{22} = \underline{0} \\ &\underline{P}'_{12}\underline{B} + \underline{B}'\underline{P}_{12} + \underline{D}'\underline{Q}_y\underline{D} + \underline{Q}_u - \underline{P}_{22}\underline{Q}_u^{\bullet -1}\ \underline{P}_{22} = \underline{0} \end{aligned} \tag{101}$$

The estimate $\hat{\underline{x}}(t)$ is obtained from the cascade combination of a Kalman filter and predictor that compensate optimally for the human's observation noise and time-delay, respectively. The filter is defined in terms of the augmented state vector $\underline{\chi} = \text{col}\,[\underline{x}(t), \underline{u}(t)]$. The filter generates $\underline{p}(t) = E\{\underline{\chi}(t-\tau)\,|\,\underline{y}(\sigma), \sigma \leq t\}$ at time $t \geq \tau$ of the past state $\underline{x}(t-\tau)$ and control $\underline{u}(t-\tau)$ from

$$\frac{d}{dt}\,\underline{p}(t) = \tilde{\underline{A}}\,\underline{p}(t) + \tilde{\underline{B}}\,\underline{u}_c(t-\tau) + \underline{\Sigma}\,\tilde{\underline{C}}'\tilde{\underline{V}}_y^{-1}[\underline{y}_p(t) - \tilde{\underline{C}}\,\underline{p}(t)] \tag{102}$$

where

$$\tilde{\underline{A}} = \left[\begin{array}{c|c} \underline{A} & \underline{B} \\ \hline \underline{0} & -\underline{T}_n^{-1} \end{array}\right] \quad ; \quad \tilde{\underline{B}} = \left[\begin{array}{c} \underline{0} \\ \hline \underline{T}_n^{-1} \end{array}\right] \quad ; \quad \tilde{\underline{C}} = \left[\begin{array}{c|c} \underline{C} & \underline{D} \end{array}\right] \tag{103}$$

and $\tilde{\underline{V}}_y$ is given by

$$\tilde{\underline{V}}_y(t) = \text{diag}\,[V_{yi}(t)/\overline{f}_{yi}] \tag{104}$$

The matrix $\underline{\Sigma}(t)$, $t \geq \tau$ satisfies the time-varying equation

$$\dot{\underline{\Sigma}}(t) = \tilde{\underline{A}}\,\underline{\Sigma}(t) + \underline{\Sigma}(t)\tilde{\underline{A}}' + \tilde{\underline{W}}(t) - \underline{\Sigma}(t)\tilde{\underline{C}}'\tilde{\underline{V}}_y^{-1}\,\tilde{\underline{C}}\,\underline{\Sigma}(t) \tag{105}$$

where

$$\tilde{\underline{W}}(t) = \left[\begin{array}{c|c} \underline{EWE}' + \underline{\dot{F}\dot{Z}F}' & \underline{0} \\ \hline \underline{0} & \underline{T}_n^{-1}\,\underline{V}_u\,\underline{T}_n'^{-1} \end{array}\right] \tag{106}$$

and $\underline{Z}(t) = \text{diag}\,[\dot{z}_1^2(t), \dot{z}_2^2(t), \ldots, \dot{z}_{n_z}^2(t)]$ (n_z = no. of deterministic inputs). The initial conditions on Eqs. (102) - (105) are

$$\underline{p}(\tau) = \hat{\underline{\chi}}_o \quad , \quad \underline{\Sigma}(\tau) = \underline{\Sigma}_o \tag{107}$$

where $\hat{\underline{\chi}}_o$ is the man's a priori estimate of the mean state $E\{\underline{\chi}(t)\}$ at $t=0$. $\underline{\Sigma}_o$ is the man's initial uncertainty in this estimate.

The predictor generates the best estimate of $\underline{\chi}(t)$ denoted by $\hat{\underline{\chi}}(t)$ from the estimator output $\underline{p}(t)$ according to

$$\begin{aligned} \frac{d}{dt}\hat{\underline{\chi}}(t) &= \tilde{\underline{A}}\,\hat{\underline{\chi}}(t) + \tilde{\underline{B}}\,\underline{u}_c(t) + e^{\tilde{\underline{A}}\tau}\,\underline{\Sigma}\,\tilde{\underline{C}}'\tilde{\underline{V}}_y^{-1}\,[\underline{y}_p(t) - \tilde{\underline{C}}\,\underline{p}(t)] \\ \hat{\underline{\chi}}(\tau) &= e^{\tilde{\underline{A}}\tau}\,\underline{p}(\tau) \end{aligned} \tag{108}$$

The above equations (83) - (108) define completely the input-output model of the pilot-vehicle system. Note that the model is time-varying since the matrix $\underline{\Sigma}$ varies with time.* These equations can be used to predict pilot response in closed-loop tracking tasks. The model inputs include the vehicle dynamics, cost functional weightings and human limitation parameters. The model outputs include statistical predictions of system performance. In steady-state situations, one may also compute input-output transfer functions and power density spectra.[2]

3.2 COVARIANCE EXPRESSIONS AND STATISTICS

Analyzing the behavior of a time-varying system is best accomplished using covariance propagation methods. This results in predictions of both the mean system response and the standard deviation in this response. The mean response is the system response to a specific input $\underline{z}(t)$ in Eq. (83), and represents the result one would expect to find by (ensemble) averaging the results of many trials, each with the same $\underline{z}(t)$. The standard deviation results from the randomness $\underline{v}_y(t)$ and $\underline{v}_u(t)$ that the human injects into the loop, as well as from any gust inputs $\underline{w}(t)$.

---

*If $\dot{\underline{z}}(t) \to \underline{0}$ and $\underline{W}(t) \to \underline{W}$ = constant, then the man-model reaches a time-invariant steady-state.

In this section, we present equations for the propagation of $\bar{\underline{\chi}}(t)$ = mean state and the covariance $\underline{X}(t) = E\{[\underline{\chi}(t) - \bar{\underline{\chi}}(t)] \cdot [\underline{\chi}(t) - \bar{\underline{\chi}}(t)]'\}$. These expressions give us the capability of analyzing the statistics of the closed-loop system response, and are needed to compute $E\{y_i^2(t)\}$ and $E\{u_i^2(t)\}$ in Eqs. (88) and (99).

The required results are most easily derived using the equations for the estimation error (see Ref. [4])

$$\underline{e}_1(t) = \underline{\chi}(t-\tau) - \underline{p}(t) \tag{109}$$

and the predicted estimate $\underline{\chi}(t)$. These quantities satisfy

$$\dot{\underline{e}}_1(t) = \underline{A}_f \underline{e}_1(t) + \underline{K}(t)\underline{v}_y(t-\tau) + \underline{F}\,\dot{\underline{z}}(t-\tau) + \tilde{\underline{B}}\,\underline{v}_u(t) \tag{110}$$

$$\dot{\hat{\underline{\chi}}}(t) = \underline{A}_c \hat{\underline{\chi}}(t) + \bar{\underline{K}}(t)\,[\tilde{\underline{C}}\,\underline{e}_1(t) + \underline{v}_y(t-\tau)] \tag{111}$$

where

$\underline{A}_f = \tilde{\underline{A}} - \underline{K}\,\tilde{\underline{C}}$ = closed-loop filter matrix

$\underline{A}_c = \tilde{\underline{A}} - \tilde{\underline{B}}\,\underline{L}$ = closed-loop control matrix

$\underline{K} = \underline{\Sigma}\,\tilde{\underline{C}}'\tilde{\underline{V}}_y^{-1}$ = estimator gain at time t

$\bar{\underline{K}} = e^{\tilde{A}\tau}\underline{K}$

The total state $\underline{\chi}(t)$ at time t is given by

$$\underline{\chi}(t) = \hat{\underline{\chi}}(t) + e^{\tilde{\underline{A}}\tau}\,\underline{e}_1(t) + \underline{e}_2(t) \tag{112}$$

where $\underline{e}_2(t)$ is the prediction error,

$$\underline{e}_2(t) = \int_{t-\tau}^{t} e^{\tilde{\underline{A}}(t-\sigma)} \left[\underline{F}\ \dot{\underline{z}}(\sigma) + \tilde{\underline{B}}\ \underline{v}_u(\sigma)\right] d\sigma \tag{113}$$

The mean-state at time t is obtained by taking the expected value of the above equations. The results are

$$\bar{\underline{\chi}}(t) = \bar{\hat{\underline{\chi}}}(t) + e^{\tilde{\underline{A}}\tau}\ \bar{\underline{e}}_1(t) + \bar{\underline{e}}_2(t) \tag{114}$$

where

$$\frac{d}{dt}\ \bar{\underline{e}}_1(t) = \underline{A}_f\ \bar{\underline{e}}_1(t) + \underline{F}\ \dot{\underline{z}}(t-\tau) \tag{115}$$

$$\frac{d}{dt}\ \bar{\hat{\underline{\chi}}}(t) = \underline{A}_c\ \bar{\hat{\underline{\chi}}}(t) + \bar{\underline{K}}(t)\ \tilde{\underline{C}}\ \bar{\underline{e}}_1(t) \tag{116}$$

$$\bar{\underline{e}}_2(t) = \int_{t-\tau}^{t} e^{\tilde{\underline{A}}(t-\sigma)}\ \underline{F}\ \dot{\underline{z}}(\sigma)\ d\sigma \tag{117}$$

$$\bar{\hat{\underline{\chi}}}(\tau) = e^{\tilde{\underline{A}}\tau}\ \underline{p}(\tau),\ \bar{\underline{e}}_1(\tau) = E\{\underline{\chi}(0)\} - \underline{p}(\tau) \tag{118}$$

Expressions for the covariances

$$\begin{aligned}
\hat{\underline{X}}(t) &= E\{[\hat{\underline{\chi}}(t) - \bar{\hat{\underline{\chi}}}(t)] \cdot [\hat{\underline{\chi}}(t) - \bar{\hat{\underline{\chi}}}(t)]'\} \\
\underline{E}_1(t) &= E\{[\underline{e}_i(t) - \bar{\underline{e}}_i(t)] \cdot [\underline{e}_i(t) - \bar{\underline{e}}_i(t)]'\} \quad ;\ i=1,2 \\
\underline{X}(t) &= E\{[\underline{\chi}(t) - \bar{\underline{\chi}}(t)] \cdot [\underline{\chi}(t) - \bar{\underline{\chi}}(t)]'\} \\
&= \hat{\underline{X}}(t) + e^{\tilde{\underline{A}}\tau}\ \underline{M}(t) + \underline{M}'(t)\ e^{\tilde{\underline{A}}'\tau} + e^{\tilde{\underline{A}}\tau}\ \underline{E}_1(t)\ e^{\tilde{\underline{A}}'\tau} + \underline{E}_2(t)
\end{aligned} \tag{119}$$

where $\underline{M}(t)$ is the cross covariance between $\hat{\underline{x}}(t)$ and $\underline{e}_1(t)$, are derived by subtracting Eqs. (115) - (117) from Eqs. (110) - (111) and (113) and taking the autocovariance. The results are a coupled set of linear matrix equations

$$\dot{\underline{E}}_1(t) = \underline{A}_f\underline{E}_1(t) + \underline{E}_1(t)\underline{A}'_f + \underline{K}(t)\tilde{\underline{V}}_y(t-\tau)\ \underline{K}'(t) + \tilde{\underline{B}}\ \underline{V}_u\tilde{\underline{B}}'$$

$$\dot{\underline{M}}(t) = \underline{A}_c\underline{M}(t) + \underline{M}(t)\underline{A}'_f + \overline{\underline{K}}(t)\tilde{\underline{C}}\ [\underline{E}_1(t) - \underline{\Sigma}(t)] \tag{120}$$

$$\dot{\hat{\underline{x}}}(t) = \underline{A}_c\hat{\underline{x}}(t) + \hat{\underline{x}}(t)\underline{A}'_c + \overline{\underline{K}}(t)\tilde{\underline{C}}\ \underline{M}'(t) + \underline{M}(t)\tilde{\underline{C}}'\overline{\underline{K}}'(t) + \overline{\underline{K}}(t)\tilde{\underline{V}}_y(t-\tau)\overline{\underline{K}}'(t)$$

$$\underline{E}_2(t) = \int_{t-\tau}^{t} e^{\tilde{\underline{A}}(t-\sigma)}\ \underline{B}\ \underline{V}_u(\sigma)\tilde{\underline{B}}'\ e^{\tilde{\underline{A}}(t-\sigma)}d\sigma \tag{121}$$

where $\underline{\Sigma}(t)$ satisfies Eq. (105). The initial conditions on $\hat{\underline{x}}$, $\underline{E}_1$, $\underline{M}$, are taken as

$$\hat{\underline{x}}(\tau) = \underline{M}(\tau) = \underline{0},\ \underline{E}_1(\tau) = \underline{X}(0) = \text{given}$$

Finally, the mean and covariance of $\underline{y}(\cdot)$ at time t are simply

$$\overline{\underline{y}}(t) = \tilde{\underline{C}}\ \overline{\underline{x}}(t) \tag{122}$$

$$\underline{Y}(t) = \text{cov}[\underline{y}(t)] = \tilde{\underline{C}}\ \underline{X}(t)\tilde{\underline{C}}' \tag{123}$$

Efficient computer programs have been developed for integrating the mean and covariance equations (114) - (123) presented above.

The above expressions for the signal means and covariances are of special interest in predicting the probability densities of system variables. Since the white noise random inputs $\underline{w}(t)$, $\underline{v}_y(t)$ and $\underline{v}_u(t)$ are assumed to be Gaussian, and since the closed-loop system is linearized, the system states $x_1,\ldots,x_n$ are Gaussian random variables. The x_i are non-stationary when the Kalman filter gains $\underline{K}$ in Eq. (110) are functions of time.

For a Gaussian variable x, the mean m and variance σ^2 are sufficient statistics for defining the probability density of x,

$$p(x) = \frac{1}{\sqrt{2\pi}\,\sigma} \exp\left\{-\frac{(x-m)^2}{2\sigma^2}\right\} \tag{124}$$

Thus, for any state variable $x_i(t)$, with mean $\bar{x}_i(t)$ given by Eq. (114), and variance $\sigma_i^2(t) = X_{ii}(t)$ given by Eq. (119),

$$p(x_i(t)) = \frac{1}{2\pi\,\sigma_i(t)} \exp\left\{-\frac{[x_i - \bar{x}_i(t)]^2}{2\sigma_i^2(t)}\right\} \tag{125}$$

is the probability density function of x_i at time t. Similar expressions hold for $p(y_i(t))$ and $p(u_i(t))$.

Equation (125) is the univariate density of $x_i(t)$. Since the $x_i(t)$ are correlated, the multivariate density of $\underline{x} = (x_1, x_2, \ldots, x_n)$ is given by the general expression,[6]

$$p_t(x_1, x_2, \ldots, x_n) = \frac{1}{2\pi^n |\underline{X}(t)|} \exp\left\{-\frac{1}{2}[\underline{x}-\bar{\underline{x}}(t)]'\underline{X}^{-1}[\underline{x}-\bar{\underline{x}}(t)]\right\} \tag{126}$$

where $\underline{X}$ is the state covariance matrix and $|\underline{X}| = \det \underline{X}$. The multivariate distribution of $\underline{y} = [y_1, y_2, \ldots, y_m]$ can also be written using the expressions for $\bar{\underline{y}}(t)$ and $\underline{Y}$ in Eqs. (122) - (123).

3.3 TERMINAL CONTROL

The above section described the pilot model that has been developed to treat regulation (i.e., tracking) tasks. Modeling pilot response during flare requires that we treat the terminal control, or finite time aspects, of the task--namely, to land the aircraft at some intended point on the runway, with a desired sink rate and attitude.

For the aircraft system defined by

$$\dot{\underline{x}}(t) = \underline{A}\,\underline{x}(t) + \underline{B}\,\underline{u}(t) + \underline{E}\,\underline{w}(t) + \underline{F}\,\dot{\underline{z}}(t)$$

$$\underline{y}(t) = \underline{C}\,\underline{x}(t) + \underline{D}\,\underline{u}(t) \tag{127}$$

with

$$\underline{x}(t=0) = \underline{x}(0) = \text{given}$$

it is assumed that a general set of terminal conditions

$$\underline{H}\,\underline{x}(T_d) + \underline{c} = 0 \tag{128}$$

must be satisfied where T_d is the intended touchdown time.

In order to extend the human operator model to include the terminal control task, it is assumed that the human generates a control input $\underline{u}_o(t)$ such that the response $\underline{x}_o(t)$ of the unforced system,

$$\dot{\underline{x}}_o(t) = \underline{A}\,\underline{x}_o(t) + \underline{B}\,\underline{u}_o(t), \quad \underline{x}_o(0) = \underline{0}$$

$$\underline{y}_o(t) = \underline{C}\,\underline{x}_o(t) + \underline{D}\,\underline{u}_o(t) \tag{129}$$

meets the terminal conditions

$$\underline{H}\,\underline{x}_o(T_d) + \underline{c} = 0 \tag{130}$$

Clearly, many controls can accomplish this transfer. However, we assume that the pilot's control is the one generated with least control effort. Thus, we require $\underline{u}_o(t)$ to minimize

$$J_o = \int_0^{T_d} \dot{\underline{u}}_o'(t)\,\underline{Q}_{\dot{u}}\,\dot{\underline{u}}_o(t)\,dt \tag{131}$$

where the cost functional weightings $q_{ui}^{\cdot}$ on control rate are chosen as discussed in Section 3.1.3. The requirement that $\underline{u}_o$ minimize J_o was motivated by the fact that a pilot tends to control an aircraft smoothly, minimizing any unnecessary rapid control motions.*

The control $\underline{u}_o(t)$ that meets the terminal constraint (130) while minimizing the "smoothness" criterion (131) is derived in Appendix A. $\underline{u}_o(t)$ is an <u>open-loop</u> (i.e., feedforward) control given by

$$\dot{\underline{u}}_o(t) = - \underline{Q}_u^{-1} \underline{B}_o \underline{h}(t) \tag{132}$$

where the time function $\underline{h}(t)$ is generated by

$$\dot{\underline{h}}(t) = - \underline{A}_o' \underline{h}(t) \tag{133}$$

with the boundary condition

$$\underline{h}(T_d) = \underline{H}_o' [\underline{H}_o \underline{W}(0,T_d) \underline{H}_o']^{-1} \underline{c} \tag{134}$$

where

$$\underline{W}(0,T_d) = \int_0^{T_d} e^{\underline{A}_o(T_d-\sigma)} \underline{B}_o \underline{Q}_u^{-1} \underline{B}_o' e^{\underline{A}_o'(T_d-\sigma)} d\sigma \tag{135}$$

The matrices $\underline{A}_o$, $\underline{B}_o$, $\underline{H}_o$ are

---

*A more general cost functional

$$J_o = \int_0^{T_d} [\underline{y}_o' \underline{Q}_y \underline{y}_o + \underline{u}_o' \underline{Q}_u \underline{u}_o + \dot{\underline{u}}_o' \underline{Q}_u \dot{\underline{u}}_o] dt$$

could also be considered. In the present effort, Eq. (131) seemed most reasonable in view of general pilot technique.

$$\underline{A}_o = \left[\begin{array}{c|c} \underline{A} & \underline{B} \\ \hline \underline{0} & \underline{0} \end{array}\right] \quad ; \quad \underline{B}_o = \left[\begin{array}{c} \underline{0} \\ \hline \underline{I} \end{array}\right] \quad ; \quad \underline{H}_o = \left[\underline{H} \mid \underline{0}\right] \tag{136}$$

The control $\underline{u}_o(t)$ and the resulting state trajectory $\underline{x}_o(t)$ and displayed outputs $\underline{y}_o(t)$ meet the terminal condition (128) only when there are no external input forcing functions, wind gusts, or pilot randomness entering Eq. (127). The fact that there are such external disturbances that act on the system give rise to deviations between the actual $\underline{x}(t)$, as generated by Eq. (127), and the nominal $\underline{x}_o(t)$. Let

$$\begin{aligned} \underline{\delta}\,\underline{x} &= \underline{x}(t) - \underline{x}_o(t) \\ \underline{\delta}\,\underline{y} &= \underline{y}(t) - \underline{y}_o(t) \end{aligned} \tag{137}$$

denote these deviations. Also, let the pilot's control input be

$$\underline{u}(t) = \underline{u}_o(t) + \underline{\delta}\,\underline{u}(t) \tag{138}$$

where $\underline{\delta}\,\underline{u}(t)$ is the pilot's corrective control action. The pilot generates $\underline{\delta}\,\underline{u}(t)$ to keep variations $\underline{\delta}\,\underline{x}(t)$ from the nominal flight path "small".

From equations (127) - (129), $x(t)$ is given by

$$\begin{aligned} \dot{\underline{\delta}}\,\underline{x}(t) &= \underline{A}\,\underline{\delta}\,\underline{x}(t) + \underline{B}\,\underline{\delta}\,\underline{u}(t) + \underline{E}\,\underline{w}(t) + \underline{F}\,\dot{\underline{z}}(t) \\ \underline{\delta}\,\underline{x}(0) &= \underline{x}(0) \end{aligned} \tag{139}$$

and

$$\underline{\delta}\,\underline{y}(t) = \underline{C}\,\underline{\delta}\,\underline{x}(t) + \underline{D}\,\underline{\delta}\,\underline{u}(t) \tag{140}$$

We assume that $\underline{\delta}\,\underline{u}(t)$ minimizes the quadratic corrective cost functional (see Eq. (94))

$$J(\underline{\delta}\,\underline{u}) = \lim_{T\to\infty} E\left\{\frac{1}{T}\int_0^T [\underline{\delta}\,\underline{y}'(t)Q_y\,\underline{y}(t) + \underline{\delta}\,\underline{u}'(t)Q_u\underline{\delta}\,\underline{u}(t) + \dot{\underline{\delta}}\,\underline{u}'(t)\,Q_u\dot{\underline{\delta}}\,\underline{u}(t)]dt\right\} \tag{141}$$

Hence, the human "tracks" the nominal trajectory $\underline{x}_o$, minimizing the deviations $\underline{\delta}\,\underline{x}(t)$ subject to his inherent limitations.* It is assumed that $\underline{y}_o(t)$ is "known" to the pilot so that $\underline{\delta}\,\underline{y}(t)$ can be obtained from the actual observations $\underline{y}(t)$ by Eq. (137).

The equations for determining the optimal $\underline{\delta}\,\underline{u}(t)$, based on the observed deviations (140), are the same as the human operator model equations presented in Section 3.1.4. It is only necessary to make the replacements

$$\underline{x}(t) \to \underline{\delta}\,\underline{x}(t), \quad \underline{y}(t) \to \underline{\delta}\,\underline{y}(t), \quad \underline{u}(t) \to \underline{\delta}\,\underline{u}(t)$$

in Eqs. (83) - (108). The result is that the optimal regulating control component $\underline{\delta}\,\underline{u}(t)$ is generated by

$$T_n\dot{\underline{\delta}}\,\underline{u}(t) + \underline{\delta}\,\underline{u}(t) = -\underline{L}\,\underline{\delta}\,\hat{\underline{x}}(t) + \underline{v}_u(t) \tag{142}$$

where $\underline{\delta}\,\hat{\underline{x}}(t)$ is the best estimate of the deviations $\underline{\delta}\,\underline{x}(t)$. The estimate is generated by a Kalman filter-Predictor combination according to equations (102) - (108) but with $\underline{\chi}(t)$ replaced by $\underline{\delta}\,\underline{\chi}(t) - [\underline{\delta}\,\underline{x}(t), \underline{\delta}\,\underline{u}(t)]$, etc. Closed-form expressions for the statistics of the variations $\underline{\delta}\,\underline{x}(t)$, $\underline{\delta}\,\underline{u}(t)$, $\underline{\delta}\,\underline{y}(t)$ are obtained from Eqs. (114) - (123) with the obvious replacements. Note that the variations $\underline{\delta}\,\underline{x}$ will contain a mean component $\overline{\underline{\delta}\,\underline{x}}$ due to the

*The assumption $T\to\infty$ is most valid when the terminal time T_d is larger than closed loop system time constants. $T\to\infty$ conveniently simplifies the model structure since various feedback gains become constants.

"deterministic" inputs $\underline{z}(t)$, plus a random component $\underline{\delta x} - \overline{\underline{\delta x}}$ due to wind gusts and pilot-induced randomness.

The total state $\underline{x}(t)$ at time t is, therefore,

$$\underline{x}(t) = \underline{x}_o(t) + \underline{\delta x}(t) .$$

The mean, or ensemble average state trajectory is

$$E\{\underline{x}(t)\} = \overline{\underline{x}}(t) = \underline{x}_o(t) + \overline{\underline{\delta x}}(t) \tag{143}$$

and the covariance of $x(t)$ is

$$\text{cov}\,[\underline{x}(t)] = \text{cov}\,[\underline{\delta x}(t)] = E\{(\underline{\delta x} - \overline{\underline{\delta x}})(\underline{\delta x} - \overline{\underline{\delta x}})'\} \tag{144}$$

By defining $\underline{u}_o(t)$ and the resulting $\underline{x}_o(t)$ and $\underline{y}_o(t)$ in the above manner, we have tacitly assumed that the pilot is well-trained, i.e., in an "ideal" situation he can control the aircraft to meet the terminal conditions. The decision to omit deterministic inputs $\dot{\underline{z}}(t)$ from the nominal path definition of $\underline{x}_o$ is because otherwise the control $\underline{u}_o(t)$ at time t would be a function of the entire future input $\dot{\underline{z}}(\sigma)$, $t \leq \sigma \leq T_d$.[7] It is unrealistic to assume that a pilot has precise a priori knowledge of $\dot{\underline{z}}(\sigma)$, $t \leq \sigma \leq T_d$ especially since this input is a function of aircraft future attitude. By assuming that pilot control is dependent on only instantaneous (and past) $\dot{\underline{z}}(t)$, along with any a priori estimates of $\underline{z}(t)$, the "deterministic" inputs are included naturally in $\underline{\delta x}(t)$. The pilot model then estimates $\underline{z}(t)$ continuously, along with the other system state variables, and uses the present estimate of $\underline{z}(t)$ in generating the present control.

3.4 APPLICATION TO THE STOL LANDING PROBLEM

In order to use the model to predict pilot performance in a landing task it is necessary to prespecify:

a. the vehicle dynamics and input disturbances,

b. the primary display instruments,

c. the terminal conditions,

d. numerical values for the human response parameters,

e. the cost functional weightings, and

f. initial conditions at the flare window.

For the three different STOL configurations to be studied, the vehicle dynamics have been developed in Section 2.4 and are presented in the state space format

$$\underline{\dot{x}}(t) = \underline{A}\,\underline{x}(t) + \underline{B}\,\underline{u}(t) + \underline{F}\,\underline{z}(t) \tag{145}$$

to be compatible with the human operator model. Numerical values for $\underline{A}$, $\underline{B}$ are given in Appendix B. Below, we discuss the display format, the a priori selection of human response parameters and the cost functional weightings.

3.4.1 Fully Augmented Aircraft

With the autospeed and pitch command-and-hold systems engaged, the pilot's task is to control altitude using the throttles. The primary displays used are thus the altimeter and rate-of-sink indicator. Since we assume that a pilot obtains directly both the position and rate of change of displayed quantities, the information base is

$$\underline{y}(t) = \text{col}\,[h_{CG}(t),\ \dot{h}(t),\ \ddot{h}(t)] \tag{146}$$

where $h_{CG}(t)$ is obtained from the altimeter and $\dot{h}(t)$ and $\ddot{h}(t)$ from the rate-of-sink meter.* With the aid of Eq. (81) displayed outputs may be written as,

*$\dot{h}(t)$ is also obtained (redundant information) from the altimeter--but not to the degree of accuracy as from the $\dot{h}$ instrument directly.

$$\underline{y}(t) = \underline{C}\,\underline{x}(t) + \underline{y}_o(t), \quad t \geq 0 \tag{147}$$

where, for the augmented aircraft, $\underline{x} = \text{col}\,[C_{Lge}, \alpha', \delta h', \delta T]$ and

$$\underline{C} = \begin{bmatrix} 0 & 0 & 126 & 0 \\ 0 & -126 & 0 & 0 \\ 7.9 & 70 & 0 & 16.9 \end{bmatrix} \tag{148}$$

The additional term $\underline{y}_o(t) = \text{col}[53. - 13.2t, -13.2, 0]$ is included since the mathematical state $\underline{x}$ represents <u>deviations</u> from an equilibrium 6° glideslope.

Figure 4 shows the flare geometry. The flare maneuver begins at an altitude $h_{LG} = 41$ ft. ($h_{CG} = 53'$). At this altitude, on a 6° glideslope, the plane is at $R = -140'$ from the runway threshold. The desired touchdown point is taken as the center of the touchdown zone. Thus, $R_{T_d} = 475$. Since the airspeed is $V_o = 126$ ft/sec, the nominal touchdown time T_d is

$$T_d = \frac{615}{126} = 4.9 \text{ sec.}$$

In the mathematical model, Eq. (145), $126x_5 = h$ is the altitude deviation from the equilibrium 6° glideslope. In order that $h(T_d) = 0$, we require

$$\delta h(T_d) = 225 \tan 6° = 23.53 \tag{149}$$

Sink rate at touchdown should be no greater than -3 ft/sec. We, therefore, choose a nominal $\dot{h}(T_d) = -2$ ft/sec. Since $\dot{h} = -13.2 + \dot{\delta h}$, the boundary condition on $\dot{\delta h}(T_d)$ is

$$\dot{\delta h}(T_d) = 11.2 \tag{150}$$

The boundary conditions (149) - (150) may be put in the form

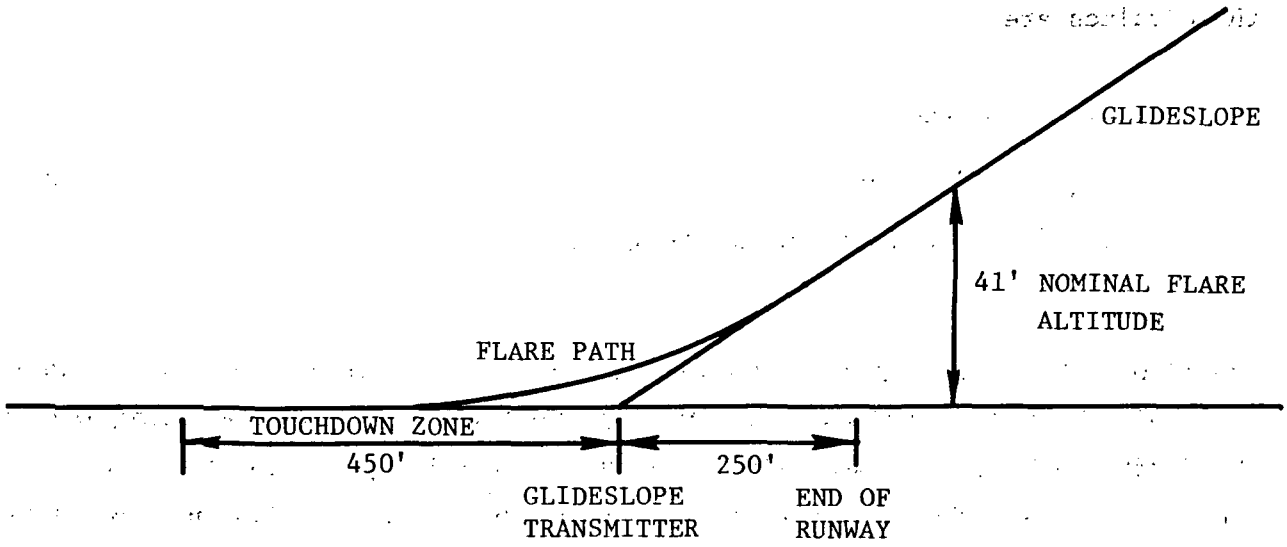

FIGURE 4 TOUCHDOWN GEOMETRY

$$\underline{H}\,\underline{x}(T_d) + \underline{c} = 0 \tag{151}$$

where

$$\underline{H} = \begin{bmatrix} 0 & 126 & 0 & 0 \\ 0 & 0 & -126 & 0 \end{bmatrix}, \quad \underline{c} = \begin{bmatrix} -23.53 \\ -11.2 \end{bmatrix}$$

Nominal values for the human response limitations are chosen on the basis of past experience with the optimal control model. As discussed in Section 3.1, these values are

$$\begin{aligned} \tau &= .2 \text{ sec} \\ \rho_u &= .003\pi = -25\text{dB} \\ \rho_{y1} &= \rho_{y2} = \rho_{y3} = .01\pi/.5 = -17\text{dB} \end{aligned} \tag{152}$$

where the observation noise/signal ratios have been adjusted to -17dB in assuming equal allocation of attention to both instruments. Any effects of pilot monitoring other instruments (e.g., pitch attitude, engine RPM) that are not needed explicitly for control are neglected. Thresholds, a_i, for the instruments are dependent upon display gain and scale markings, and relate to the accuracy with which one can read a given variable. For the standard type set of instruments used in this study, a priori values

$$a_1 = 5 \text{ ft}, \quad a_2 = .8 \text{ ft/sec}, \quad a_3 = .4 \text{ ft/sec}^2 \tag{153}$$

were chosen rather crudely. a_1 and a_2 correspond to one-half the minimal scale division on the altimeter and rate-of-sink instruments, respectively. By assuming that a signal must move through its threshold in 2 sec in order for motion to be discerned, we obtain $a_3 = .4$ ft/sec^2. Fortunately, model predictions were not found to be highly sensitive to changes (by a factor of 2) in the threshold values. Thus, for the STOL landing problem, the numbers a_i can be assumed to be (within a factor of 2) representative of the standard h, $\dot{h}$ instruments.

The cost functional weightings in $J(\underline{\delta u})$ are determined a prior as discussed in Section 3.1.3. These weightings relate to the task of optimal regulation about the nominal flare path. Representative values can be determined in part from analyzing the approach task, which is totally a regulation task. We first choose a weighting on altitude deviations δh. During the approach, it is assumed that the pilot desires to maintain glideslope error within $\pm .3°$. We assume, therefore,

$$\delta\gamma_{max} = .3° = .0052 \text{ rad}$$

Since $\delta h = R\delta\gamma$, we have at the flare initiation point,

$$\delta h_{max} = 390*(.0052) = 2.05' .$$

This value of δh_{max} is used for the entire flare path. The weighting $q_{\delta h}$ is, therefore, by Eq. (95),

$$q_{\delta h} = \frac{1}{(2.05)^2} \simeq .25 \tag{154}$$

Since the throttle input is limited in magnitude, δT_c is weighted in the cost functional. On the approach $\delta T_c = .98$ which corresponds to 13,200 lbs of thrust; δT_c increases nominally to 1.4 during flare. Since the range of δT_c is approximately 0 - 2.4, δT_c, max $\simeq$ 1.0. Therefore, the weighting on δT_c^2 is chosen

$$q_{\delta T_c} = 1.0 \tag{155}$$

The final weighting to be chosen is the control rate weighting. As discussed in Section 3.1.3, $q_{\delta T_c}$ is chosen to yield a $\tau_n \simeq .1$ sec. For the augmented aircraft, the required weighting was found to be

$$q_{\delta T_c} = .022 \tag{156}$$

This corresponds to a maximum rate of throttle motion of $\simeq 7$ units of thrust/sec, or movement through the entire throttle range 0 - 2.4 in approximately .3 sec.

Finally, the initial conditions on the state covariances appropriate to flare initiation must be specified.* These were obtained from the model by "flying" the aircraft down the approach path and stopping at an altitude of $h_{CG} = 53'$. The predicted variances of the system state variables at $h = 53'$ were then used as initial conditions for the flare segment of the landing task. The values used were

$$\sigma_{\delta\alpha'} = .005,\ \sigma_{\delta h'} = .006,\ \sigma_{\delta T} = .06,\ \sigma_{\delta T_c} = .1 \tag{157}$$

These values were subsequently compared with NASA simulator data taken at the flare initiation window. Generally, model and data results agreed within a factor of 1.5. Slight errors in these quantitites are relatively unimportant as regards touchdown, since the effects of the initial model covariances damp out after approximately 1 sec. Initial conditions on the mean state $\underline{\bar{x}}(0)$ are zero, since the plane is assumed to be on the glideslope (on the average) and the C_L ground effect has not as yet built up.

3.4.2 Aircraft with Autospeed Only

With the autospeed system, the aircraft can approach the flare initiation point in the 2° nose-up attitude desired for touchdown. As discussed in Section 2.3.3, the flaps δf_3 must be backed-off -13.1°, and the equilibrium tail position is $\delta t = -3.5°$. The pilot is required to regulate pitch deviations from 2° through controlling the tail input. Pitch deviations occur through cross terms in the throttle input, and directly from the C_M ground effect.

*This is necessary to avoid transients in the model response over the first second of the flare. These might arise if the model were started "cold".

The equations of motion for the STOL dynamics with autospeed are given in Section 2.4.5. For this task, the pilot's major displays are the altimeter and rate-of-sink meter as well as the pitch attitude indicator on the eight-ball. The pilot's information base is, therefore,

$$\underline{y}(t) = \text{col}\,[h_{CG}(t),\ \dot{h}(t),\ \ddot{h}(t),\ \theta(t),\ q(t)] \tag{158}$$

or

$$\underline{y}(t) = \underline{C}\,\underline{x}(t) + \underline{D}\,\underline{u}(t) + \underline{y}_o(t) \qquad t \geq 0 \tag{159}$$

where in this case $\underline{x} = \text{col}\,[C_L,\ C_M,\ \alpha',\ q,\ \theta,\ \delta h',\ \delta T]$, $\underline{u} = \text{col}\,[\delta T_c,\ \delta t]$ and

$$\underline{C} = \begin{bmatrix} 0 & 0 & 0 & 0 & 0 & 126 & 0 \\ 0 & 0 & -126 & 0 & 126 & 0 & 0 \\ 7.9 & 0 & 70 & 0 & -3.3 & 0 & 16.9 \\ 0 & 0 & 0 & 0 & 57.3 & 0 & 0 \\ 0 & 0 & 0 & 57.3 & 0 & 0 & 0 \end{bmatrix} \qquad \underline{D} = \begin{bmatrix} 0 & 0 \\ 0 & 0 \\ 0 & 12.2 \\ 0 & 0 \\ 0 & 0 \end{bmatrix}$$

$$\underline{y}_o(t) = \text{col}\,[53\text{-}13.2t,\ -13.2,\ 0,\ 2°,\ 0]$$

The equation for $\ddot{h}(t)$ is obtained by substituting for $\dot{\theta} - \dot{\alpha}' = \delta\ddot{h}'$.

The terminal conditions on δh and $\delta\dot{h}$ for this problem are given, as before, by Eqs. (149) - (150). In addition, terminal conditions are placed on $\delta\theta$ (deviation from 2° equilibrium) and q, i.e.,

$$\theta(T_d) = 0.,\quad q(T_d) = 0. \tag{160}$$

The four terminal conditions are put in the general form (151) with

$$\underline{H} = \begin{bmatrix} 0 & 0 & 0 & 0 & 0 & 126 & 0 \\ 0 & 0 & -126 & 0 & 126 & 0 & 0 \\ 0 & 0 & 0 & 0 & 57.3 & 0 & 0 \\ 0 & 0 & 0 & 57.3 & 0 & 0 & 0 \end{bmatrix} \qquad \underline{c} = \begin{bmatrix} -25.53 \\ -11.2 \\ 0 \\ 0 \end{bmatrix}$$

Nominal values for the human response parameters are

$$\tau = .2 \text{ sec}$$

$$\rho_{u_1} = \rho_{u_2} = .003\pi = -25\text{dB} \tag{161}$$

$$\pi_{y_1} = \frac{.01\pi}{.33} \simeq -15\text{dB}, \quad i=1,\ldots,5$$

The observation noise/signal ratios have been adjusted to -15dB assuming equal allocation of attention to all three display instruments. The thresholds a_i for the altimeter and rate-of-sink indicator are given by Eq. (153). For the pitch attitude indicator we assume,

$$a_4 = 1.0 \text{ deg} \quad , \quad a_5 = .5 \text{ deg/sec.} \tag{162}$$

The cost functional weightings for the autospeed case must reflect the fact that the pilot is required to regulate both altitude deviations and pitch deviations from the nominal flare path. The cost functional weightings on δh and δT_c are chosen as in the augmented case. Thus,

$$q_{\delta h} = .25, \quad q_{\delta T_c} = 1.0 \tag{163}$$

In the past modeling efforts using the optimal control model, pitch regulation was treated by including a cost functional weighting on q.[3-4] This assures that pitch error corrections are made smoothly, and corresponds with pilots' subjective control behavior. In the present study, we assume

$$\delta q_{max} = 1 \text{ deg/sec}$$

Thus, the cost functional weighting on pitch rate deviations is

$$q_{\delta q} = 1. \tag{164}$$

For the STOL aircraft under consideration, it was found that weighting $q(t)$ alone resulted in large pitch angle deviations during both approach and flare. This is due to the poor pitch damping of the aircraft. It is assumed necessary for the pilot to control pitch angle directly; we assume a maximum tolerance

$$\delta\theta_{max} = 2^\circ$$

so that the aircraft would land with $\theta \geq 0$. Hence,

$$q_{\delta\theta} = \left(\frac{1}{2}\right)^2 = .25 \tag{165}$$

The control weighting on tail deflection δt is determined from the tail position limits. The tail is free to move through a total range -10 to +10 degrees. Since the trim position is -3.5°, the maximum allowable deviation is $6.5^\circ \simeq .11$ rad. Thus,

$$q_{\delta t} = \left(\frac{1}{.11}\right)^2 = 81. \tag{166}$$

The control rate weighting on commanded throttle $u_1 = \delta T_c$ was chosen to yield a resultant $\tau_{n1} = .1$ sec. The required value was found to be (as in the augmented case)

$$q_{\delta \dot{T}_c} = .022 \tag{167}$$

The control rate weighting on tail position $u_2 = \delta t$ was chosen to yeild a resultant $\tau_{n2} = .1$ sec. The required control rate weighting $q_{\delta t}^{\bullet}$ was found to be

$$q_{\delta t}^{\bullet} = 16. \tag{168}$$

which corresponds to a maximum tail rate of approximately .25 rad/sec $\simeq 15°$/sec.

Initial standard deviations for the model states were determined from prediction at the flare window. For the autospeed case, it was found

$$\delta\alpha' = .008,\ \delta q = .003,\ \delta\theta = .006,\ \delta h' = .003$$
$$\delta T = .14,\ \delta T_c = .23,\ \delta t = .004 \tag{169}$$

One simplifying assumption is made in modeling the pitch ground effect in the autospeed case. The C_M ground effect begins at an altitude of $h_{LG} = 60'$. We wish to start the flare model at $h_{LG} = 41'$. Prior to flare initiation, the pilot's major role is to regulate pitch deviations, including those that arise from C_M between $h_{LG} = 60 - 41'$. We, therefore, assume that pitch deviations $\delta\theta = \delta q = 0$ at $h_{LG} = 41'$, so that it is only necessary to consider the <u>additional</u> C_M ground effect that is introduced for $h_{LG} \leq 41$. This enables us to begin the model propagation at $h = 41'$ $(t=0)$ with $\delta x(0) = 0$. The equation $\dot{C}_M = \dot{z}_2(t)$ for generating $C_M(h(t))$ remains as in Eq. (76), but with $C_M(41') = 0$. The additional pilot tail input at $h = 41'$ is computed from the average value of C_M between $h = 60'$ and $41'$ which is $\overline{C}_M \simeq .05$. From the q equation, the tail deflection necessary to balance this average moment is $-.5°$. Thus, since the equilibrium tail position is $-3.5°$, we have at flare initiation $\delta t \simeq -4°$.

3.4.3 <u>Unaugmented Aircraft</u>

The basic aircraft approaches flare initiation in a $-4.1°$ nose-down configuration. The pilot must rotate the plane to achieve a $2°$ nose-up configura-

tion at touchdown. Since the aircraft is pitched down, a higher equilibrium thrust (17,500 lb) is needed to generate the required lift to maintain equilibrium.

The equations of motion for the basic STOL dynamics are given in Section 2.4.5. For this task, as for the autospeed case, the pilot's main displays are the altimeter and rate-of-sink meter, and the pitch attitude indicator. The display information base is, therefore, given by Eq. (158). This may be written

$$\underline{y}(t) = \underline{C}\,\underline{x}(t) + \underline{D}\,\underline{u}(t) + \underline{y}_o(t) \tag{170}$$

with $\underline{x}(t) = \text{col}\,[C_L,\ C_M,\ u',\ \alpha',\ q,\ \theta,\ \delta h',\ \delta T]$, and

$$\underline{C} = \begin{bmatrix} 0 & 0 & 0 & 0 & 0 & 0 & 126 & 0 \\ 0 & 0 & -13.2 & -126 & 0 & 126 & 0 & 0 \\ 7.9 & 0 & 66.5 & 70 & 0 & 0 & 0 & 0 \\ 0 & 0 & 0 & 0 & 0 & 57.3 & 0 & 0 \\ 0 & 0 & 0 & 0 & 57.3 & 0 & 0 & 0 \end{bmatrix} \quad \underline{D} = \begin{bmatrix} 0 & 0 \\ 0 & 0 \\ 0 & 12.2 \\ 0 & 0 \\ 0 & 0 \end{bmatrix}$$

$$\underline{y}_o(t) = [53\ -13.2t,\ -13.2°,\ 0,\ -4.1,\ 0].$$

The equation for $\ddot{h}$ is obtained from differentiating $\dot{\delta h}' = -.105u' - \alpha' + \theta$ and subsituting for $\dot{u}'$, $\dot{\alpha}'$, q.

The terminal conditions on δh and $\dot{\delta h}$ are given by Eqs. (149) - (150). The terminal conditions on θ (deviations from -4.1°) and q are

$$\theta(T_d) = +6.1, \quad q(T_d) = 0. \tag{171}$$

In the general form (151) we have

$$\underline{H} = \begin{bmatrix} 0 & 0 & 0 & 0 & 0 & 0 & 126 & 0 \\ 0 & 0 & -13.2 & -126 & 0 & 126 & 0 & 0 \\ 0 & 0 & 0 & 0 & 0 & 57.3 & 0 & 0 \\ 0 & 0 & 0 & 0 & 57.3 & 0 & 0 & 0 \end{bmatrix} \quad \underline{c} = \begin{bmatrix} -25.53 \\ -11.2 \\ -6.1 \\ 0 \end{bmatrix}$$

For the basic aircraft, we do not assume that the pilot controls speed directly (indeed speed variations on the flare are small). Thus, we have not included u' as a displayed variable, nor is it necessary to include a weighting on u' in the cost functional. The nominal human response parameters for this case are, therefore, the same as Eq. (161). The thresholds a_i are the same as those before, namely

$$a_1 = 5 \text{ ft}, \; a_2 = .8 \text{ft/sec}, \; a_3 = .4 \text{ ft/sec}^2, \; a_4 = 1.0 \text{ deg}, \; a_5 = .5 \text{ deg}$$

The cost functional weightings on δh, δq and $\delta\theta$ are the same as those chosen for the augmented case. The cost functional weighting on δT_c is somewhat higher than before since the available throttle range from nominal is smaller than in the autospeed and augmented case.* Thus,

$$q_{\delta T_c} = 1.5 \tag{172}$$

Also, since the equilibrium tail position is -1°, $\delta t_{max} = 9°$. Hence,

$$q_{\delta t} = \left(\frac{57.3}{9}\right)^2 \simeq 36. \tag{173}$$

The control rate weightings on throttle and tail are adjusted to yield $\tau_{n_i} = .1$.

*nominal throttle setting is 17,500 lbs as opposed to 13,200 lbs.

The required values are

$$q_{\delta T_c}^{\bullet} = .033, \quad q_{\delta t}^{\bullet} = 16. \tag{174}$$

The initial standard deviations for $\underline{\delta x}$ were determined from model predictions at the flare window. The values found were

$$\begin{aligned} &\delta u' = .02, \ \delta\alpha' = .01, \ \delta q = .003, \ \delta\theta = .006 \\ &\delta h' = .01, \ \delta T = .14, \ \delta T_c = .23, \ \delta t = .004 \end{aligned} \tag{175}$$

As in the autospeed case, the pilot was assumed to have compensated for the C_M ground effect over the range $h = 60 - 41'$ so that the model could conveniently be initialized at $t=0$ at $h = 41'$. This introduces an additional tail deflection at flare initiation of .5°. Thus, initial tail deflection is -1.5°.

3.4.4 Model Initial Estimates

It is necessary, when applying the optimal control model to study problems involving "deterministic" inputs, to specify the human's a priori estimate $\hat{\underline{x}}(0)$ of the system state, $\underline{x}$, as in Eq. (107). For the landing task being studied, the aircraft is nominally on the glideslope at flare initiation. Hence vehicle states which represent deviations from the equilibrium 6° glide-path are zero at $t=0$, and it is reasonable to assume that the pilot's estimate of these states is also zero. Therefore, it remains necessary to specify the pilot's a priori estimate of the ground effect terms $\hat{x}_1 = \hat{C}_L$, $\hat{x}_2 = \hat{C}_M$.

We assume values for the initial a priori estimates $\hat{C}_L$, $\hat{C}_M$ equal to 20% of the maximum values for C_L and C_M.

Thus,

$$\hat{C}_M(h_{LG} = 60') = -.06$$

$$\hat{C}_L(h_{LG} = 41') = -.09$$

As discussed in Section 3.4.2, the initial estimate on C_M enables us to introduce a simplification in the model. Since $-C_M$ increases from 0 to .1 between $h = 60'$ and $h = 41'$, it can be assumed that the pilot, because of his initial estimate, has corrected for the C_M pitching moment during this time interval. Thus, we assume $\delta\theta \simeq 0.$ and $\delta q \simeq 0.$ at $h = 41'$, and it becomes necessary to consider only the increase $C_M = .1$ for $h \leq 41'$. With an initial estimate $\hat{C}_M = -.06$, the pilot's estimate of C_M by the time $h = 41'$ will be approximately $-.1 \pm .02$. Thus, it can be assumed that the pilot's estimate of the increase $C_M + .1$ at $h = 41'$ is zero.

As a result, the flare portion of the flight including the pilot reaction to the ground effect can be modeled as beginning at $h - 41'$, where we set $t=0$, with

$$\hat{x}_1 = -.09; \ \hat{x}_2 = 0; \ \hat{x}_i \simeq 0, \quad i=3,\ldots,n$$

where $x_2 = C_L + .1$.

3.5 TOUCHDOWN PREDICTIONS

The independent variable in the pilot model is time. At any time, t, the model generates predictions of the mean and standard deviation of all system variables according to the covariance propagation equations derived in Section 3.2. In addition, as discussed in Section 3.2, these quantities are used to generate the state and output probability densities as functions of time. Of prime interest in a landing task are the probability densities and mean values of key system variables (especially sink-rate) at touchdown. We have model predictions available as functions of time. The transformation from the time predictions to the touchdown predictions is complicated because the touchdown time, T_d, is a random variable ($E\{T_d\} \simeq 4.9$ sec). Below it is shown how we can generate touchdown predictions, including the probability densities of touchdown time (which translates into range dispersions) and sink-rate.

For ease of exposition, let $z_1(t) = h_{LG}(t)$ and let $z_2(t)$ be any model output whose mean and/or probability density at touchdown is sought. Let

$$m_i(t) = E\{z_i(t)\} \qquad i=1,2$$
$$\sigma_{ij}(t) = E\{(z_i(t) - m_i)(z_j(t) - m_j)\} \qquad i,j=1,2 \tag{176}$$

be the mean and covariance at time t of the Gaussian random variables z_1 and z_2. The quantities m_i and σ_{ij} are available directly from the results of Section 3.2.

The joint probability density $p(z_1(t), z_2(t))$ is written as

$$p(z_1,z_2) = \frac{1}{2\pi[\sigma_{11}\sigma_{22}(1 - \bar{\rho}^2)^{\frac{1}{2}}} \exp -\left[\frac{z_1^2 - 2z_1z_2 + z_2^2}{2(1 - \bar{\rho}^2)}\right] \tag{177}$$

where

$$z_1 = \frac{a_1 - m_1(t)}{\sqrt{\sigma_{11}(t)}} \quad , \quad z_2 = \frac{z_2 - m_2(t)}{\sqrt{\sigma_{22}(t)}} \tag{178}$$

and

$$\bar{\rho} = \sigma_{12}/\sqrt{\sigma_{11}\sigma_{22}} \tag{179}$$

is the correlation coefficient between $z_1(t)$ and $z_2(t)$. The univariate probability density of $z_1(t)$ is

$$p(z_1(t)) = \frac{1}{\sqrt{2\sigma\pi_{11}}} \exp\left(-\frac{z_1^2}{2}\right) \tag{180}$$

Let T_d be the touchdown time and let $p(T_d)$, to be determined, be the probability density of T_d. The mean of z_2 at touchdown is given by

$$E\{z_2(T_d)\} = \int_0^\infty E\{z_2(t) \mid t = T_d\}\, p(T_d)\, dT_d \tag{181}$$

where the condition mean is defined as

$$E\{z_2 \mid T_d\} = \int_{-\infty}^{\infty} z_2 p(z_2 \mid T_d)\, dz_2 \tag{182}$$

In the process of integrating Eq. (181), we do not wish to include those trajectories that overflare. The model that has been developed is not appropriate for predicting pilot response to an overshoot of the landing zone. Thus, in computing $E\{z_2(T_d)\}$ from the model predictions only those flights that land within a prescribed time $\hat{T} \simeq T_f$ may be considered. Flights that have not landed by $t=\hat{T}$ are assumed to have overflared. In our analysis, $\hat{T}$ is taken to be the first time $t \geq T_f = 4.9$ sec at which $E\{\dot{h}(t)\} = 0$. The result of considering $T_d < \hat{T}$ is to modify Eq. (181), i.e.,

$$E\{z_2(T_d) \mid T_d \leq \hat{T}\} = \frac{\int_0^{\hat{T}} E\{z_2(t) \mid t = T_d\} p(T_d) dT_d}{\int_0^{\hat{T}} p(T_d)\, dT_d} \tag{183}$$

It thus remains to compute $E\{z_2 \mid T_d\}$ and $p(T_d)$. By definition, the conditional density $p(z_2 \mid T_d)$ is also given as

$$p(z_2(t) \mid t = T_d) = p(z_2(t) \mid z_1(t) = 0) \tag{184}$$

since $z_1(t) = 0$ implies $t = T_d$. The Gaussian density $p(z_2(t)|z_1(t)$ is obtained by dividing Eq. (177) by Eq. (180), yielding

$$p(z_2|z_1) = \frac{1}{[2\pi\sigma_{22}(1 - \bar{\rho}^2)]^{\frac{1}{2}}} \exp - \left[\frac{(z_2 - \bar{\rho}z_1)^2}{2(1 - \bar{\rho}^2)}\right]$$

Evaluating the conditional mean (182) with $z_1 = 0$ gives

$$E\{z_2(t)|t = T_d\} = - \bar{\rho} \sqrt{\frac{\sigma_{22}}{\sigma_{11}}} m_1 + m_2 = - \frac{\sigma_{12}}{\sigma_{11}} m_1 + m_2 \qquad (185)$$

The density of T_d is obtained by noting that

$$\Pr\{\text{landing between time t and t + dt}\}$$

$$= p(T_d)dt$$

$$= -p(h(t) = 0)dh$$

Thus, the required density is

$$p(T_d) = - p(h=0) \frac{dh}{dt} = - p(h=0) \cdot E\{\dot{h}(t)\} \qquad (187)$$

where

$$p(h=0) = \frac{1}{\sqrt{2\pi\sigma_{11}}} e^{-m_1^2/2\sigma_{11}} \qquad (188)$$

and where $E\{\dot{h}(t)\}$ = the mean sink rate <u>at time t</u> is obtained from the model predictions of Eqs. (114) - (118). Therefore, the mean of z_2 at touchdown may be computed from Eq. (183) upon substituting Eqs. (185) and (188). Note

that it is possible to carry through the above process to compute any moment $E\{z_2^n(T_d)\}$ $n \geq 2$, in addition to the mean $z_2(T_d)$.

The probability density of $z_2(T_d)$ in general can be computed by first finding $p(T_d|z_2)$ and then using Bayes rule, or by numerically obtaining a histogram. Either method is cumbersome. Analytic results are obtainable when $E\{z_2(t)\}$ is a monotone function of t, i.e., $E\{z_2(t)\}$ has the same sign for all $t > 0$. Sink rate $z_2(t)$ satisfies this condition. Consider a given time t. From Eq. (185) we can evaluate $E\{z_2(t)|t = T_d\} \triangleq \hat{z}$; we wish to determine $p(z(T_d))$ evaluated at $z(T_d) = \hat{z}$. The probability that $z(T_d)$ lies between $\hat{z}$ and $\hat{z} + dz$ is equal to the probability that touchdown occurs between time t and $t + dt$ since $z_2(t)$ is monotone in t. Thus,

$$p(z(T_d))\Big|_{z(T_d) = \hat{z}} = p(T_d)\left|\frac{dt}{dz_2}\right| = \frac{p(T_d)}{\left|E\{z_2(t)\}\right|} \tag{189}$$

Eq. (189) will be used to compute the probability density of $\dot{h}$ at touchdown.

IV. MODEL RESULTS

In this section, model covariance propagation results are compared with experimental data obtained on the NASA-Langley Research Center Real Time Dynamic Simulator. Three cases are studied; namely, the fully augmented STOL, the basic aircraft with autospeed and the unaugmented aircraft. Thus, we will be able to examine the effects on pilot response of the two augmentation schemes.

4.1 DESCRIPTION OF EXPERIMENTS

The experiments were conducted on the NASA Langley Research Center Real Time Dynamic Simulator. The simulation was fixed-base, and only the longitudinal flight model was simulated on the CDC 6600 digital computer with table look-ups used for the various aircraft coefficients and throttle/thrust characteristics.

The aircraft was positioned initially R = -5000 ft from the runway threshold. The pilot had to acquire the glideslope, and then trim the aircraft to maintain equilibrium flight down the 6° glideslope. Flare initiation was at h_{CG} = 53', at which point a flare initiation light came on. A "get ready" light came on at approximately 5 sec prior to flare initiation. The flare geometry is shown in Figure 4. The pilot was instructed to land the aircraft, and no go-arounds were permitted. Only the basic set of instruments were available for landing the aircraft: pitch attitude indicator, altimeter, sink rate, and airspeed dials. No external visual cues were provided.

4.1.1 Data Analysis

Ten flights of each of the three conditions

- Fully Augmented Aircraft
- Autospeed System Only
- Basic Aircraft

were made in sequence. Flare (and approach) data consisted of the sampled time histories of all pertinent system variables to touchdown. The sampling time was .25 sec during flare. Data from only one pilot was provided for validating the model developed in the present effort.

Ensemble statistics were computed for various flight quantities during flare. For a given variable, x, the sample mean and standard deviation as functions of time were computed according to

$$\bar{x}(t_i) = \frac{1}{N} \sum_{k=1}^{N} x_k(t_i) \tag{190}$$

$$\sigma_x(t_i) = \left[\frac{1}{N} \sum_{k=1}^{N} x_k^2(t_i) - \bar{x}^2(t_i) \right]^{\frac{1}{2}} \tag{191}$$

where $x_k(t)$ is the k^{th} sample path and where N is the total number of sample paths ($N = 10$). For convenience, we define $t = 0$ to be the time at which the aircraft is at $h_{CG} = 53'$.

For the augmented STOL, the ensemble mean and RMS were computed for sink-rate ($\dot{h}$), throttle (T_c), total thrust (T). For the autospeed and unaugmented cases, additional statistics were also computed for pitch angle (θ) and tail deflection (δt). In the following section, these human-generated statistics are compared with the model predictions. However, it should be borne in mind, when viewing the comparisons, that because of the relatively low number of sample paths averaged, the variance in $\bar{x}(t_i)$ and $\sigma_x(t)$ is high.* Therefore, these experimental quantities can only be viewed as approximations to the true ensemble statistics.

*The variance in the sample mean and RMS decreases as $N^{-\frac{1}{2}}$. Thus, with $N = 10$, any one sample path can have a pronounced effect on the resultant ensemble statistics.

4.2 MODEL-DATA COMPARISONS

In this section, model covariance propagation results, obtained using the expressions derived in Section 3.2, are compared with ensemble statistics computed from the pilot-simulator data. In addition, probability densities of touchdown time and sink-rate at touchdown (Eqs. 187 - 189) are presented. The model predictions have been generated using the model parameters as chosen a priori in Section 3.4. Thus, the model results are a priori predictions, and not the consequences of model-data matching.* After presenting the results for the three different STOL configurations, model attributes and deficiencies will be discussed indicating possible changes in the a priori parameter values and the model structure.

4.2.1 Fully Augmented STOL

With both the autospeed and pitch hold systems engaged, it might be expected that the pilot is capable of controlling the aircraft with minimal flight path dispersions. Figure 5 shows $h_{CG}(t)$ for each of the ten data trails, i.e., a scatter diagram of $h_{CG}(t)$. vs. t. The dashed lines enclose the model's predicted 95% confidence limits on altitude dispersion,

$$\Delta h(t)\Big|_{95\%} = [\bar{h}(t) - 2\sigma_h(t),\ \bar{h}(t) + 2\sigma_h(t)] \tag{192}$$

where $\bar{h}(t)$ and $\sigma_h^2(t)$ are the model predictions of mean altitude and variance at time t.** For $t > 4.9$ sec, which is the nominal touchdown time, model predictions are obtained by setting $u_{nom}(t) = u_{nom}(4.9) =$ constant, since $\dot{u}_{nom}(4.9) = 0$.

---

*Indeed, Systems Control, Inc. did not receive the NASA data until after model predictions were generated.

**Since h(t) is assumed to be a Gaussian random variable, the 2σ band about the mean is the 95% predicted confidence limit.

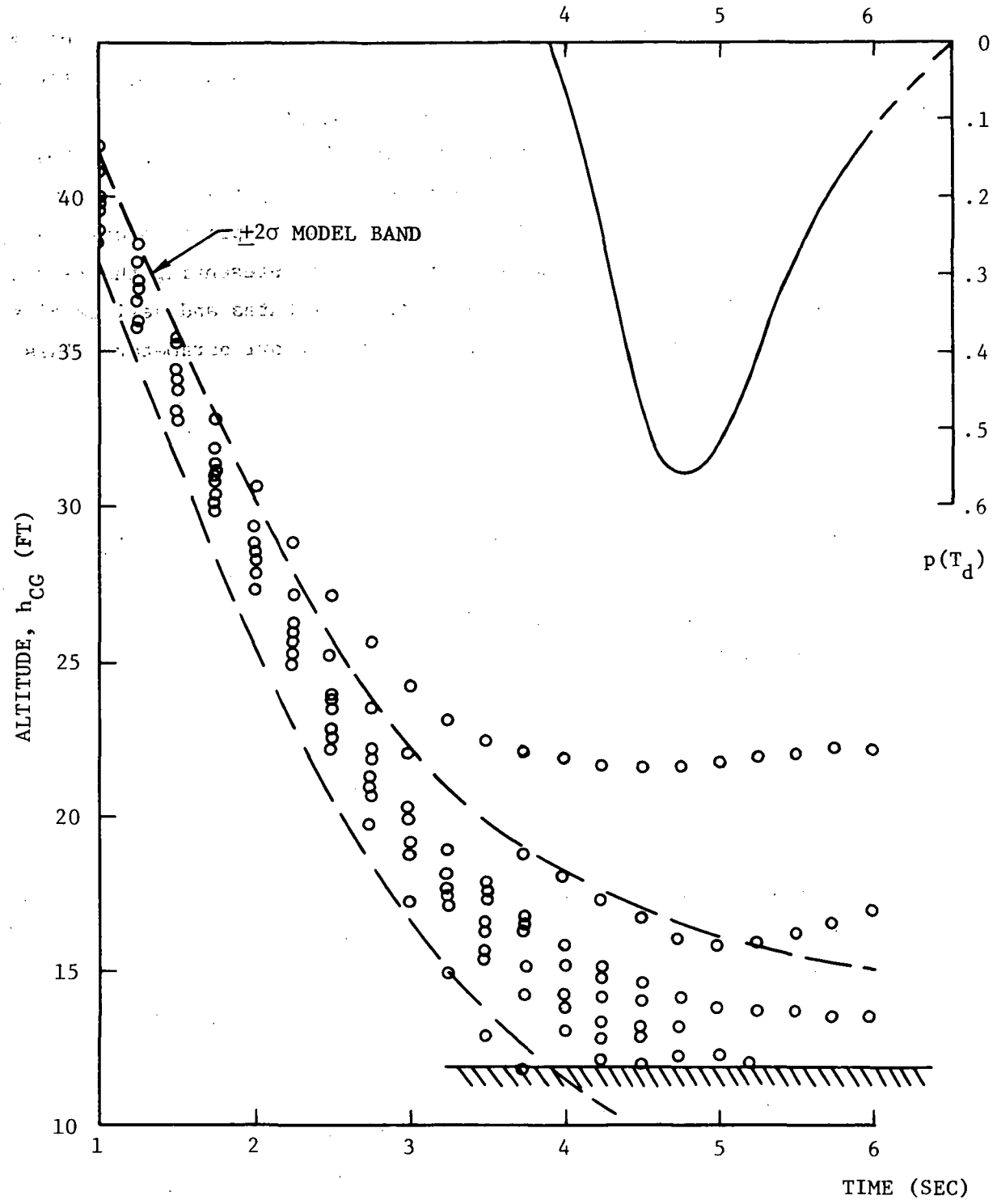

FIGURE 5 FLIGHT PATH DISPERSIONS, AUGMENTED STOL

As can be seen in Figure 5, model and data dispersions are in general agreement, with the pilot showing a somewhat greater tendency to overflare. Three flights have not yet terminated by $t = 6$ sec, and one trajectory is on the outer limits of any distribution. The probability density $p(T_d)$ of touchdown time (Eq. (187)) for $T_d \leq 6.5$ is superimposed on the dispersion diagram. This density is non-Gaussian. $p(T_d)$ increases rapidly for $t > 4$ sec and has a well defined peak between $4.25 < T_d < 5.5$, indicating a high likelihood of touchdown in this time interval. As t increases, $p(T_d)$ decreases more slowly, indicating a somewhat greater tendency to land long as opposed to landing short. Because of the low number of sample runs, a histogram of T_d was not computed for comparison with the predicted $p(T_d)$.

The probability of landing prior to $t = \hat{T}$ sec is given by

$$\Pr\{T_d \leq \hat{T}\} = \int_0^{\hat{T}} p(T_d)dT_d \triangleq P(\hat{T}) \tag{193}$$

The value of $\hat{T}$ such that $P(\hat{T}) = 0.5$ is defined as the median touchdown time, and must coincide with the touchdown time of the mean flight path $\bar{h}(t)$.* For this case the median touchdown time is 5.15 sec. We note that this is <u>not</u> equal to the average touchdown time due to the asymmetry of $p(T_d)$. Evaluating the integral (193) for $\hat{T} = 5.9$ and $\hat{T} = 6.5$ yields $P(5.9) = 0.69$ and $P(6.5) = 0.73$, respectively. This indicates that approximately 30% of all flights are predicted to land more than one second later than the nominal $T_f = 4.9$, and approximately 25% land more than 1.6 seconds late. Translation into range at touchdown ($R_{td} = V_o T_d$) implies an approximate 0.25 probability of overflaring the touchdown zone. It should be emphasized again that model predictions are not valid much beyond $t = 6.0$ sec. Once a pilot realizes that he is about to overflare his (cost functional and) control strategy may change drastically, e.g., diving for the deck, cutting all power, etc. Thus, although the model predicts that 30% of all flights land at $T_f > 6.0$ sec, the existing model cannot predict the subsequent pilot control inputs.

*Since the density of $h(t)$ is Gaussian, it is symmetric about its mean.

Figures 6 and 7 compare model and data sink rate, throttle input and resultant thrust. Model predictions consist of the mean (solid line) and the $\pm 1\sigma$ band about the mean (dashed line). The pilot data consists of the ensemble mean (Eq. (190)) and the $\pm 1\sigma$ ensemble deviation (Eq. (191)) at .25 sec intervals. The model and pilot data are in reasonable agreement. The pilot's mean response generally lies within the 1-sigma band of the model predictions. The model and data standard deviations agree generally within a factor of two. Model and pilot sink-rates agree within 0.5 ft/sec over the entire flare. Note that the average pilot sink-rate at $t \cong 0$ is -13.6, which is slightly greater than the assumed nominal of -13.2.

Both model and pilot throttle inputs increase rapidly during the first .5 sec. This is primarily in response to the initial estimate of the C_L ground effect. The pilot's commanded T_c continues to increase for $.5 < t < 1$ whereas the model does not show this trend. Possible reasons for this slight discrepancy include the slightly greater pilot initial sink-rate as noted above, an initial pilot estimate of C_L greater than the -.09 assumed in the model, (or an a priori pilot estimate of both C_L and an initial rate of change $\dot{C}_L$),* or slight differences between the actual throttle/thrust characteristics and the simplified first-order lag assumed in Eq. (66). On the average, the net throttle input of the pilot is slightly greater than the model's, yielding a pilot sink rate approximately .5 ft/sec lower than the model as touchdown approaches.

The basic assumption in modeling the terminal time aspects of the landing task was that in the absence of all external disturbances, the pilot would generate a minimum rate open-loop control input that met the terminal state conditions. In the presence of external disturbances, the pilot would then try to regulate about the so-generated nominal flight path. The pilot data provides an opportunity to validate this hypothesis. Figure 8 shows the sink-rate and throttle for the nominal flight path (solid curve), mean model predictions that

*Section 4.3.1 discusses the effects on model predictions of other characterization of C_L, specifically allowing the pilot model to continually estimate both C_L and its rate of increase.

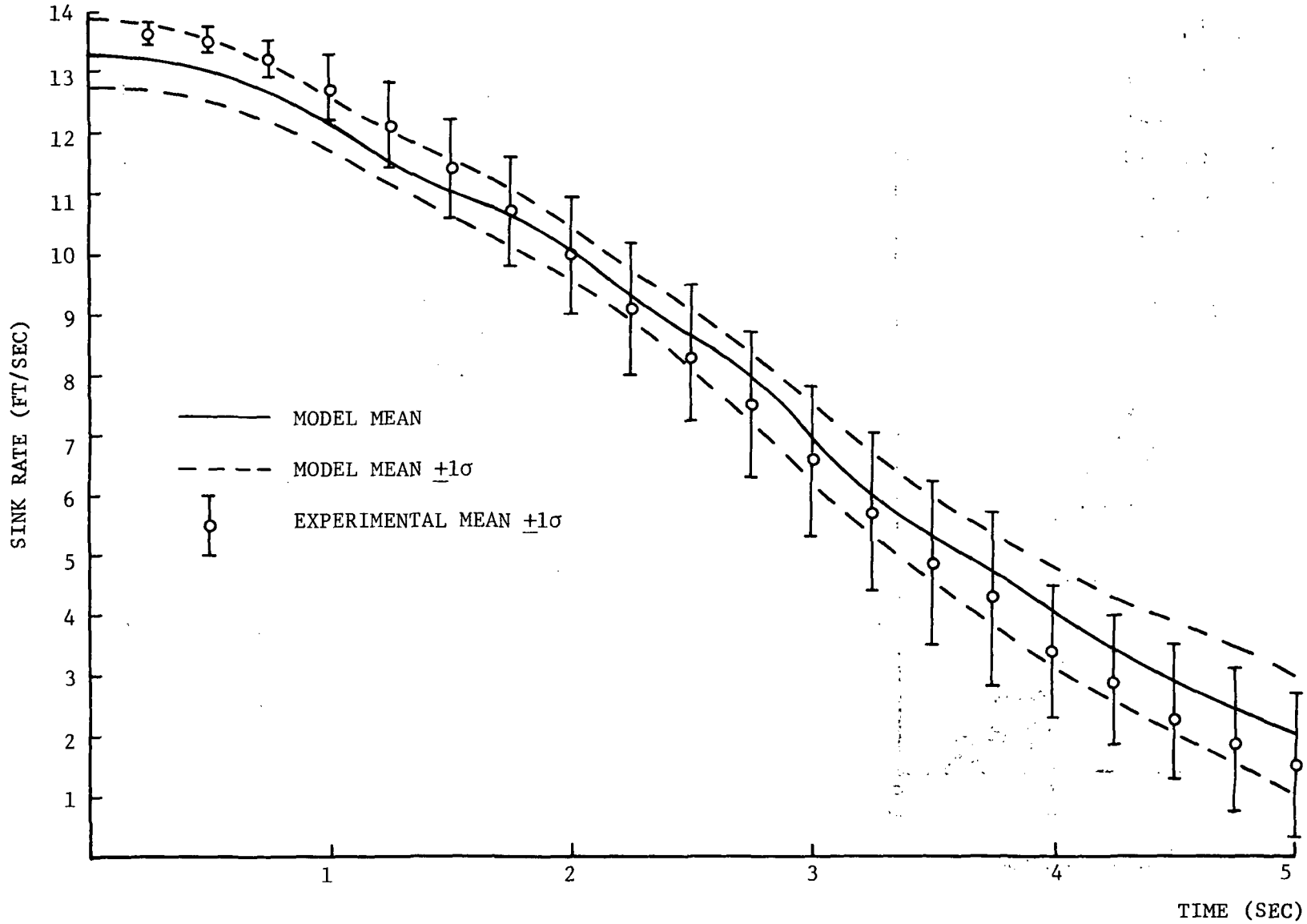

FIGURE 6 SINK RATE, AUGMENTED STOL

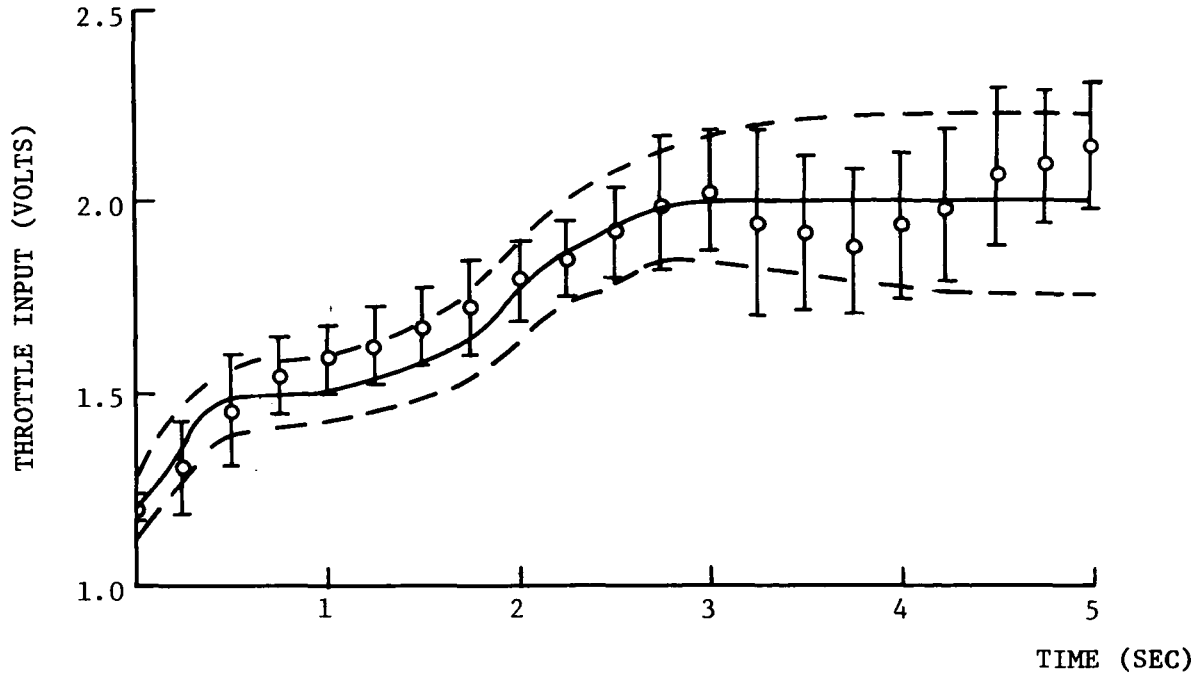

a) Commanded Throttle Input

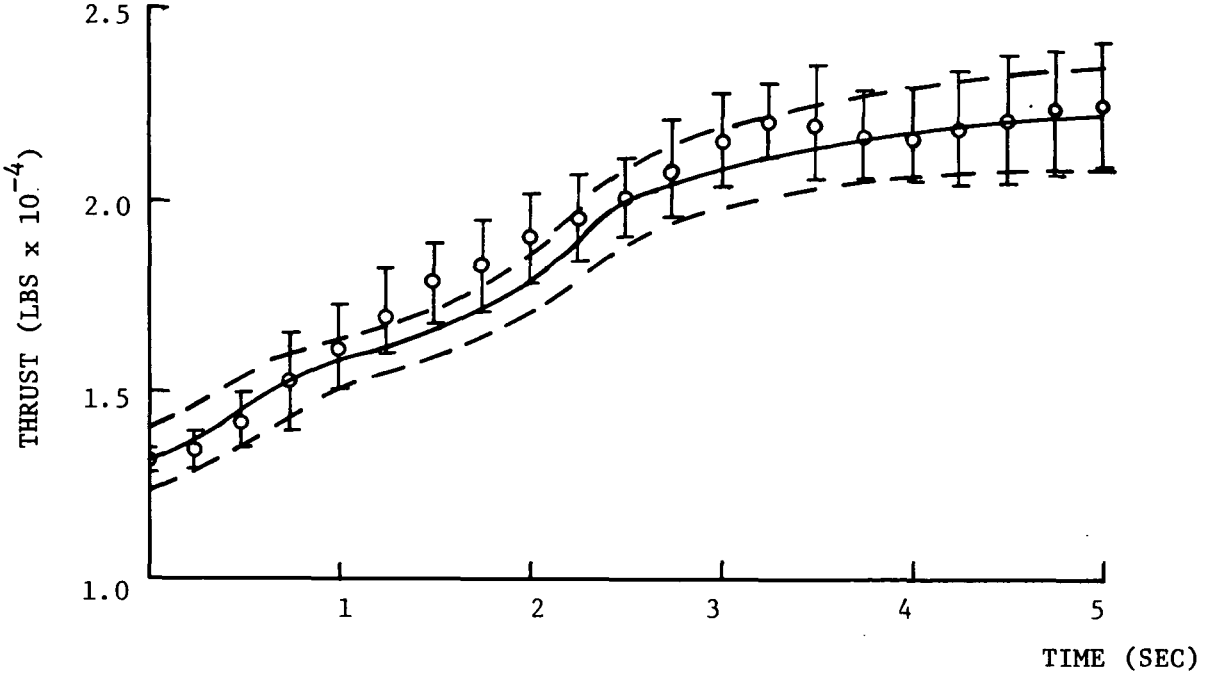

b) Engine Thrust

FIGURE 7 THROTTLE/THRUST INPUTS, AUGMENTED STOL

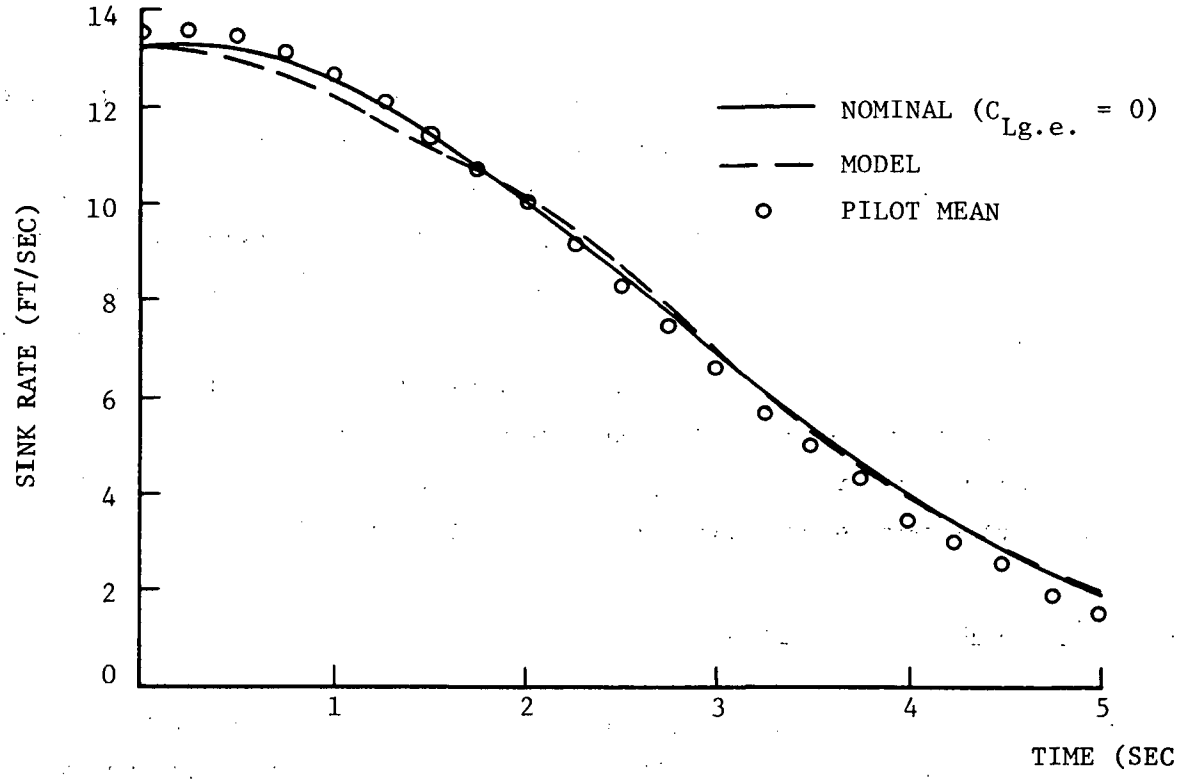

a) Sink Rate Deviations

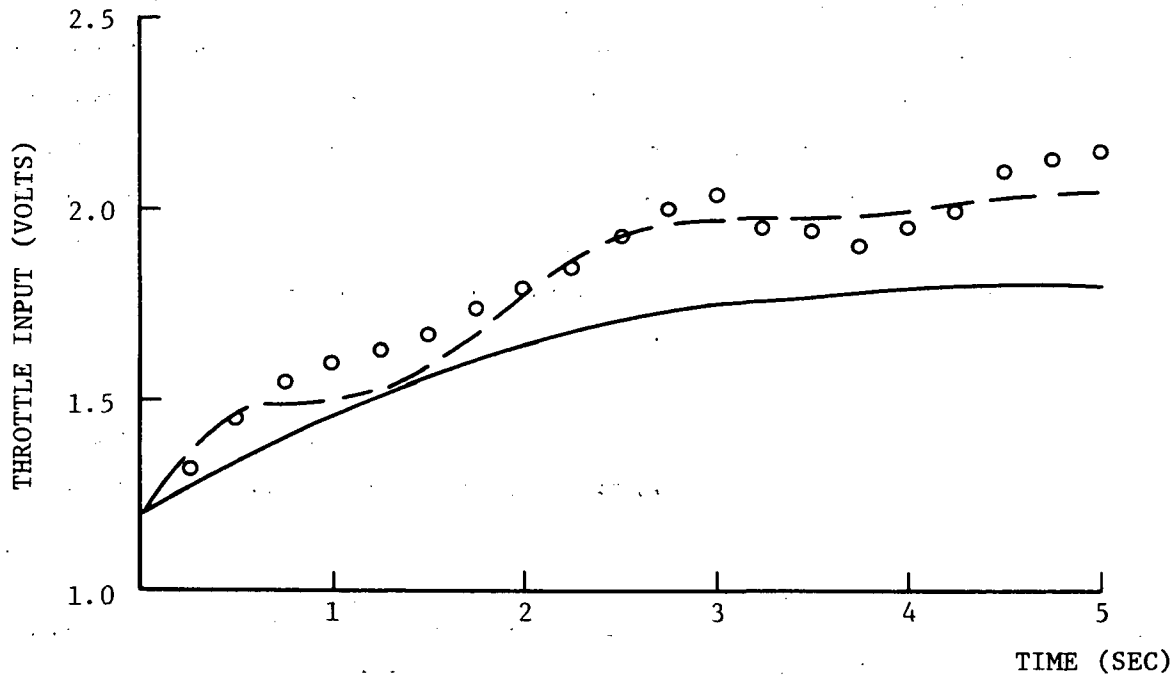

b) Commanded Throttle Input

FIGURE 8 REGULATION ABOUT NOMINAL FLARE PATH, AUGMENTED STOL

include all external disturbances (dashed curve) and the pilot data ensemble average. There is an excellent agreement between the mean pilot sink rate and the nominal sink rate. This indicates that our assumption of pilot regulation about a minimal control rate nominal flight path is most reasonable. Indeed, the pilot seems to do a better job than the model in regulating disturbances about the nominal altitude path. This is probably due to the pilot's having a better internal characterization of C_L than was assumed in the model. The difference between the nominal T_c and the model/pilot T_c in Figure 8b is the additional control input T_c applied to correct for C_L. The pilot appears to have corrected more precisely, and earlier, than did the model.

4.2.2 STOL with Autospeed Only

With the autospeed system engaged, the pilot can still maintain a +2° pitch attitude on the approach. During flare, it is only necessary for the pilot to regulate the deviations in θ-2°. Consequently, it might be expected that the altitude control (i.e., flare) behavior of the pilot would not differ substantially from that observed in the augmented case. Figure 9 shows the altitude dispersions from of the sample flare paths, and the 95% model confidence band. Comparing the pilot data in Figure 9 with that of Figure 5 (discounting the one or two "strange" runs) shows a noted similarity in altitude dispersions in the vicinity of touchdown. The tighter clustering of the scatter points in Figure 9 indicates that the pilot's control strategy has probably become less variable by the time the autospeed experiments were performed.* Therefore, external effects of learning may be biasing the experimental results since the pilot's control strategy is continuing to stabilize on a run-to-run basis.

Comparing the model flight path statistics of Figure 9 with those of Figure 5, we see an almost identical variance but a mean flight path that lands

*The augmented STOL runs were the first series of 10 experiments, and no warm-up runs were made. The autospeed case was the third set of 10 experiments actually performed. An intermediate augmentation scheme involving pitch damping was also simulated. However, this case is not discussed herein. Thus, a possible explanation of the decreased variability is that by the time the autospeed-only runs were made, the pilot had "warmed-up". Obviously, this is a short-term adjustment phenomenon only.

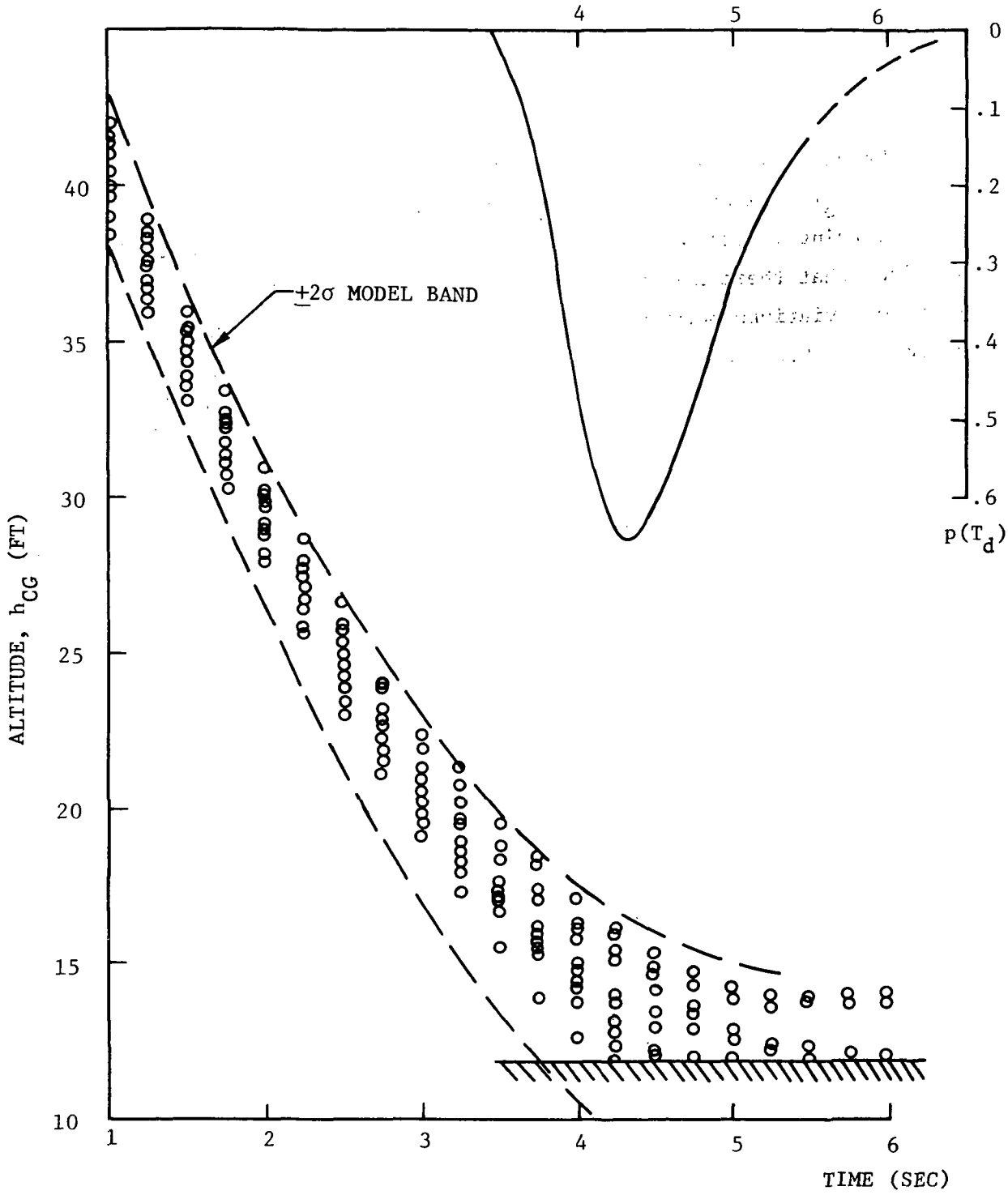

FIGURE 9 FLIGHT PATH DISPERSIONS, AUTOSPEED STOL

sooner at $t \simeq 4.7$ sec. The scatter points of Figure 9 also indicate that our prediction of altitude dispersion is reasonable, but the model is slightly low in its mean altitude and touchdown time predictions. The probability density $p(T_d)$ is also shown in Figure 9. The results are much the same as in Figure 5, but with a .5 sec shift towards earlier touchdown times. Indeed, integrating Eq. (193) with $T = 6.5$ indicates that only 20% of all flights might be expected to overflare compared with 25% in the augmented case. Unfortunately, the trend towards lower touchdown times does not appear in the pilot autospeed data.

Comparisons of model vs. data statistics of sink-rate, throttle input and thrust are shown in Figures 10, 11a and 11b, respectively. In all cases, the ensemble standard deviations are much smaller than their counterparts in Figures 5-6. This is further evidence of the reduced variability in the pilot response caused in part by underlying adjustment phenomena inherent in the experimental procedure.* The model predictions of the standard deviations $\sigma_{\dot{h}}$, σ_{T_c} and σ_T are noticeably greater than the pilot data. Several reasons for these discrepancies are:

a. The pilot may be devoting more attention to the sink-rate indicator than we have assumed. More precise estimates of $\dot{h}$ will result in less throttle variability and more accurate $\dot{h}$ control.

b. Cost functional weightings, other than the ones chosen, may be more representative of pilot behavior. For example, weighting $y_2 = \delta\dot{h}$ or $y_3 = \delta\ddot{h}$ in the cost functional would have a very pronounced effect on reducing both throttle and sink-rate variability.

c. A lower value of the motor-noise ratio ρ_u may be appropriate. This will result directly in less control input variability, and, hence, less closed-loop randomness.

---

*Indeed, with "equal" training in both augmented and autospeed landing tasks, one would expect the pilot to show a greater variability in the latter since it is a somewhat more difficult overall task. It is implicitly assumed that the pitch-hold augmentation is working properly (i.e., $q \simeq 0$), and that adverse interaction between pitch-hold augmentation and pilot control is minimal during flare, allowing, in effect, pitch-loop decoupling.

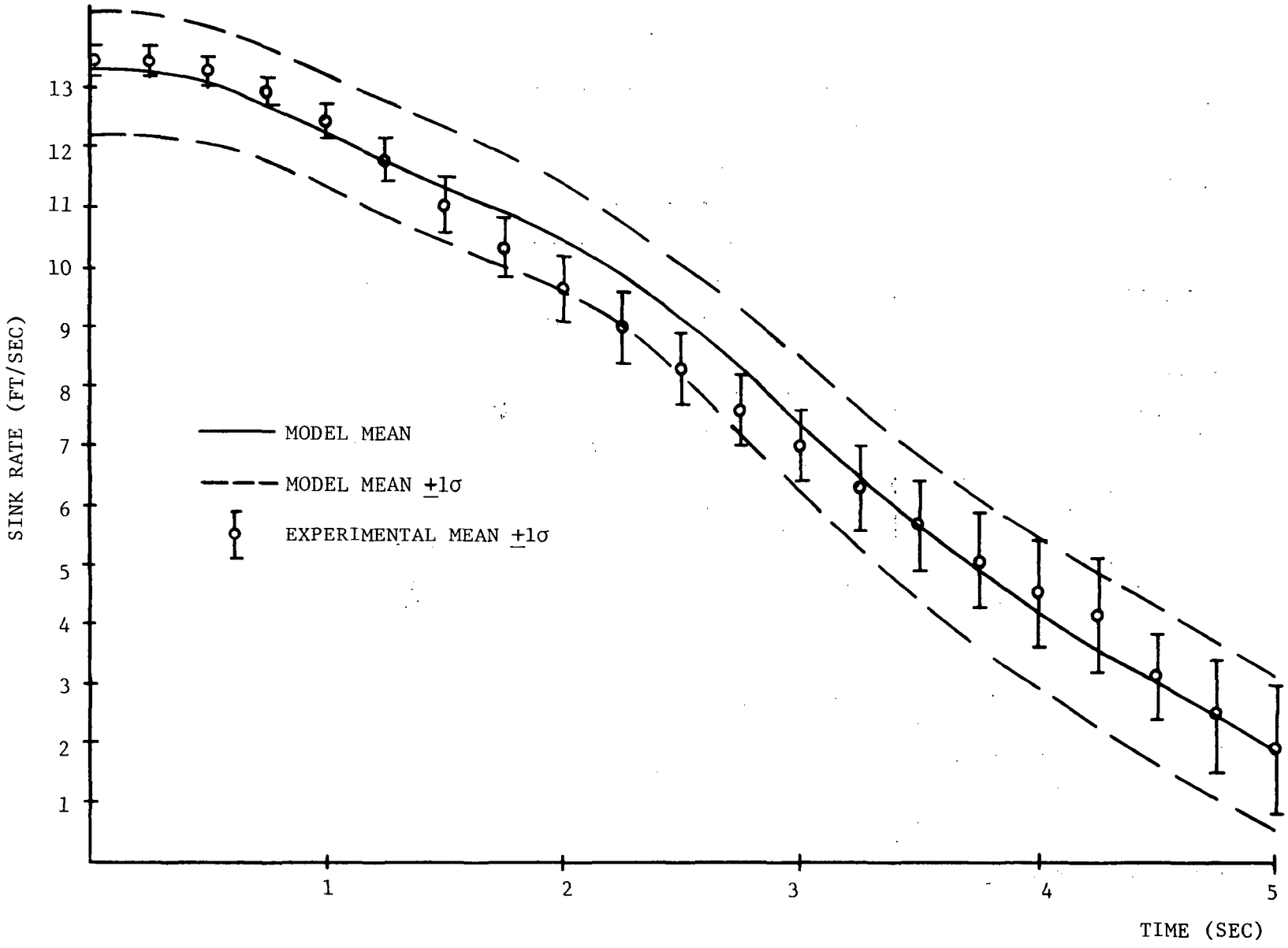

FIGURE 10 SINK RATE, AUTOSPEED STOL

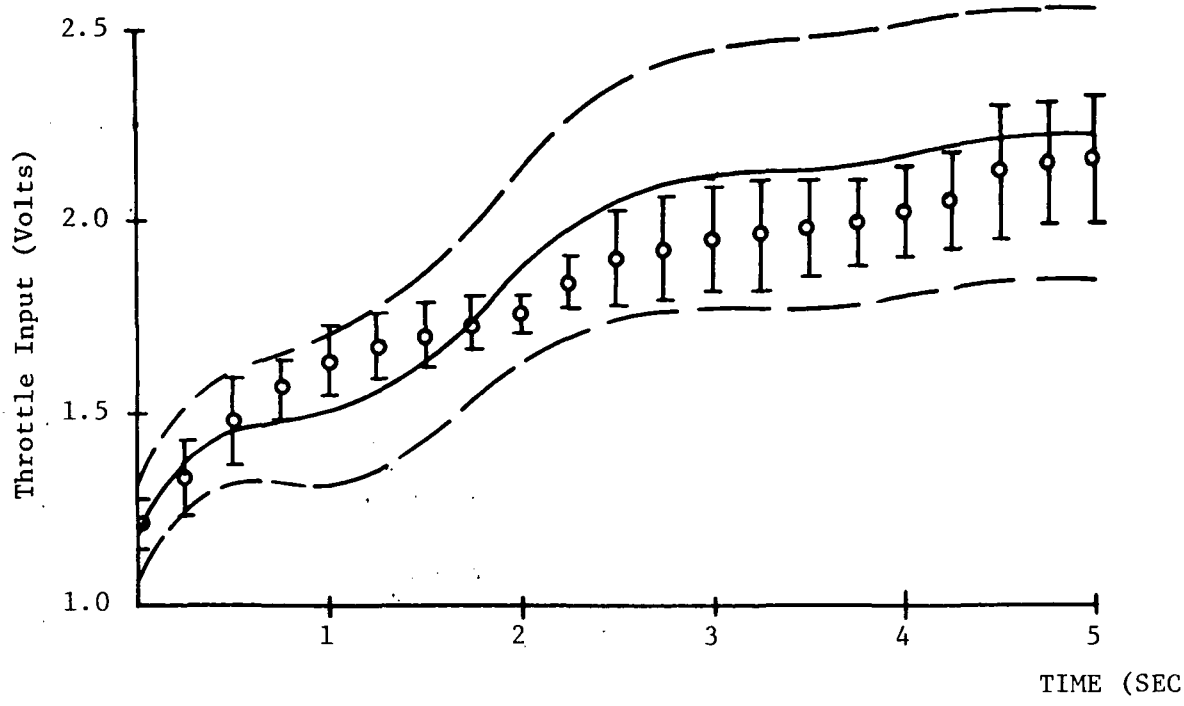

a) Commanded Throttle Input

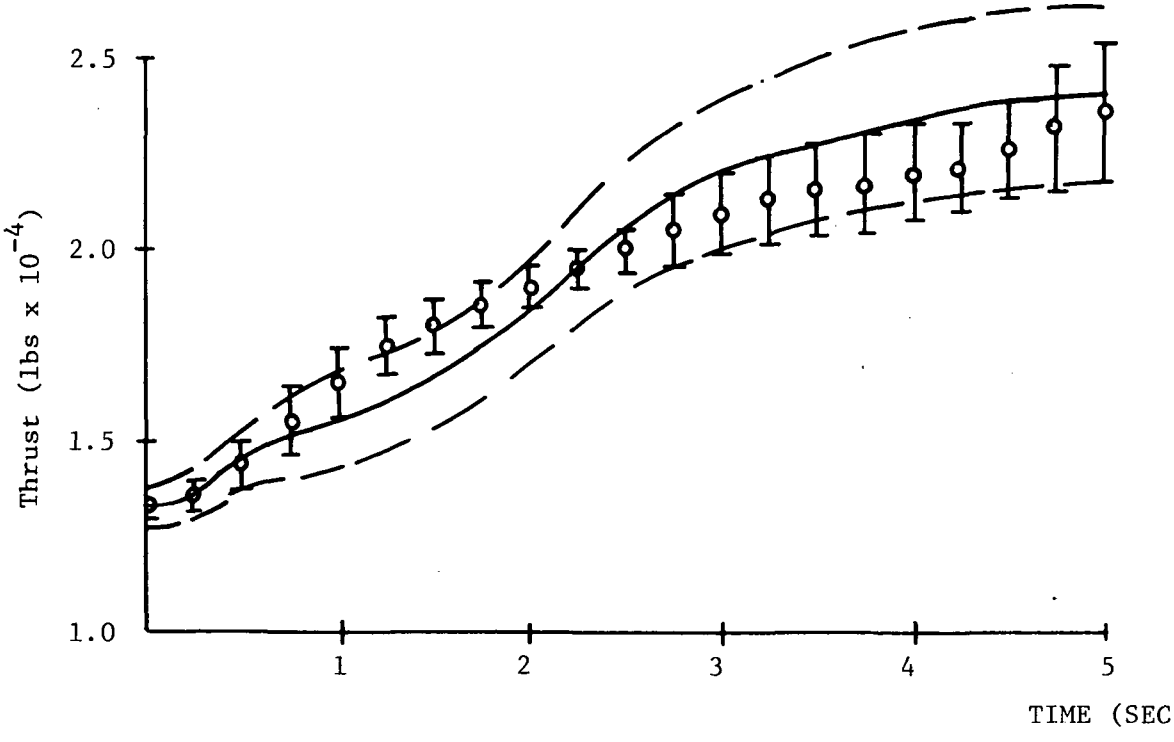

b) Engine Thrust

FIGURE 11 THROTTLE/THRUST INPUTS, AUTOSPEED STOL

d. A larger value of T_n may be appropriate for the specific pilot. This would lower the bandwidth, and, consequently, the power, of the injected motor noise (see Eq. (97)).

Items (c) and (d) suggest that a reexamination of the model's treatment of motor noise is in order. In fact, other applications of the human modeling techniques to study time-varying problems have arrived at similar conclusions.[5]

Comparison of the model mean with the ensemble average for $\dot{h}$, shows a well-defined difference between model and pilot response. For $1.5 < t < 3$ sec, the model's sink rate is considerably (.3 - .8 ft/sec) higher than the pilot's. This difference arises from the higher level of pilot thrust (yielding more lift) between $.75 < t < 2$ sec as shown in Figure 11b. For $t > 2$ sec, the model must correct the compounded effects of the high sink-rate and more thrust is applied to put the aircraft back onto its nominal flare path.* The net result, as seen, is that the model's mean flight path lands somewhat earlier than the nominal. The cause of the model's behavior can be traced directly to its estimate of the C_L ground effect. The model corrects for its initial estimate $C_L = -.09$, but does not anticipate a further increase in C_L until 1 sec later--when the effects of the $C_{L,ge}$ are eventually observed in $\dot{h}$, $\delta\dot{h}$ and $\delta\ddot{h}$. Correction for $C_{L,ge}$ is, therefore, applied late. The pilot, on the other hand, seems to be aware earlier of the ground effect. He compensates earlier and needs to generate less lift nearer the ground.

The comparisons of both the average pilot response and the mean model response with the nominal sink rate are striking. Figure 12 shows that the pilot is doing an excellent job of regulating $\dot{h}$ about the open-loop model-generated nominal. Our basic assumption that the pilot regulates about a "least workload" (minimum $\dot{u}$) nominal flight path is demonstrated convincingly for the second time. However, our model for how this regulation task is accomplished, and how the pilot compensates for $C_{L,ge}$ needs modification. In Figure 12b,

*We see here the interplay between the open-loop generation of a "nominal" flare path, and the closed-loop requirements to minimize deviations from this flight trajectory.

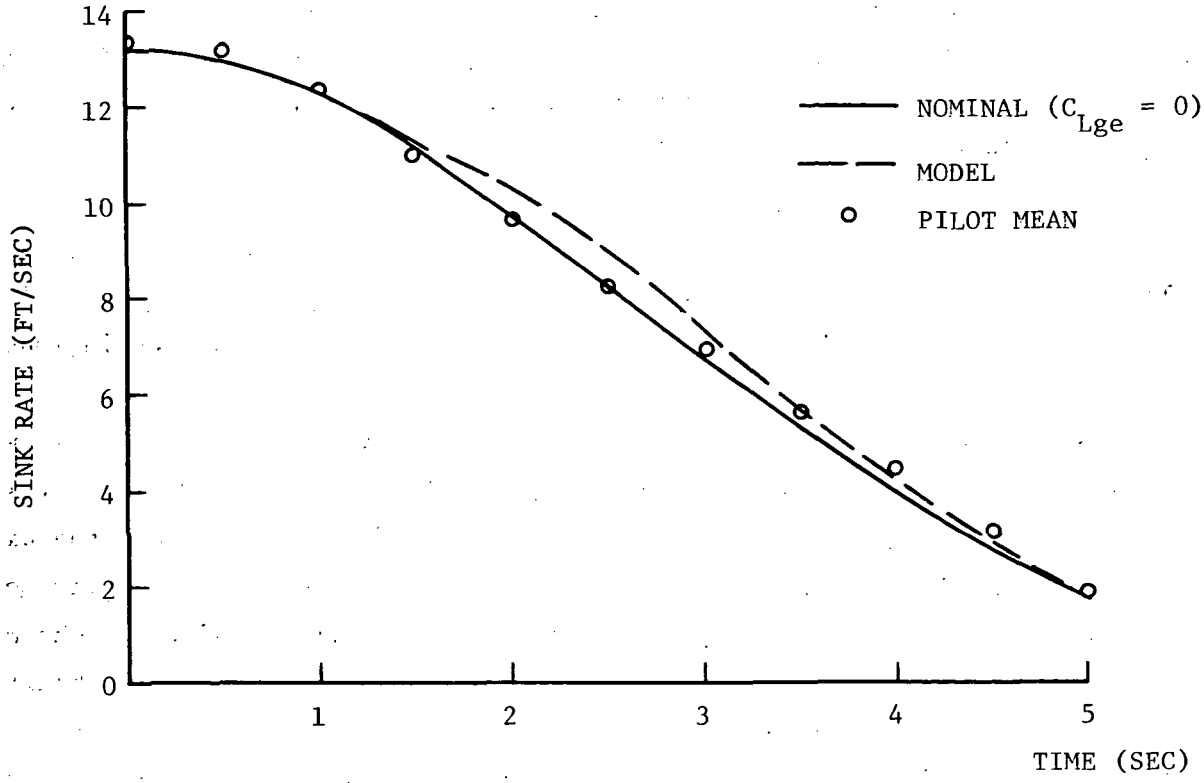

a) Sink Rate Deviations

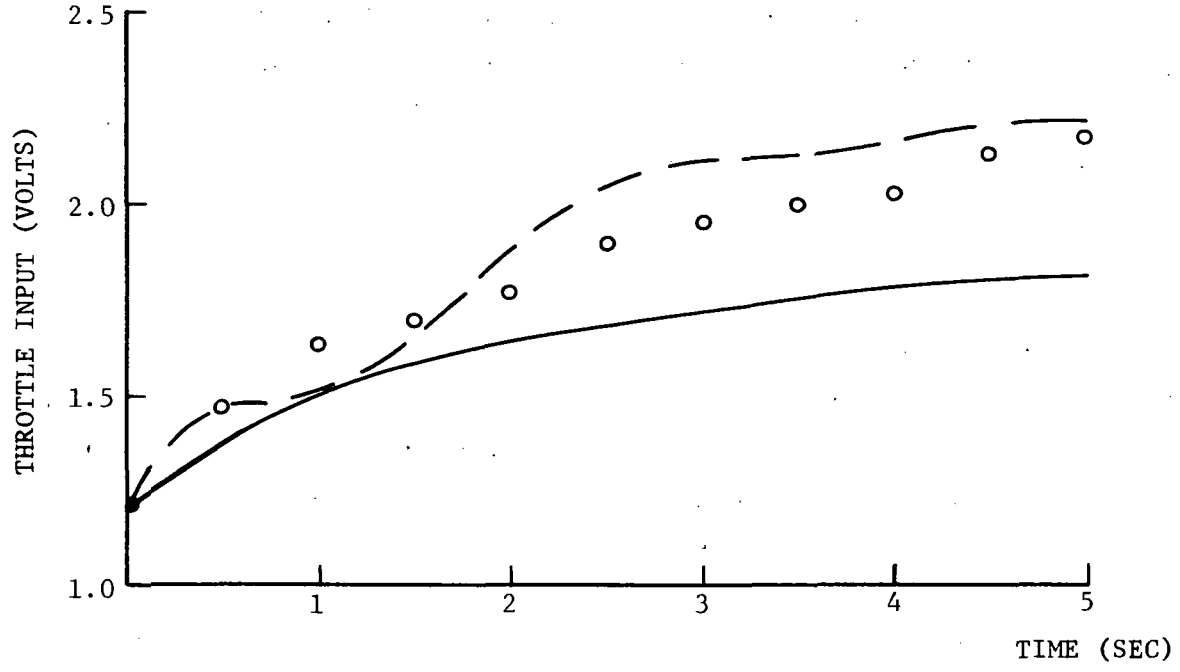

b) Commanded Throttle Input

FIGURE 12 REGULATION ABOUT NOMINAL FLARE PATH, AUTOSPEED STOL

the additional throttle inputs δT_c needed to counterbalance C_L indicate that the model requires a larger initial estimate of C_L, or an estimate of C_L that increases with time, to generate a control input that would match the pilot's.

The aspects of the pitch regulation task are shown in Figure 13. It is apparent that the pilot has devoted little, if any, attention to regulating pitch about the 2° nominal. The elevator input is essentially held constant during the flare. Pitch excursions are highly variable. The model predictions also show virtually no elevator input to regulate θ which is predicted to decrease to 0.5° at touchdown. The major difference between pilot and model pitch response lies in the variance. The most plausible reasons why pilot variability is larger than the model's are the following:

a. The pilot is probably devoting most of his attention to the altimeter and/or rate-of-sink instruments. Therefore, the observation noise on θ and q would be higher than the -15dB assumed, resulting in poorer estimates of pitch deviations and, consequently, less control of them. The fact that pilot variability of h, $\dot{h}$ are lower than the model, while variability of θ is greater than model predictions gives further evidence to greater pilot attention to altitude control.

b. The pilot's strategy in controlling θ may show a run-to-run variability. Indeed, the sensitivity of model predictions with respect to changes in the cost functional weighting on $\delta\theta^2$ is high and can account for the observed variability. The nominal weighting on q_θ is .25. Varying q_θ over the range $.25 \pm .25$ results in pitch angles at touchdown between $0.5 \pm 1.0°$, yet has little effect on other model predictions. The high sensitivity of θ to small variations in pilot response (caused by the poor inherent pitch damping of the STOL) is one reason for the poor pilot rating.[1]*

*In past applications of the optimal control model to pitch regulation tasks, only pitch rate was included in the pilot's cost functional. The fact is that with $q_\theta = 0$, pitch deviations are -2.5°, which indicates a serious handling quality deficiency. Thus, the pilot must adopt a pitch regulation strategy somewhat different from his "usual".

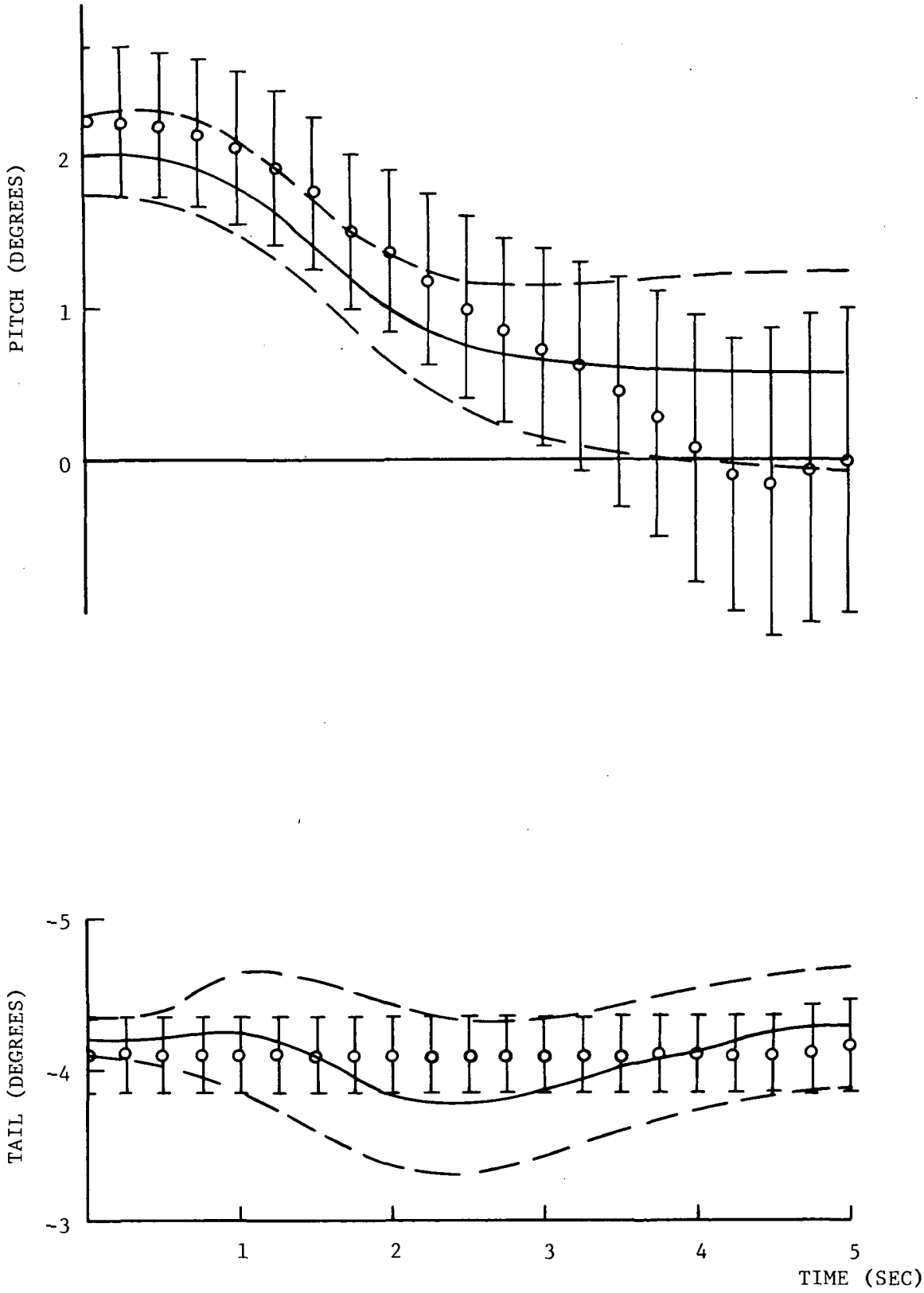

FIGURE 13 PITCH CONTROL RESULTS, AUTOSPEED STOL

4.2.3 Unaugmented STOL

The model predictions and pilot data for the unaugmented STOL are shown in Figures 14 - 17. From the results, it is apparent that: (a) the aircraft is near impossible to fly, or (b) the pilot is not well-trained on this task. The fact that the model seems to control the aircraft is evidence of the latter. The flight path dispersions are shown in Figure 14. Only eight trajectories are shown, yet it is apparent that pilot variability is exceptionally high, with a marked tendency to overflare. The model predicts a higher variability in altitude dispersions for the basic STOL configuration than in the preceeding cases. The model's median touchdown time, however, is only 4.65, i.e., the model shows a tendency to land early, as in the autospeed case. The probability of landing at $t > 6$ sec is only 0.2; this seems low in view of the observed pilot trajectories.

Sink-rate and throttle inputs are shown in Figures 15-16, respectively. Pilot variance is extremely high, about twice as great as the model predictions. The large variance leads to the belief that pilot strategy is highly variable on a run-to-run basis, so that the effects of learning have not yet stabilized. Unfortunately, it is not possible, at the current state-of-the-art in man-machine modeling, to predict the degree of training a pilot needs before his control strategy stabilizes. The given pilot data does seem to violate the underlying assumption in the optimal control model--that the pilot is well-trained.

Comparing the mean sink-rate and throttle input for the pilot and model shows that the pilot is probably overcorrecting for $C_{L,ge}$, whereas the model is undercorrecting. This results in larger pilot throttle inputs and lower sink-rates than the model, and a subsequent tendency for the pilot to overflare. (Note the rapid pilot attempt to compensate for $t > 3$ sec.)

Pitch angle and tail input are shown in Figure 17. The basic aircraft approaches the flare window in a -4° nose-down attitude. The pilot is required to (try to) land with a positive 2° pitch. Neither the pilot nor the model is capable of achieving a nose-up attitude at touchdown. The pilot data shows

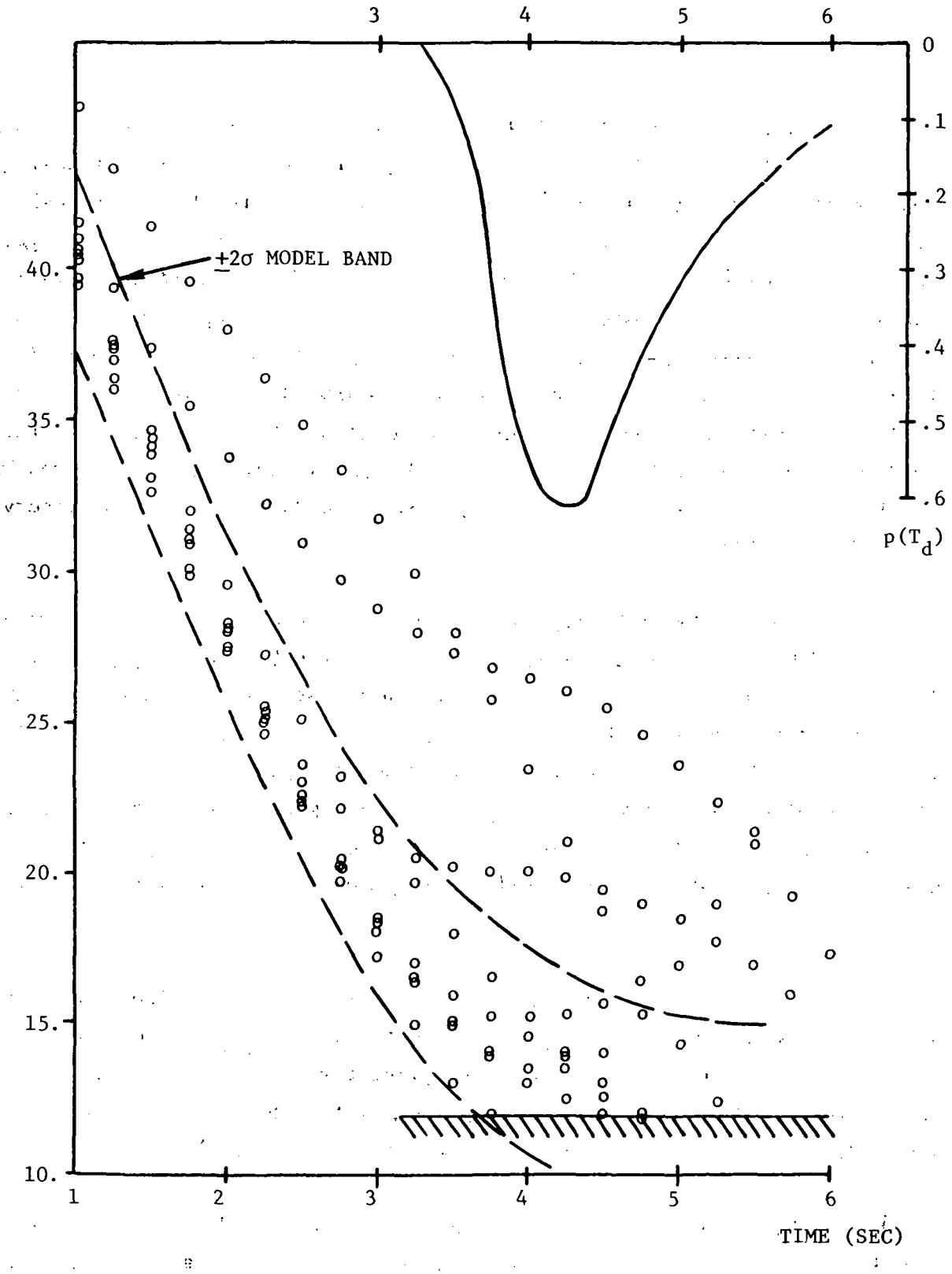

FIGURE 14 FLIGHT PATH DISPERSIONS, UNAUGMENTED STOL

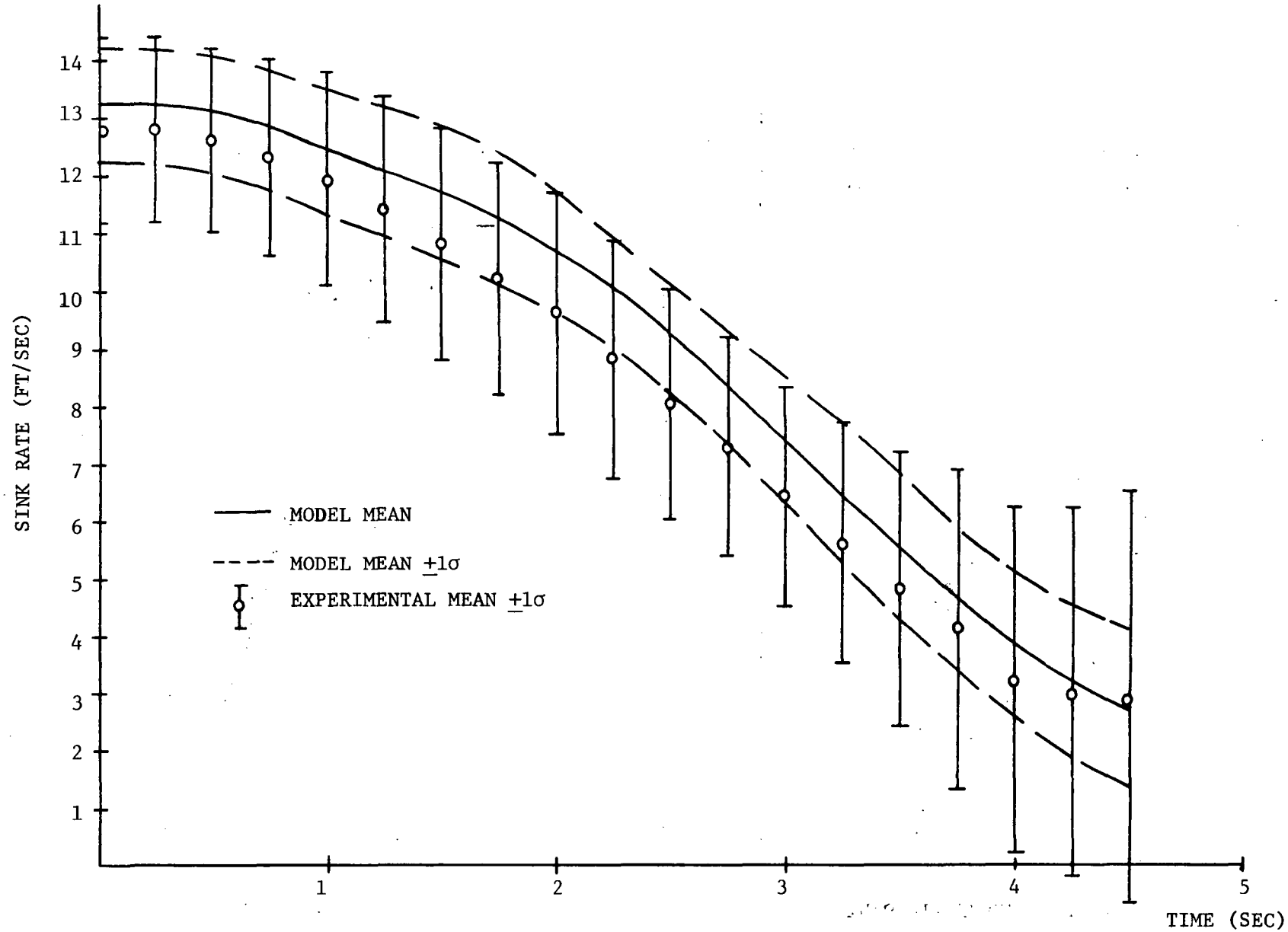

FIGURE 15 SINK RATE, UNAUGMENTED STOL

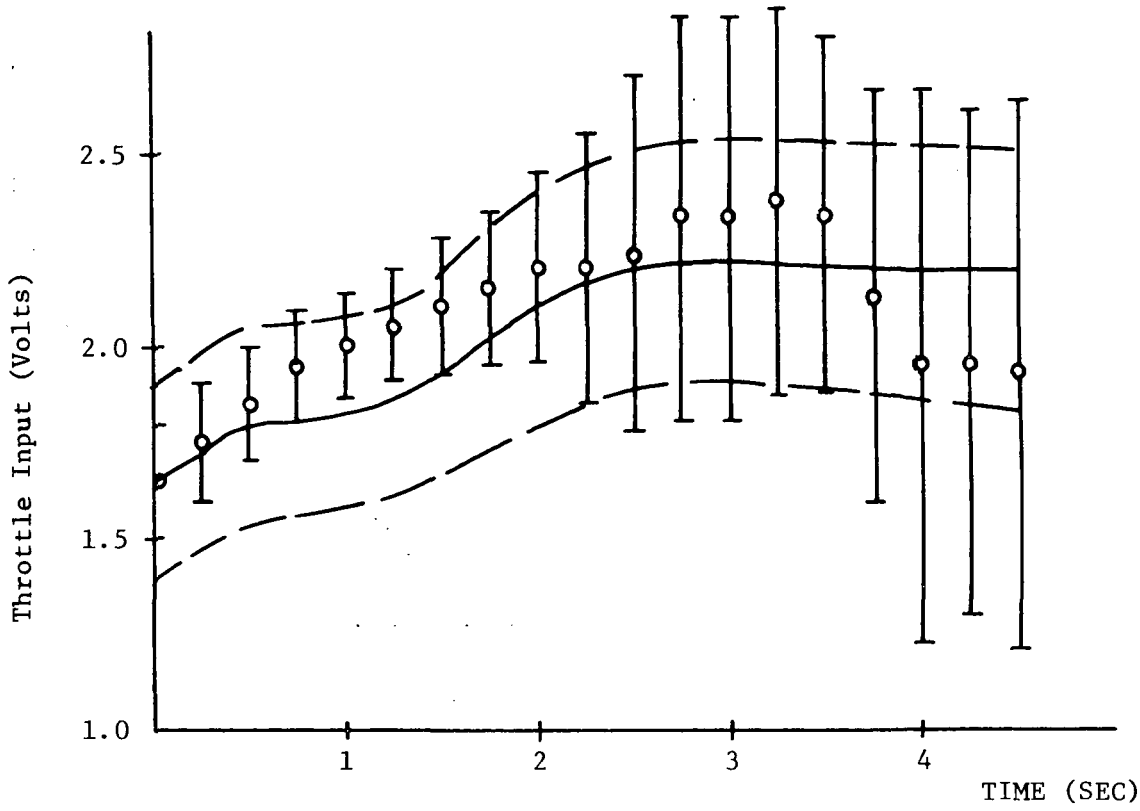

a) Commanded Throttle Input

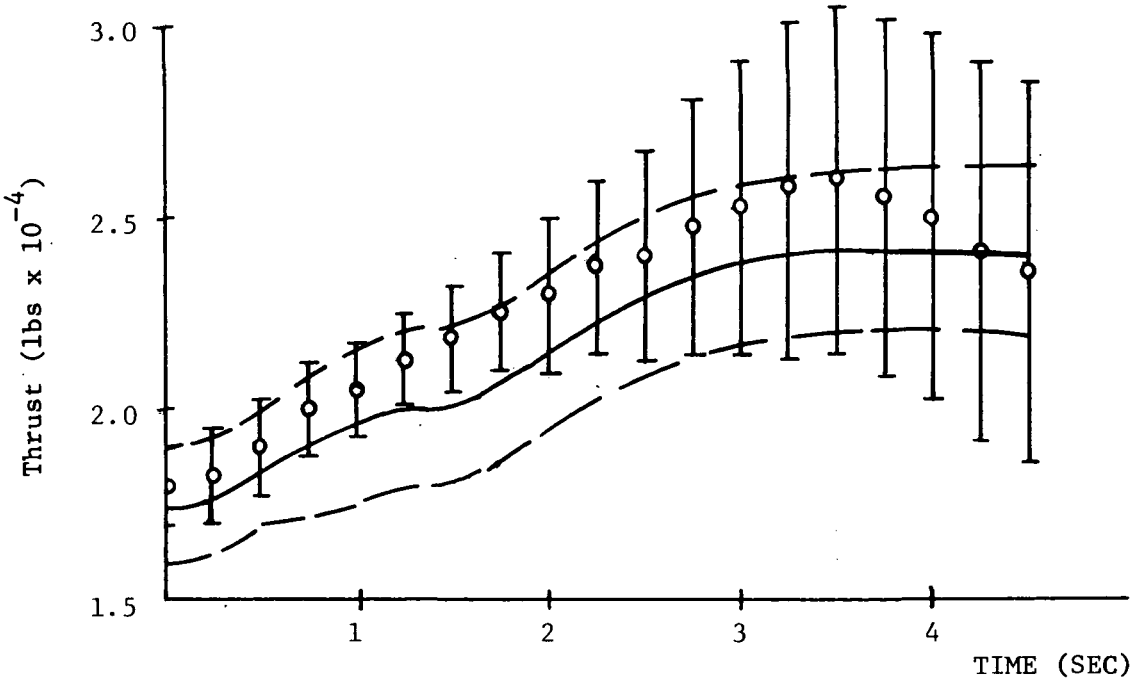

b) Engine Thrust

FIGURE 16 THROTTLE/THRUST INPUTS, UNAUGMENTED STOL

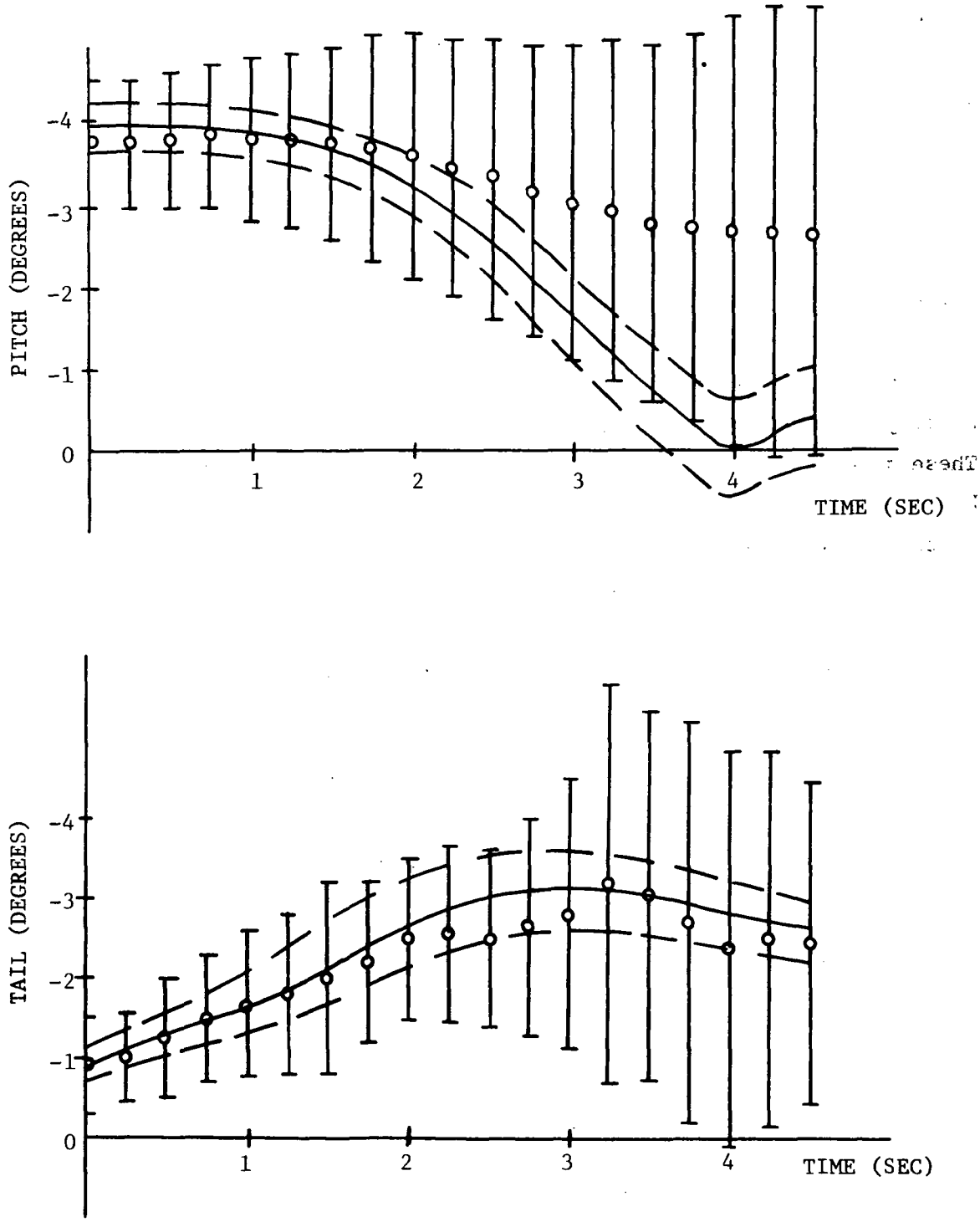

FIGURE 17 PITCH CONTROL RESULTS, UNAUGMENTED STOL

a much higher variability than does the model. The apparent reasons for this are much the same as in the autospeed case, i.e., run-to-run variability in pilot strategy and low attentional allocation to the pitch attitude indicator. The model's pitch response was found to be quite sensitive to changes in q. For example, $q_\theta = 0$ yields a model prediction $\theta_{td} \simeq -2°$. The mean tail input for both model and pilot are in close agreement with the pilot input being only 1/4° less on the average for $t > 2$ sec.*

4.2.4 Sink-Rate Predictions at Touchdown

Among the most important predictions generated by the model are the probability density of the touchdown velocity and the mean touchdown velocity. These quantities are given by Eqs. (189) and (185), respectively. It should be re-emphasized that our predictions of touchdown statistics are based only on those flight paths that terminate within approximately 1 sec of the nominal touchdown time. The one second "cutoff" has been chosen arbitrarily; for flights tending to land late, model predictions are probably not highly representative of pilot actions.

Figure 18 shows the model's prediction of the touchdown velocity probability density (conditioned on $T_d \leq 5.9$ sec) for the three STOL configurations. The comparisons are interesting. The augmented STOL density shows a well-defined peak at $\dot{h} \simeq -2.25$ ft/sec. In the autospeed case, the density peak has shifted to -3.25 ft/sec indicating the higher touchdown velocities associated with earlier landing times (see Figure 9). In addition, the density has broadened, predicting more variability in touchdown velocity. The unaugmented results show an even greater flattening of the touchdown density, to correspond with a highly variable sink-rate at touchdown.**

Because of the limited number of experimental runs that terminate prior to $t = 5.9$, it is not realistic to compute a probability density or histogram

---

*The sensitivity of θ to δt is evident by comparing the mean responses of Figure 17a and 17b.

**The density of $\dot{h}$ increases for $-\dot{h} < 1.5$ ft/sec since $\dot{h} \to$ constant $\simeq 1.35$ for $T_d > 5.4$ sec. Ideally, there would be an impulse at $\dot{h} = -1.35$ with area $\simeq .2$.

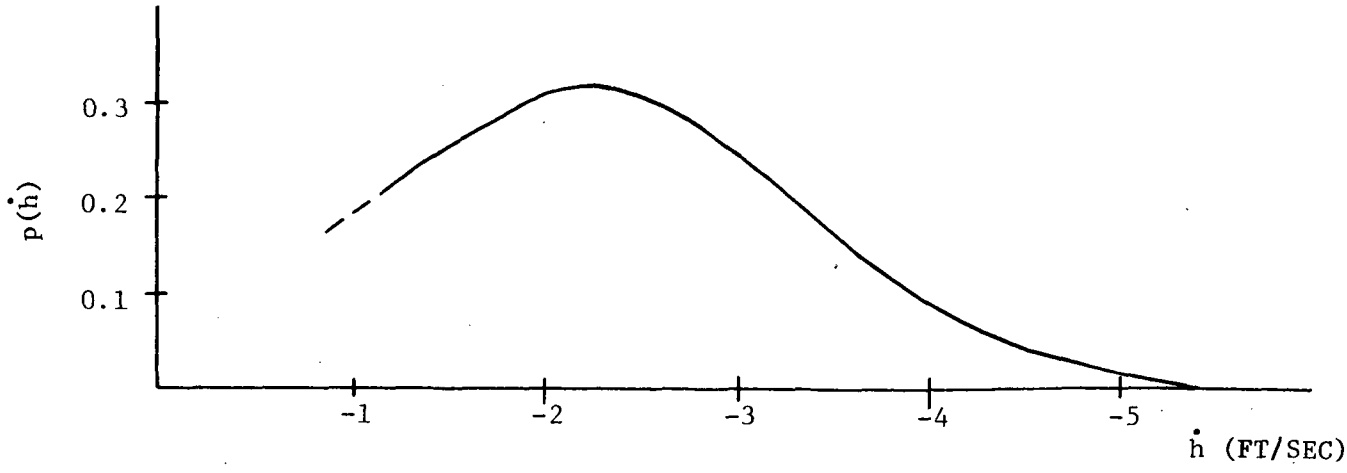

a) Augmented STOL

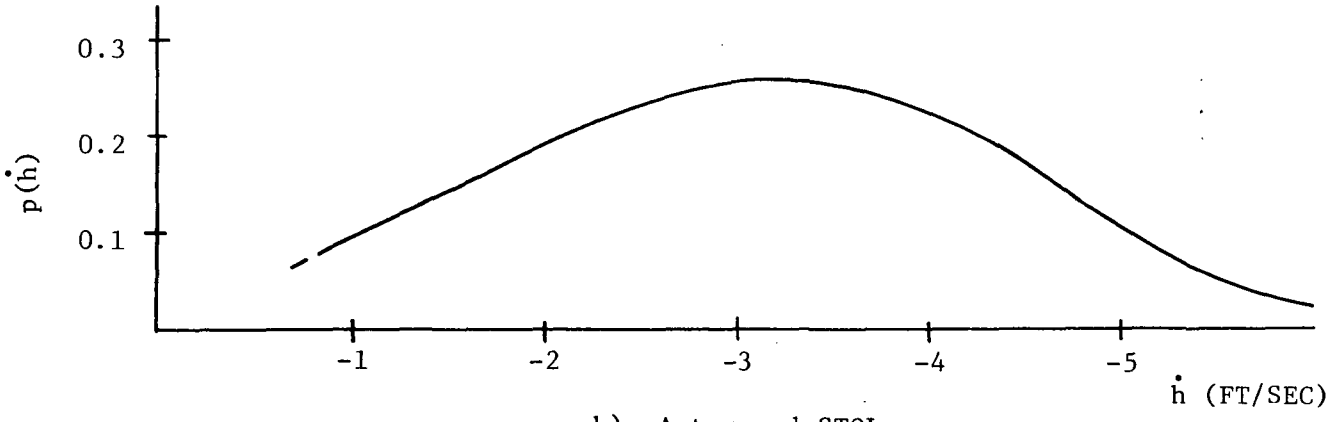

b) Autospeed STOL

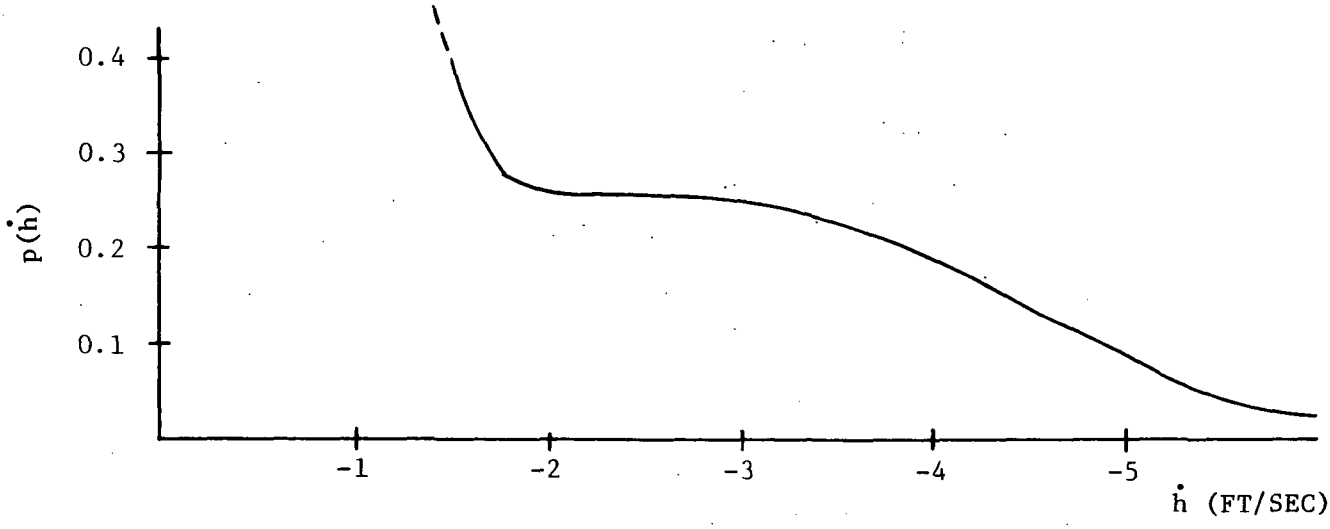

c) Unaugmented STOL

FIGURE 18 PROBABILITY DENSITY OF TOUCHDOWN VELOCITY, $T_d < 5.9$

of $\dot{h}_{TD}$. However, it is plausible to compare the average touchdown velocity as computed by Eq. (183) with the average sink-rate of those data trials that land prior to t = 5.9. Table 1 shows this comparison. P(5.9) is the predicted probability of landing prior to t = 5.9. N_i is the number of data runs that have landed by this time. The model and data results are in reasonable agreement, despite the low N_i, which gives rise to the large standard deviation in the data mean.

TABLE 1

MEAN SINK-RATE FOR TOUCHDOWN $\leq$ 5.9 SEC

	MODEL		DATA			
Condition	p(5.9)	$\bar{\dot{h}}_{td}$	N_i	$\frac{N_i}{N}$	$\bar{\dot{h}}_{td}$	S.D.
Augmented	.69	2.25	7	.7	3.4	1.7
Autospeed	.79	3.10	8	.8	3.3	1.5
Unaugmented	.80	3.10	5	.62	5.0	2.0

4.3 POTENTIAL MODEL MODIFICATIONS

When viewed in total, the results of Section 4.3 show that the model has the capability of predicting pilot performance in a landing task. Certain aspects of the model (e.g., our treatment of the terminal control aspects of the landing) were validated by the data. On the other hand, the model was found to possess certain deficiencies that indicate modifications to the model's a prior structure and/or parameter values.

4.3.1 Estimation of Ground Effect

The data for the three conditions studied showed that as the task became more difficult, the pilot exhibited a greater tendency to overflare. The model, on the other hand, indicated a trend towards landing short. The pilot seems to be overcorrecting for $C_{L,ge}$ while the model is undercorrecting. The undercorrection of the optimal control model is evident in the thrust predictions of Figures 7, 11 and 16. As each condition increases in difficulty, the differences between pilot and model δT_c become more pronounced.

The optimal control model has the ability to estimate $C_{L,ge} = x_1$ continuously from displayed information given an a priori estimate $\hat{x}_1(0) = -.09$. There is no ability to estimate $\dot{x}_1$, or to use an initial estimate of $\dot{x}_1$. Therefore, as the quality of the pilot's information base decreases and as the task becomes more difficult, the estimate $\dot{x}_1(t)$ changes less quickly.* In terms of the model elements, the Kalman filter has larger time constants. Figure 19 shows clearly this trend. In the augmented case, the pilot's estimate of $C_{L,ge}$ lags the true value with a .05 estimation error. In the unaugmented case, the estimation error has doubled; as a result, pilot compensation for C_L is too small.

From the above discussion, and the results of Section 4.2, it is apparent that the model should have the ability to estimate (at least) $\dot{C}_{L,ge}$. This is easily accomplished within the model framework by defining two states $x_1 = C_L$, $x_2 = \dot{C}_L$, with

$$\begin{aligned} \dot{x}_1(t) &= x_2(t) \\ \dot{x}_2(t) &= \ddot{C}_L(t) \triangleq \dot{z}(t) \end{aligned} \tag{194}$$

The above equation (194) would then replace the equation for C_L in the STOL model. In this case, $\dot{z}(t)$ will be a function of $\ddot{h}(t)$. Since the model's

*In the limiting case of no display information $\hat{x}_1(t) = \hat{x}_1(0)$ for all t.

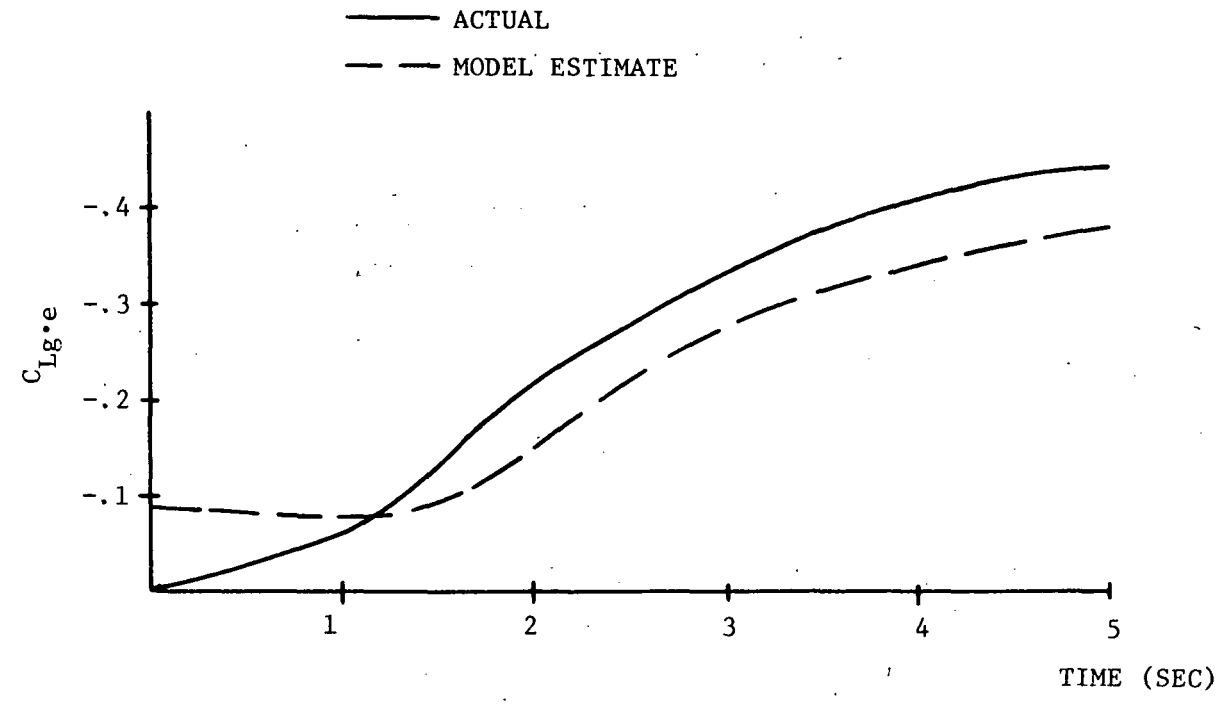

a) Augmented STOL

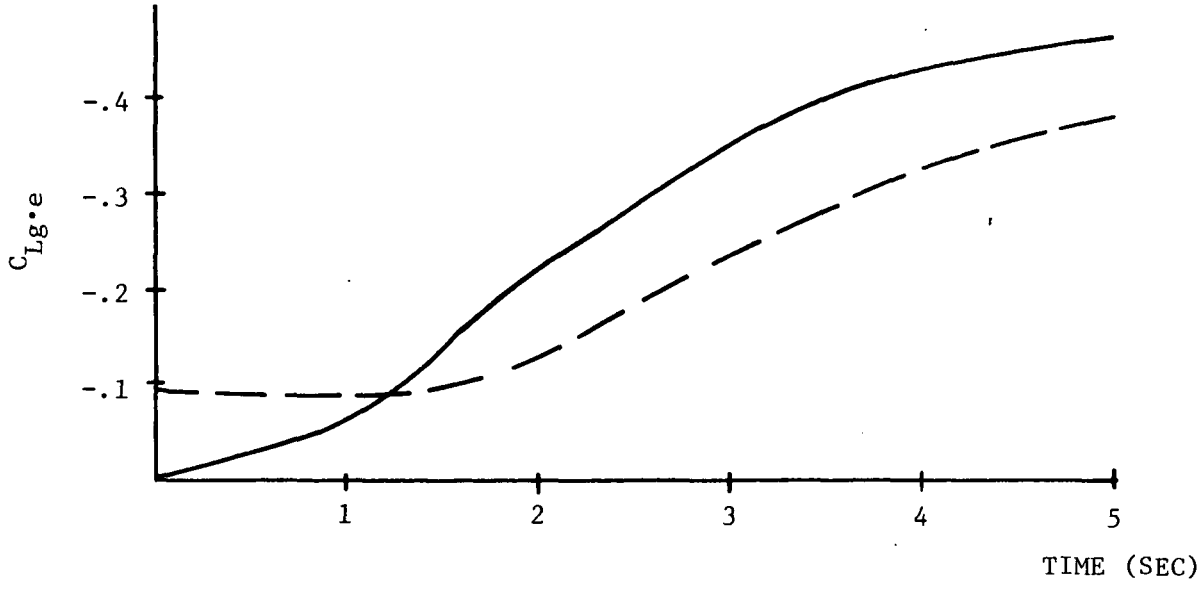

b) Unaugmented STOL

FIGURE 19 MODEL ESTIMATION OF GROUND EFFECT FROM DISPLAY INFORMATION

Kalman filter generates estimates of all states $x_i(t)$, the filter will continuously estimate $\dot{C}_L(t)$. The net result would be an estimation of C_L that is closer to the actual value, but showing a tendency to overestimate since the Kalman fitler would always be expecting C_L to increase.

The above discussion is also appropriate to the estimation of the pitching moment ground effect, $C_{M,ge}$. However, no conclusions can be drawn from the poor pilot pitch data, as regards the need for modifying the estimation of C_M. Better estimation of C_M will probably produce little effect on the model's pitch response due to the overwhelming effect of the STOL's poor pitch damping.

4.3.2 Cost Functional Weightings

The cost functional weightings for the optimal control model were chosen as described in Section 3.3 by considering pilot regulation about a nominal trajectory. With respect to altitude regulation, only a weighting on deviations δh was included. The results of Figures 8 and 12 indicate that the pilot is probably regulating about $\dot{h}_{nom}$, and possibly $\ddot{h}_{nom}$, as well. Therefore, it seems appropriate that any model modifications should include cost functional weightings on $\delta\dot{h}$ and (possibly) $\delta\ddot{h}$. It can be shown that if these deviations were weighted, it becomes unnecessary to include $u^2 = \delta T_c^2$ in the cost functional.* The control input δT_c is implicitly kept small by the model in order that $\delta\ddot{h}$ remain small. A reexamination of the data with emphasis on model-data matching or identification techniques is warranted. This is a relatively important task as regards further modeling efforts, since one must determine whether a pilot tends to control altitude deviations directly, or indirectly via control of sink-rate deviations.

Changes in the cost functional weighting on θ deviations was found to induce relatively large changes in the model's resulting pitch response. Since the model, on the average, controlled pitch somewhat better than the pilot, it appears that the a priori value of $q_\theta = .25$ is too large. Setting $q_\theta = 0$

*In most past modeling efforts, it was not necessary to weight u^2.

would bring model predictions more in line with the data. However, any attempt to identify an accurate "value" of q_θ is virtually impossible from the available pitch data. It appears that the q_θ associated with the pilot response is variable on a run-to-run basis.

4.3.3 Human Parameter Values

Slight changes in the human response parameters (τ, ρ_{yi}, a_i, τ_{ni}, etc.) generally did not have a great effect on the model predictions for the STOL problem studied. The only parameters for which the data-model trends indicate potential changes are τ_{ni} (or ρ_{ui}) and the attentional allocation parameters η_i in Eq. (90). It appears that the pilot is probably devoting more attention to the sink-rate indicator during the flare. Our assumption that $\eta_i = 1/(\text{no. of instruments})$ is probably somewhat inaccurate. A posteriori analysis of the data can be used to indicate the relative values of η_i, since the variance of a given display quantity will be related inversely to the associated η_i. Methods for predicting a priori fractional allocation of attention or scanning behavior are beyond the scope of the immediate effort. However, this topic is of central importance for display design and panel layout.

Lower values for the motor noise/signal ratio, or corresponding higher values for τ_{ni}, seem to be indicated by the autospeed data. In this case, the model's control variability is greater than the pilot's. It should be emphasized that there is relatively little data available in the manual control field pertinent to multiple control input tasks. We have assumed values for $\tau_{ni} \simeq .1$ on the basis of past single-axis task studies. In multiple control situations, it may be reasonable to expect increased values of τ_{ni} depending, for example, on the relative use the pilot makes of each control.*

*The concept of pilot control allocation is interesting, and may have a counterpart to the display allocation problem.

4.3.4 System Modeling Errors

In developing the human operator model, it was necessary to derive a linearized state-space model for the vehicle dynamics. These dynamics are highly nonlinear with respect to angle-of-attack variations, thrust variations, etc. Thus, slight differences between the model predictions and pilot data might be attributed to imprecise linearization. For example, changes in the pitch damping terms in the linearized model have a pronounced effect on the short period mode; changes in the thrust characteristics will change the manner in which in which the pilot applies control, etc. In addition to the above, there are modeling errors introduced in our simple modeling of the autospeed and pitch command-and-hold systems. When the autospeed system is engaged, we have set $u' = 0$; the pitch hold system implied $\delta\theta = \delta q = 0$ in our model. In actuality, these augmentation systems are not perfect and introduce changes in the model states. For example, the pitch hold system in the fully augmented case was found capable of controlling θ to within only .5° during flare. A more extensive model analysis could include the dynamics of the augmentation systems, but the price to pay is an increased model complexity.

V. CONCLUSIONS

Optimal control and estimation techniques have been combined with human response theory to develop a model for the pilot in a STOL landing task. This model extends previous work in man-machine systems analysis where only the approach portion of the landing task was considered. The ability to carry model predictions through flare, to touchdown, now exists.

The model development began with the nonlinear, longitudinal equations of motion for the aircraft. These equations were linearized about the equilibrium flight conditions, to develop a linear model for the STOL dynamics suitable for analytic investigation. The linear model coefficients were obtained from NASA wind tunnel measurements. The ground effects, which are an important aspect of the STOL landing problem, were included in the model equations.

The optimal control approach to human operator modeling provided the basis for developing the pilot model. The underlying assumption in this approach is that the well-trained pilot will behave in an optimal manner subject to his inherent limitations and the task requirement. Thus, the model that has been developed includes such pilot limitations as time-delay, inherent randomness, visual threshold effects, display attentional allocation, and "neuro-motor" dynamics. The terminal control aspects of the landing task were modeled by assuming that the pilot regulates the aircraft motion about a nominal flight path that meets the desired touchdown conditions. The nominal path has the property of being generated with minimal control effort.

The pilot model is time-varying, with the time-variation arising from the terminal control aspects of the task and the pilot's estimation of, and adaptation to, the ground effects. The model's output predictions are of a covariance propagation type, i.e., for any system variable, we obtain the mean and standard deviation as a function of time from flare initiation. The mean and standard deviation are sufficient statistics for predicting the joint probability density of the system state at any given time. These probability densities were translated into probability densities at touchdown to give model predictions of touchdown time and touchdown velocity.

The model was applies to predict flare performance for three different levels of STOL augmentation:

1. autospeed plus pitch command and hold,

2. autospeed system only, and

3. no augmentation.

Parameter values were chosen a priori on the basis of the task requirements and existing results in human response theory. The same set of model parameter values were used across the three STOL cases studied. The model predictions were compared with pilot data obtained on the NASA-LRC Real-Time Dynamic Simulator. The comparisons were generally in agreement, with the most accurate predictions being obtained for the fully augmented aircraft. The data indicated that certain aspects of the model were valid, e.g., our method for treating the terminal control problem, but that other facets require slight modification, e.g., the pilot's estimation of the ground effect. Some suggested modifications to the model, that will enhance its predictive capability, were discussed.

The pilot landing model can serve as a very useful design tool in analytic investigation of landing performance. It is relatively easy to study the effects of changing the display information, display gains, etc., thus obtaining probabilistic predictions associated with different display formats. Adding, or deleting, vehicle stability augmentation systems can be studied merely by changing the vehicle parameters; the parameters associated with the pilot (.e.g., time-delay, cost functional weightings, etc.) remain the same. Thus, it is possible to exercise the computer model in a straightforward, repetitive manner to study the effects on performance of vehicle and/or display modifications. Extensive simulation programs can be eliminated, since the model can serve to glean the most promising configurations for subsequent pilot simulation tests.

Further efforts in extending the modeling techniques that have been developed include the following:

1. Generation of Computer Simulation Flight Trajectories

The predictions generated by the optimal control model are of a probabilistic nature. Thus, with a single computer run, we generate the statistics associated with an entire ensemble of trajectories. However, in certain applications it may be desirable to obtain representative sample flight paths in order to investigate potential oscillations, overshoots, etc., that might not be readily apparent from the averaged statistics. The ability to use the model in a "Monte Carlo" manner would certainly enhance its flexibility, and is a relatively straightforward extension to the present effort.

2. Display Attentional Allocation

As discussed earlier, it is important to include within the pilot model the capability to predict a pilot's fractional attention allocation among a set of display indicators. This is a necessary step towards the eventual use of the pilot model for display design. One method of approach is to assume that pilot scanning (or attention) strategy is chosen to minimize the uncertainty in estimating those state variables most important for feedback control.[3] Accurate pilot scanning data will be necessary for validating any such scanning submodel that is eventually developed.

3. Pilot Control in Terminal Areas

The model that has been developed is appropriate for the specific pilot task of landing approach and flare. However, the methodology we have used can be extended to model a pilot's ability in following curved approach paths (or multi-segment paths) appropriate in a terminal configured vehicle context. Thus, one would have the ability to determine the degree of pilot error in executing given maneuvers, including compensation for changes in relative wind, timed arrival at given waypoints, etc.

4. Optimization of Display Information

One of the ultimate goals of the pilot model is its application to optimizing the information content of a display panel. To achieve this goal, it will be necessary to develop (either via experiment or analytically) more precise relationships between a display symbol and related model parameters such as observation noise, perceptual thresholds, etc. A model can then be used to rank-order proposed display panel formats, with model predicted performance serving as a figure of merit.

5. Display Monitoring

The model's information base consists presently of those instruments used by the pilot in generating a given control input. There is no explicit treatment of pilot monitoring displays that are not directly appropriate for control, but may relate to vehicle "status". It will prove important to model these peripheral sources of information when considering pilot identification of system failures, and the broader aspect of total flight management. The model has the capability to treat such "status" information as discrete information, obtained periodically, as opposed to "control" information that is processed continuously. Modifying the model to include continuous and discrete-time information is an area for further effort, especially as regards to pilot monitoring in automated and/or semi-automated systems.

APPENDIX A

SOLUTION OF THE LINEAR OPTIMAL TERMINAL CONTROL PROBLEM

This appendix derives the solution to the linear regulator problem where it is required to meet prescribed set of terminal conditions.

Problem Formulation

The system dynamics are described by the linear time-invariant equations

$$\dot{x}(t) = Ax(t) + Bu(t) \tag{A.1}$$

$$x(t_o) = x_o = \text{given} \tag{A.2}$$

where $x = \text{col}\,[x_1, x_2, \ldots, x_n]$ is the system state and $u = \text{col}\,[u_1, u_2, \ldots u_r]$ is the control. It is desired to drive the sytem from the initial state x_o to a terminal state $x(t_1)$ that satisfies the p boundary conditions

$$Hx(t_1) + c = 0 \tag{A.3}$$

where H is a given $p \times n$ matrix of full rank $p \leq n$ and c is a p-vector. In addition, the control that accomplishes the transfer must minimize the cost functional

$$\hat{J}(u, x_o, t_o) = x'(t_1)Fx(t_1) + \int_{t_o}^{t_1} [x'(t)Qx(t) + u'(t)Ru(t)]dt \tag{A.4}$$

where F and Q are positive semi-definite matrices and R is positive definite.

It is assumed that there exists at least one control that can drive the system from x_o to an $x(t_1)$ satisfying (A.3) so that the optimization problem

posed is non-vacuous. If the system (A.1) is completely controllable, this assumption will be satisfied.

Problem Solution

In order to solve the optimization problem, the constraint equation (A.3) is appended to the cost function $\hat{J}(u,x_o,t_o)$ by introducing a Lagrange multiplier ν. Thus, we define a new cost functional,

$$J(u,x_o,t_o) = (Hx(t_1) + c)'\nu + \hat{J}(u,x_o,t_o) \tag{A.5}$$

where ν will be chosen such that the terminal condition $Hx(t_1) + c$ will be small--hopefully zero.

The minimization of J subject to Eq. (A.1) is easily accomplished using Hamilton Jacobi theory.[7] Define the Hamiltonian

$$H\left(x, \frac{\partial J}{\partial x}, u\right) = x'Qx + u'Ru + \frac{\partial J'}{\partial x}(Ax + Bu) \tag{A.6}$$

where the function $J(x,t)$ of x and t is the optimal cost

$$J(x,t) = \min_u J(u,x,t) \tag{A.7}$$

for the system (A.1) with initial state x at time t. Clearly, at $t = t_1$,

$$J(x,t_1) = x'Fx + (Hx + c)'\nu \tag{A.8}$$

The optimal control, u^*, must minimize the Hamiltonian. Thus,

$$\frac{\partial H}{\partial u} = 0 \tag{A.9}$$

which yields

$$u^* = -\frac{1}{2} R^{-1} B' \frac{\partial J}{\partial x} \tag{A.10}$$

The Hamilton-Jacobi theory then states that the function $J(x,t)$ satisfies the partial differential equation

$$\frac{\partial J}{\partial x} + H\left(x, \frac{\partial J}{\partial x}, u^*\right) = 0 \tag{A.11}$$

with the boundary condition (A.8). Substituting Eq. (A.10) in (A.11) gives

$$\frac{\partial J}{\partial t} + \frac{\partial J'}{\partial x} \cdot Ax + x'Qx - \frac{1}{4} \frac{\partial J'}{\partial x} BR^{-1}B' \frac{\partial J}{\partial x} = 0 \tag{A.12}$$

The solution $J(x,t)$ can be shown to be, by direct substitution,

$$J(x,t) = x'K(t)x + x'h(t) + r(t) \tag{A.13}$$

where the matrix $K(t)$, $t \leq t_1$ satisfies the Riccati equation

$$\dot{K}(t) = -K(t)A + A'K(t) + K(t)BR^{-1}B' K(t) - Q \tag{A.14}$$

with boundary condition

$$K(t_1) = F \tag{A.15}$$

Note that if $F = Q = 0$, then $K(t) \equiv 0$.

The function $h(t)$, $t \leq t_1$ is generated by

$$\dot{h}(t) = -(A - BR^{-1}B' K(t))' h(t) = -\bar{A}'(t) h(t) \tag{A.16}$$

$$h(t_1) = H'\nu \tag{A.17}$$

Finally, $r(t) = \nu' c$. Hence, the optimal control is

$$u(x,t) = - R^{-1}B'K(t)\, x(t) - R^{-1}B'h(t) \tag{A.18}$$

It remains to determine ν such that the boundary condition (A.3) is satisfied. We note that the solution for $h(t)$ is given by

$$h(t) = \bar{\Phi}'(t_1,t)H'\nu \tag{A.19}$$

where $\bar{\Phi}(t,\tau)$ is the state transition matrix corresponding to $\bar{A}(t)$, i.e.,

$$\frac{d}{dt}\bar{\Phi}(t,\tau) = \bar{A}(t)\,\bar{\Phi}(t,\tau), \quad \bar{\Phi}(t,\tau) = I^{\dagger} \tag{A.20}$$

The state trajectory of Eq. (A.1) is then generated according to

$$\begin{aligned} \dot{x}(t) &= (A - BR^{-1}B'K(t))\, x(t) - BR^{-1}B'h(t) \\ &= \bar{A}(t)\, x(t) - BR^{-1}B'\,\bar{\Phi}'(t_1,t)H'\nu \end{aligned} \tag{A.21}$$

$x(t_1)$ is then given by

$$x(t_1) = \bar{\Phi}(t_1,t_o)x_o - W(t_1,t_o)H'\nu \tag{A.22}$$

where

$$W(t_1,t_o) = \int_{t_o}^{t_1} \bar{\Phi}(t_1,\tau)\, BR^{-1}B'\,\bar{\Phi}'(t_1,\tau)\, d\tau \tag{A.23}$$

---

†If $K(t) = 0$, $\bar{\Phi}(t,\tau) = e^{A(t-\tau)}$.

The matrix $W(t_1,t_o)$ is invertible if the system (A.1) is completely controllable.[7]

Premultiplying Eq. (A.22) by H it can be seen that for $Hx(t_1) = -c$, the vector ν should be chosen as

$$\nu = [H\, W(t_1,t_o)H']^{-1} \cdot [H\, \bar{\Phi}(t_1,t_o)x_o + c] \tag{A.24}$$

The required inverse exists if the system is completely controllable, and since H was assumed to have full rank.* This completes the solution to the originally posed problem.

Extension to Control Rate Weighting

In the optimal control of human response, the cost functional $\hat{J}(u,x_o,t_o)$, Eq. (A.4), is of the (general) form

$$\hat{J}(u,x_o,t_o) = x'(t_1)\, Fx(t_1) + \int_{t_o}^{t_1} (x'Qx + u'Ru + \dot{u}'G\dot{u})dt \tag{A.25}$$

The system dynamics and boundary conditions (A.1) - (A.3) remain unchanged. In order to apply the above results to solve this problem, we define an augmented $n+r$ state vector $\chi = \text{col}\,[x,u]$ and define $\mu(t) = \dot{u}(t)$. Thus, the equation (A.1) becomes

$$\dot{\chi}(t) = A_o\chi(t) + B_o\mu(t) \tag{A.26}$$

$$\chi(t_o) = \chi_o \tag{A.27}$$

*The assumption of full rank is tantamount to having non-conflicting boundary conditions.

where

$$A_o = \left[\begin{array}{c|c} A & B \\ \hline 0 & 0 \end{array}\right], \quad B_o = \left[\begin{array}{c} 0 \\ \hline I \end{array}\right], \quad \chi_o = \left[\begin{array}{c} x_o \\ \hline 0 \end{array}\right] \tag{A.28}$$

The cost functional Eq. (A.25) and terminal condition Eq. (A.3) may then be written as

$$\hat{J}(\mu,\chi_o,t_o) = \chi'(t_1)F_o\,\chi(t_1) + \int_{t_o}^{t_1} (\chi'Q_o + \mu'G\mu)dt \tag{A.29}$$

$$H_o\chi(t_1) + c = 0 \tag{A.30}$$

where

$$F_o = \text{diag}\,(F,0), \quad Q_o = \text{diag}\,(Q,R), \quad H_o = [H,0]. \tag{A.31}$$

The derived results of Eqs. (A.14) - (A.24) are now applicable to the problem of minimizing control rate, with the replacements $A \to A_o$, $B \to B_o$, $Q \to Q_o$, $R \to G$, $H \to H_o$, $x \to \chi$, $u \to \mu = \dot{u}$, etc.

APPENDIX B

NUMERICAL SPECIFICATION OF THE STOL MODELS

The elements of the state space STOL models are functions of velocity, physical characteristics of the aircraft, and the aerodynamic coefficients. These elements are analytically specified by Eqs. (57) - (61) in the text. In this appendix, the numerical values for the $\underline{A}$ and $\underline{B}$ matrices are presented for the basic aircraft, the aircraft with autospeed, and the aircraft with pitch command and autospeed.

Basic Aircraft

The basic aircraft approaches at an initial airspeed of 75 knots on a 6° glideslope. The centerline of the aircraft is initially pitched down -4.1°. The A and B matrices are given by:

$$\underline{A} = \begin{bmatrix} 0.0 & 0.0 & 0.0 & 0.0 & 0.0 & 0.0 & 0.0 & 0.0 \\ 0.0 & 0.0 & 0.0 & 0.0 & 0.0 & 0.0 & 0.0 & 0.0 \\ 0.0 & 0.0 & -.0373 & .0855 & 0.0 & -.255 & 0.0 & 0.0 \\ -.063 & 0.0 & -.522 & -.566 & 1.0 & .0268 & 0.0 & -.134 \\ 0.0 & .63 & .2087 & -1.2 & -1.47 & -.0107 & 0.0 & -.0212 \\ 0.0 & 0.0 & 0.0 & 0.0 & 1.0 & 0.0 & 0.0 & 0.0 \\ 0.0 & 0.0 & -.105 & -1.0 & 0.0 & 1.0 & 0.0 & 0.0 \\ 0.0 & 0.0 & 0.0 & 0.0 & 0.0 & 0.0 & 0.0 & -2.0 \end{bmatrix}$$

$$\underline{B} = \begin{bmatrix} 0.0 & 0.0 \\ 0.0 & 0.0 \\ 0.0 & -.0043 \\ 0.0 & -.096 \\ 0.0 & -3.5 \\ 0.0 & 0.0 \\ 0.0 & 0.0 \\ 2.0 & 0.0 \end{bmatrix}$$

Aircraft With Autospeed

The aircraft with autospeed approaches at an airspeed of 75 knots on a 6° glideslope. The airspeed is held at 75 knots and the centerline of the aircraft is initially pitched up 2°. The $\underline{A}$ and $\underline{B}$ matrices are given as

$$\underline{A} = \begin{bmatrix} 0.0 & 0.0 & 0.0 & 0.0 & 0.0 & 0.0 & 0.0 \\ 0.0 & 0.0 & 0.0 & 0.0 & 0.0 & 0.0 & 0.0 \\ -.063 & 0.0 & -.556 & 1.0 & .0268 & 0.0 & -.134 \\ 0.0 & 0.0 & -1.2 & -1.47 & -.0107 & 0.0 & -.0212 \\ 0.0 & .63 & 0.0 & 1.0 & 0.0 & 0.0 & 0.0 \\ 0.0 & 0.0 & -1.0 & 0.0 & 1.0 & 0.0 & 0.0 \\ 0.0 & 0.0 & 0.0 & 0.0 & 0.0 & 0.0 & -2.0 \end{bmatrix}$$

$$\underline{B} = \begin{bmatrix} 0.0 & 0.0 \\ 0.0 & 0.0 \\ 0.0 & -.096 \\ 0.0 & -3.65 \\ 0.0 & 0.0 \\ 0.0 & 0.0 \\ 2.0 & 0.0 \end{bmatrix}$$

Aircraft With Autospeed and Pitch Command and Hold

The fully augmented aircraft approaches on the 6° glidelsope. The airspeed is held at 75 knots and the pitch is held at 2°. The $\underline{A}$ and $\underline{B}$ matrices are given as

$$\underline{A} = \begin{bmatrix} 0.0 & 0.0 & 0.0 & 0.0 \\ -.063 & -.556 & 0.0 & -.134 \\ 0.0 & -1.0 & 0.0 & 0.0 \\ 0.0 & 0.0 & 0.0 & -2.0 \end{bmatrix} \qquad \underline{B} = \begin{bmatrix} 0.0 \\ 0.0 \\ 0.0 \\ 2.0 \end{bmatrix}$$

In all cases, the aircraft mass is 1700 slugs and the moment of inertia about the y-axis is 2.46×10^5 slug-ft^2.

REFERENCES

1. Grantham, W.D., et al., "Fixed-Base Simulator Study of an Externally Blown Flap STOL Transport Airplane During Approach and Landing", NASA TN D-6898, October 1972.

2. Kleinman, D.L. and Baron, S., "Manned Vehicle Systems Analysis by Means of Modern Control Theory", NASA CR-1626, October 1970.

3. Kleinman, D.L., et al., "A Control Theoretic Approach to Manned Vehicle Systems Analysis", 1971 Joint Automatic Control Conference, Washington University and IEEE Trans. Auto. Control, AC-16, No. 6, December 1971.

4. Kleinman, D.L. and Baron, S., "Analytic Evaluation of Display Requirements for Approach to Landing", NASA CR-1952, November 1971.

5. Kleinman, D.L. and Perkins, T., "Modeling the Human in a Time-Varying Anti-Aircraft Tracking Loop", Proceedings of NWC Symposium on Application of Control Theory to Modern Weapons Systems, May 1973. Also to appear in IEEE Trans. Auto. Control, 1974.

6. Bryson, Jr., A.E. and Ho, Y.C., Applied Optimal Control, Blaisdell Publishing Company, Waltham, Mass., 1969.

7. Athans, M. and Falb, P.L., Optimal Control, McGraw-Hill Book Co., New York, N.Y., 1966.

8. Grantham, W.D., Sommer, R.W., and Deal, P.L., "Simulator Study of Flight Characteristic of a Jet-Flap STOL Transport Airplane During Approach and Landing", NASA TN D-6225, 1971.

9. Middleton, D.B. and Bergeron, H.P., "A Compilation and Preliminary Analysis of Typical Approach and Landing Data for an Externally Blown Flap STOL Aircraft". TN D-7497, 1974.

*U.S. GOVERNMENT PRINTING OFFICE: 1974-739-158/99

NATIONAL AERONAUTICS AND SPACE ADMINISTRATION
WASHINGTON, D.C. 20546

OFFICIAL BUSINESS
PENALTY FOR PRIVATE USE $300

SPECIAL FOURTH-CLASS RATE
BOOK

POSTAGE AND FEES PAID
NATIONAL AERONAUTICS AND
SPACE ADMINISTRATION
451

U.S.MAIL

POSTMASTER: If Undeliverable (Section 158 Postal Manual) Do Not Return

"The aeronautical and space activities of the United States shall be conducted so as to contribute . . . to the expansion of human knowledge of phenomena in the atmosphere and space. The Administration shall provide for the widest practicable and appropriate dissemination of information concerning its activities and the results thereof."

—NATIONAL AERONAUTICS AND SPACE ACT OF 1958

NASA SCIENTIFIC AND TECHNICAL PUBLICATIONS

TECHNICAL REPORTS: Scientific and technical information considered important, complete, and a lasting contribution to existing knowledge.

TECHNICAL NOTES: Information less broad in scope but nevertheless of importance as a contribution to existing knowledge.

TECHNICAL MEMORANDUMS: Information receiving limited distribution because of preliminary data, security classification, or other reasons. Also includes conference proceedings with either limited or unlimited distribution.

CONTRACTOR REPORTS: Scientific and technical information generated under a NASA contract or grant and considered an important contribution to existing knowledge.

TECHNICAL TRANSLATIONS: Information published in a foreign language considered to merit NASA distribution in English.

SPECIAL PUBLICATIONS: Information derived from or of value to NASA activities. Publications include final reports of major projects, monographs, data compilations, handbooks, sourcebooks, and special bibliographies.

TECHNOLOGY UTILIZATION PUBLICATIONS: Information on technology used by NASA that may be of particular interest in commercial and other non-aerospace applications. Publications include Tech Briefs, Technology Utilization Reports and Technology Surveys.

Details on the availability of these publications may be obtained from:

SCIENTIFIC AND TECHNICAL INFORMATION OFFICE

NATIONAL AERONAUTICS AND SPACE ADMINISTRATION

Washington, D.C. 20546